Titre: Title:	Comprehensive Characterization of an Inducible Mammalian Expression System Using 13C-Metabolic Flux Analysis
Auteur: Author:	Zahra Sheikholeslami
Date:	2013
Type:	Mémoire ou thèse / Dissertation or Thesis
Référence: Citation:	Sheikholeslami, Z. (2013). Comprehensive Characterization of an Inducible Mammalian Expression System Using 13C-Metabolic Flux Analysis [Thèse de doctorat, École Polytechnique de Montréal]. PolyPublie. https://publications.polymtl.ca/1261/

URL de PolyPublie: PolyPublie URL:	https://publications.polymtl.ca/1261/
Directeurs de recherche: Advisors:	Olivier Henry, & Mario Jolicoeur
Programme: Program:	Génie chimique

UNIVERSITÉ DE MONTRÉAL

COMPREHENSIVE CHARACTERIZATION OF AN INDUCIBLE MAMMALIAN EXPRESSION SYSTEM USING 13C-METABOLIC FLUX ANALYSIS

ZAHRA SHEIKHOLESLAMI

DÉPARTEMENT DE GÉNIE CHIMIQUE

ÉCOLE POLYTECHNIQUE DE MONTRÉAL

THÈSE PRÉSENTÉE EN VUE DE L'OBTENTION

DU DIPLÔME DE PHILOSOPHIAE DOCTOR

(GÉNIE CHIMIQUE)

OCTOBRE 2013

UNIVERSITÉ DE MONTRÉAL

ÉCOLE POLYTECHNIQUE DE MONTRÉAL

Cette thèse intitulée:

COMPREHENSIVE CHARACTERIZATION OF AN INDUCIBLE MAMMALIAN EXPRESSION SYSTEM USING 13C-METABOLIC FLUX ANALYSIS

présentée par : SHEIKHOLESLAMI Zahra

en vue de l'obtention du diplôme de : Philosophiae Doctor

a été dûment acceptée par le jury d'examen constitué de :

M. DE CRESCENZO Gregory, Ph.D., président

M. HENRY Olivier, Ph.D., membre et directeur de recherche

M. JOLICOEUR Mario, Ph.D., membre et codirecteur de recherche

M. PERRIER Michel, Ph.D., membre

M. GODIA Francesc, Ph.D., membre

DÉDICACE

To my adored parents, Mahin and Shamseddin, my first and best teachers.

Thank you for your love, support, and encouragement

AKNOWLEDGMENT

This thesis is the result of five and a half years of research whereby I have been accompanied and supported by several people. This is the opportune moment to acknowledge all who have crossed my path throughout this journey. First, I would like to thank my supervisor, Dr. Olivier Henry. Your wide knowledge and your logical way of thinking have been of great value to me. I have always enjoyed our discussions, and I never left a meeting with you without feeling motivated and optimistic about the future directions of our research. I have learned so much from you through the years. You are one of the people in my life for which I hold the utmost respect. I will certainly miss our regular meetings, but hope that our conversations will never end.

I would like to express my deep and sincere gratitude to my co-supervisor, Dr. Mario Jolicoeur for his intellectual support and encouragement and advice on my research. You made me realize that “sky is the limit” and I won't stop until I touch the top.

I have also learned a lot from Jingkui Chen and I sincerely thank him for all his help and encouragement. I would like to extend my thanks to all members of our group (past and present) who have made my stay at Ecole enjoyable and scientifically simulating. I have collaborated closely with Ines, Cyril, Eric, Alex, Claudia, Cedric, Judy, Nesrine, Massi, Benoit, Frédéric, Samantha and Charles. Thanks to summer students, Azadeh, Emil, Alexander, Saagar and Kahina who helped me. I wish to thank Dr. Alexandra Furtos and her assistant Ms. Tang Marie-Christine from Université de Montréal and all secretaries and technical staff of the chemical engineering department, as well as Dr. Patrick Benoist and Dr. Patrick Daoust of Viropro Internal Inc.

I would also like to thank my best friend and soul mate Atefeh, who has listened to my moaning and complaining and supported me every step of the way. I am so blessed to have you in my life for all these years.

I give my very special thanks to my parents to whom I owe everything I am today, for giving me the inspiration to work hard and never give up, and for always being there for me when I needed them. I also thanks to my dear brother, Majid, for his kindness and moral support and wish him all the best in his studies.

And finally, I cannot imagine having gone through this without my intelligent and supportive husband, Alireza. Your unconditional love, friendship and honesty give me the strength to follow my dreams. You are the coauthor of this thesis. I love you.

And, of course, my darling five months old son, Arad, whose love is worth it all. He is the sunshine of my life, my joy and hope no matter what.

RÉSUMÉ

La culture de cellules de mammifères constitue à ce jour la plateforme d'expression la plus utilisée dans l'industrie biopharmaceutique, en raison de la capacité inégalée de ces cellules à réaliser les modifications post-traductionnelles essentielles à la fonctionnalité des produits complexes. En raison de la forte demande pour les produits biothérapeutiques, de la volonté de diminuer les coûts associés au développement des bioprocédés et du besoin de réduire les temps de mise en marché, plusieurs progrès réalisés au cours des dernières décennies ont permis des améliorations significative en termes de rendement et de qualité du produit. Ces avancées ont été effectuées surtout grâce au développement de meilleurs vecteurs d'expression, au développement de milieux de culture plus performants et à l'application de stratégies fed-batch permettant l'atteinte de très hautes densités cellulaires. Une autre avancée récente concerne le développement de systèmes d'expression inductibles, dont l'énorme avantage est de permettre de découpler les phases de croissance et de production, conférant ainsi la possibilité d'optimiser chacune des phases indépendamment, avec des conditions opératoires spécifiques à chacune d'elles. Par ailleurs, cela permet en principe de faire croître les cellules plus rapidement avant la phase d'induction, puisque ces dernières n'ont pas à supporter la charge métabolique additionnelle qu'impose la synthèse d'une protéine recombinante. Dans de tels procédés bi-phasiques, établir le moment propice pour procéder à l'induction et élaborer une stratégie d'alimentation post-induction efficace sont deux facteurs cruciaux qui vont dicter la productivité du système. En raison de la complexité du métabolisme des cellules de mammifères, l'optimisation ciblée des procédés de culture demeure un défi, mais ce travail peut être grandement facilite par le biais de nouvelles approches du génie métabolique. C'est le cas notamment de la technique d'analyse des flux métaboliques avec traceurs isotopiques (^{13}C-MFA), qui a démontré qu'elle permet une caractérisation de l'état physiologique à la fois plus fine et plus robuste, mais qui a toutefois encore peu été exploitée dans le contexte de la culture de cellules animales.

L'objectif principal de cette thèse était donc d'appliquer la technique d'analyse des flux métaboliques avec traceurs isotopiques afin d'effectuer une caractérisation quantitative du métabolisme primaire de cellules CHO dotées d'un système d'expression inductible, afin de permettre l'établissement systématique des principales conditions de culture et le développement rationnel d'une stratégie d'alimentation post-induction. A cette fin, des protocoles expérimentaux

pour effectuer des expériences de marquage et des analyses par spectrométrie de masse, ainsi que les outils de calcul requis pour effectuer l'estimation des flux intracellulaires à partir de ces mesures ont du être développés ou adaptés à partir de méthodes décrites dans la littérature.

En premier lieu, l'approche a été utilisée afin d'analyser le métabolisme central du carbone d'une lignée de cellules CHO en lien avec la productivité cellulaire spécifique. L'objectif était d'évaluer de façon quantitative la charge imposée par la synthèse d'une protéine recombinante sur le métabolisme primaire des cellules. Ceci a été accompli par le biais d'une analyse comparative des flux métaboliques pour des cellules induites et non-induites. Des cultures avec divers substrats marqués au C^{13} ont été réalisées et les distributions de masse résultantes de plusieurs métabolites extracellulaires (lactate et trois acides aminés) ont été mesurées. Ces données ont été utilisées, de concert avec des mesures de taux spécifiques de consommation et de production, pour calculer les flux métaboliques. Cette analyse a notamment révélé que l'expression d'une protéine recombinante est associée avec des différences faibles, mais néanmoins significatives pour plusieurs voies métaboliques, particulièrement celles reliées à la formation d'ATP et de NADPH, tel que le cycle de Krebs, la voie des pentose phosphate ou la voie de l'enzyme malique. Les cellules induites présentaient un métabolisme plus efficace, puisqu'une plus grande proportion du glucose, le nutriment principal, était acheminée dans le cycle TCA. A l'inverse, aucun changement majeur n'a été détecté au niveau du métabolisme des acides aminés, dont la glutamine. Comme un changement de température a été opéré au moment de l'induction pour favoriser la productivité, cette étude se voulait également la première caractérisation détaillée du métabolisme des cellules CHO sous des conditions légèrement hypothermique.

Par la suite, l'impact du moment d'induction sur la productivité des cultures a été étudié, puisque ce paramètre influe à la fois sur la quantité de biomasse et sur la productivité spécifique des cellules. A cette fin, des cellules ont été prélevées à différents stades de croissance, puis ont été transférées pour être induites dans du milieu frais. Les cinétiques de croissance, de consommation et de production durant la phase de production ont été comparées pour l'ensemble des conditions d'induction. En comparaison avec les cultures induites à concentrations élevées, les cellules induites à faibles densités cellulaires ont atteint un pic de concentration plus faible, mais la longévité des cultures et la productivité spécifique des cellules étaient plus élevées, ce qui s'est traduit par une augmentation de la concentration finale en produit. Afin de mieux caractériser les effets observés sur le plan physiologique, une analyse des flux métaboliques par

traceurs isotopiques a été réalisée pour comparer les cultures induites respectivement à faible et à haute densité cellulaire. Pour cette étude, le nombre de mesures a été étendu en considérant également les distributions de masse de deux acides organiques. En accord avec les différences observées au niveau de la croissance et de la productivité cellulaire, il a été constaté que plusieurs flux intracellulaires sont affectés par le moment d'induction. Il en a été conclu que la disponibilité des nutriments avait un impact marqué durant la phase de production après induction. Plus particulièrement, il a été révélé que le glucose est consommé plus efficacement dans le cas des cultures à haute densité, alors que la contribution des acides aminés s'en trouvait, elle, diminuée.

Les résultats précédents ont été obtenus pour un changement de milieu complet au moment de l 'induction, une opération qui ne serait pas aisément transposable pour la production à grande échelle. Pour cette raison et parce que la disponibilité des nutriments semblent avoir un impact majeur sur la productivité et/ou la croissance, la possibilité d'augmenter les rendements par le biais d'une stratégie fed-batch a été explorée. Il a été constaté que des ajouts de solutions concentrées effectués post-induction augmentaient de façon substantielle la productivité des cultures par rapport au mode batch. Plus encore, il a été observé que lorsque la glutamine est alimentée en excès, les cultures atteignent des concentration cellulaires maximales plus grandes. Cependant, les cultures limitées en glutamine présentaient elles une productivité spécifique plus grande, ce qui a conduit à des rendements en produit similaires. Afin de mettre en lumière l'impact physiologique du niveau de glutamine dans l'alimentation, une étude comparative des flux métaboliques avec traceurs isotopiques a été réalisée dans des cultures en mode semi-continu. Les changements majeurs en terme de croissance et de productivité se traduisaient également par des différences observables au niveau de la distribution des flux métaboliques. Plus particulièrement, le métabolisme du lactate était grandement influencé par le niveau de glutamine alimenté aux cellules durant la phase d'induction.

Globalement, l'ensemble des travaux réalisés semble suggérer une corrélation inverse entre le taux de croissance et la productivité spécifique des cellules. Les caractérisations métaboliques effectuées pourraient néanmoins procurer une bonne base pour l'identification de marqueurs physiologiques de la productivité, permettant ainsi de poursuivre le développement et l'optimisation des procédés avec induction. Ces travaux démontrent également la valeur de la technique de ^{13}C-MFA comme outil de caractérisation du métabolisme.

ABSTRACT

Mammalian cell cultures have become the predominant production platform in today's multi-billion dollar biopharmaceutical industry. Mammalian cells have the unique capacity to synthesize recombinant proteins with proper folding and post-translational modifications. Due to the increasing demand for biotherapeutics, the pressure to reduce the costs associated with process development and the need to shorten the time to market, continuous efforts have been made in mammalian cell technologies to maximize both the product yields and quality. This has been mostly achieved through the design of enhanced expression vectors, improved medium formulations and the application of fed-batch strategies supporting high cell densities. In recent years, there has been also a growing interest in the development of inducible mammalian expression systems, which allow decoupling of the growth and production phases and open up the possibility to define specific operating conditions that are favorable for each phase. Moreover, cells can presumably be grown more rapidly before induction, as they do not have the extra metabolic burden associated with recombinant protein expression. In such biphasic systems, a suitable timing for induction and an efficient feeding protocol pre/post-induction are among the most crucial factors to ensure a high volumetric productivity. Due to the complex metabolism of mammalian cells, the targeted optimization of cell culture processes remains challenging, but can be greatly facilitated with the aid of new metabolic engineering approaches. In particular, the use of isotopic tracers and ^{13}C-metabolic flux analysis (^{13}C-MFA) was shown to provide a more detailed and accurate description of cellular physiology than the classical metabolite balancing technique, although its application to mammalian cells is still in its infancy.

The main objective of this work was thus to apply ^{13}C-metabolic flux analysis to quantitatively characterize the primary metabolism of recombinant CHO cells harboring an efficient inducible expression system, as a systematic approach to guide the determination of key process conditions and allow the rational development of a feeding protocol to increase culture productivity. To this end, analytical methods for conducting informative labeling experiments and mass spectrometry measurements, as well as computational tools allowing reliable metabolic flux quantification had to be developed or adapted from the literature.

First, this method was used to analyze the central carbon metabolism of a recombinant CHO cell line in relation with cellular productivity. The goal was to quantitatively evaluate the burden

imposed by recombinant protein expression on the primary metabolism of cells in culture. This was achieved by conducting a comparative study of the intracellular flux map distribution with and without the induction of recombinant protein expression. We performed cultures with multiple ^{13}C-labeled substrates and measured the resulting mass distribution of extracellular metabolites (lactate and three amino acids) by mass spectrometry. This additional data was used in conjunction with extracellular rate measurements to obtain reliable metabolic flux estimates. Through this analysis, we have notably demonstrated that heterologous protein expression is correlated with small, but significant differences in a number of important intracellular pathways, most of them related to ATP and NADPH formation, including the pentose phosphate pathway, the malic enzyme reaction and the TCA cycle. Induced cells were found to exhibit an increased flux of pyruvate into the TCA cycle, indicative of a more efficient glucose utilization. However, no significant difference could be inferred with respect to amino acid metabolism, including glutamine. Since a temperature shift was performed at the time of induction, this study was also the first comprehensive characterization of CHO cell metabolism under mild-hypothermia conditions.

We have then investigated the impact of the timing of induction on culture productivity, since this parameter can affect both the cumulative biomass concentration and the cell specific productivity. Cells taken at different stages of growth were transferred and induced in fresh medium and the kinetics of growth, nutrient consumption and product formation were compared during the production phase. Compared to cultures induced at a high cell concentration, low cell density inductions achieved lower maximum cell concentrations, but exhibited higher cell specific productivity and greater culture longevity, which gave a greater final product titers. To gain more physiological insights into the observed differences, ^{13}C-metabolic flux analysis was performed to characterize and compare the metabolism of cells induced at respectively low and high cell densities. The range of measurements was extended by including the mass distributions of two organic acids. In line with differences observed in terms of growth and productivity, several calculated intracellular fluxes were found to be affected by the timing of induction. It was inferred that the corresponding availability of nutrients had a determinant impact on the induction phase. Most notably, glucose utilization efficiency was increased in high cell density induction, whereas the contribution of amino acids became marginal.

The previous results were however obtained by doing a complete medium exchange at the time of induction, an operation which cannot be easily implemented at large-scale. For this reason and since the results implied a strong correlation between nutrient availability and cellular growth/productivity, we then explored the possibility to increase the product yield by using a fed-batch process. We found that performing concentrated feed additions post-induction greatly increase the productivity of cultures compared to induction in batch mode. More interestingly, we observed that when glutamine was fed in excess to the cells, the cultures reached greater maximum cell concentrations. While cell growth was comparatively lower in glutamine-limited fed-batch, the final product titers were found to be similar, indicative of an increased cell specific productivity. To further assess the physiological impact of glutamine levels on the cells, a comparative ^{13}C-metabolic flux analysis was conducted in semi-continuous cultures to analyze both culture regimes. The marked changes in cellular growth and productivity were clearly reflected in the metabolism of the cells. In particular, lactate metabolism was found to be greatly influenced by the amount of glutamine present in the feed during the production phase.

Overall, the results from all our studies tend to suggest that there may be some negative correlation between cell growth and cellular productivity. Nonetheless, the metabolic characterizations performed in this work may provide useful clues for the identification of physiological markers of cell growth and/or productivity that could further guide the optimization of inducible expression systems. Our work also demonstrates that ^{13}C-metabolic flux analysis is a valuable tool for characterizing cell metabolism and supporting cell culture process optimization.

TABLE OF CONTENTS

LIST OF TABLES

LIST OF FIGURES

LIST OF ABBREVIATIONS

(c)	cytosolic
(m)	mitochondrial
AcCOA	acetyl coenzyme A
ACN	acetonitrile
ADP	adenosine diphosphate
αkg	α-ketoglutarate
ALA	alanine
AMM	atom mapping matrix
ARG	arginine
ASN	asparagine
ASP	aspartate
ATP	adenosine-5'-triphosphate
BHK	baby hamster kidney
CHO	chinese hamster ovary
CI	confidence interval
CIT	citrate
CO2	carbon dioxide
CoA	coenzyme A

CSTR	continuous stirred tank reactor
CYS	cysteine
(d)AMP	(deoxy) adenosine monophosphate
(d)CMP	(deoxy) cytidine monophosphate
(d)GMP	(deoxy) guanosine monophosphate
(d)GTP	(deoxy) guanosine triphosphate
(d)TMP	(deoxy) thiamine monophosphate
DNA	deoxyribonucleic acid
E4P	erythrose 4-phosphate
ELISA	enzyme-linked immunosorbent assay
EMU	elementary metabolite unit
F6P	fructose 6-phosphate
FA	fatty acid
FAD(H2)	flavine adenosine dinucleotide (reduced)
FBPA	fructose-1,6-bisphophate aldolase
G6P	glucose 6-phosphate
GAP	glyceraldehyde 3 phosphate
GC-MS	gas chromatography mass spectrometry
GDP	guanosine diphosphate

GLC	glucose
GLN	glutamine
GLT	glutamate
GLY	glycine
H2O	water
HEK	human embryo kidney
HILIC	hydrophilic interaction liquid chromatography
HIS	histidine
HK	hexokinase
HPLC	high-pressure liquid chromatography
IDV	isotopomer distribution vector
ILE	isoleucine
IMM	isotopomer mapping matrice
IVCC	integral viable cell concentration
LAC	lactate
LB	lower bound
LC-MS	liquid chromatography mass spectrometry
LC-QTOF MS	liquid chromatography quadrupole time-of-flight mass spectrometry
LDH	lactate dehydrogenase

LEU	leucine
LYS	lysine
mAb	monoclonal antibodies
MAL	malate
MET	methionine
MFA	metabolic flux analysis
MID	mass isotopomer distribution
MS	mass spectrometry
NaBu	sodium butyrate
NADP(H)	nicotinamide adenine dinucleotide phosphate (reduced)
NMR	nuclear magnetic resonance
NON-OX-PPP	non-oxidative pentose phosphate pathway
OAA	oxaloacetate
OX-PPP	oxidative pentose phosphate pathway
P5P	pentose 5-phosphate
PBM	population balance model
PC	pyruvate carboxylase
PDC	pyruvate dehydrogenase complex
PHE	phenylalanine

PK	pyruvate kinase
PPP	pentose phosphate pathway
PRO	proline
PTFE	polytetrafluoroethylene
PYR	pyruvate
R5P	ribose 5-phosphate
RNA	ribonucleic acid
RPM	revolutions per minute
Ru5P	ribulose-5-phosphate
S7P	septulose-7-phosphate
SCM	single cell method
SER	serine
SUC	succinate
TC	total carbohydrate
TCA	tricarboxylic acid cycle
Tet	tetracycline
THR	threonine
TMB	3,3′,5,5′-tetramethylbenzidine
TRP	tryptophane

TYR	tyrosine
UB	upper bound
UMP	uridine monophosphate
UPLC-MS/MS	ultra performance liquid chromatography-tandem mass spectrometric
VAL	valine
WSR	weighted squared residuals
WSSR	weighted sum of squared residuals
X5P	xylulose 5-phosphate

CHAPTER 1 INTRODUCTION

1.1 Background

Nowadays, two thirds of top selling biopharmaceutical products are being produced by mammalian cell culture. The fact that these cells have the ability to produce proteins with human-like posttranslational modifications often makes them the most suitable host system. Due to the high and growing demand for biotherapeutics, in particular antibodies, efforts have been made to improve the efficiency of cell culture processes in order to speed up the time-to-market and reduce the development/production costs. Significant advances have been made in the field of cell culture technology over the last decades, with product concentrations now routinely reported in the 5-10 g/L range. These yields have been achieved owing to the development of improved expression vectors, the selection of high producing cell lines, the design of enhanced medium formulations, and through the development of fed-batch and perfusion processes supporting high cell density. Moreover, progresses in cellular engineering have also led to the development of new inducible promoter systems, such as the widely used tetracycline- or ecdysone-based systems (Kaufmann, Mazur, Marone, Bailey, & Fussenegger, 2001; No, Yao, & Evans, 1996), or the recent cumate gene-switch (Mullick et al., 2006). In such expression system, the growth and production phases can be effectively decoupled, in that way allowing to optimize each phase independently. Despite these advances, significant challenges still remain for further improving the efficiency of cell culture processes; the complex behavior of mammalian cells in culture is currently only partially understood because of the multitude of parameters governing cell growth, metabolism and productivity. This lack of knowledge restricts the capacity to identify robust biomarkers of productivity, to rationally develop medium formulation and feeding strategy and to efficiently engineer cells with desired characteristics (Selvarasu et al., 2012). In this context, metabolic engineering approaches are now increasingly being applied to mammalian cell systems. They involve the investigation and modification of biochemical reactions, metabolic networks and metabolic flux control (Boghigian, Seth, Kiss, & Pfeifer, 2010; T. Omasa et al., 2010). Among the various approaches, metabolic flux analysis has become a rational tool to characterize cell physiology by detailed quantification of major intracellular fluxes in the central

carbon metabolism of cells (Wiechert, 2001). However, due to the complexity of mammalian cells, conventional metabolic flux analysis has to rely typically on hardly verified assumptions to estimate intracellular flux distributions. It is now recognized that a more accurate determination of metabolic fluxes in complex biological systems can be performed with the aid of stable isotope labeling experiments and mass spectrometry measurements, a technique called "^{13}C-metabolic flux analysis".

1.2 Thesis hypothesis and objectives

This work tested the main hypothesis that there are some links between the cell metabolism and specific productivity, and that a comprehensive metabolic characterization in relation with environmental variables will allow investigation of these links and offer a huge potential for rational process design. The work was focused on investigating an inducible mammalian expression system, motivated by the facts that (1) inducible systems offer a unique opportunity for controlling the recombinant protein expression level of a single cell line (thereby allowing to highlight metabolic changes related specifically to cellular growth or productivity, and not due to clonal effects) and (2) while inducible mammalian systems are increasingly available, studies assessing the impact of key process conditions on the productivity of induced cell cultures are sparse. Hence, the main goal of the thesis was to quantitatively characterize the primary metabolism of a recombinant CHO cell line harboring an efficient inducible expression system with the aid of isotopic tracers.

The specific objectives were:

1. To develop an experimental and computational framework for acquiring isotopic stationary ^{13}C-labeling data and estimating the main intracellular fluxes in cultivated mammalian cells
2. To assess quantitatively the metabolic load imposed by recombinant protein production in an inducible mammalian expression system by isotopomer analysis
3. To investigate the main factors and process conditions affecting cell growth and productivity during the induction phase with the aid of isotopic tracers
4. To study the impact of various feeding protocols on the growth and productivity of induced cells

1.3 Thesis organization

Chapter 1 provides a general context and background, as well as the main hypothesis and research objectives of the thesis. Chapter 2 presents a literature review of the main strategies used for the enhancement of cell culture productivity, as well as the current challenges hindering process development and the need for improved metabolic characterization to address them. This is followed by a review of the main mathematical approaches to quantify intracellular flux distributions in mammalian cells and a discussion on their main advantages and limitations. The set of experimental and computational methods used during this research project is described in Chapter 3. Chapter 4 was published as a research article entitled "**Probing the metabolism of an inducible expression system**" in the ***Journal of Biotechnology***. In this paper, we quantitatively assess the metabolic load of recombinant protein production on the primary metabolism of CHO cells using an efficient inducible expression system and ^{13}C-metabolic flux analysis. This approach allowed us to obtain reliable estimates for the main intracellular fluxes, including pathways that cannot be observed from external rate measurements (e.g. the pentose phosphate pathway). Chapter 5 presents the second article of this thesis entitled "**The impact of the timing of induction on the metabolism and productivity of CHO cells**" and published in ***Biochemical Engineering Journal***. In this contribution, we have investigated how the induction conductions affect the cells' physiological state and the ensuing process productivity. In Chapter 6, entitled "**Elucidating the effects of post-induction glutamine feeding on the growth and productivity of CHO cells**", we have demonstrated that cell growth and productivity can be greatly enhanced during the induction phase through the application of a fed-batch strategy. The metabolic impact of different feeding regime was also explored with the aid of isotopic tracers. This work was submitted for publication in ***Biotechnology Progress***. Chapter 7 consists in a general discussion of all the work performed in this thesis and, finally, the conclusion and recommendations for future works are presented in Chapter 8.

CHAPTER 2 LITERATURE REVIEW

2.1 Industrial mammalian cell culture

In recent years, mammalian cell culture has become the most important method for the production of secreted products such as recombinant proteins and monoclonal antibodies (Langdom, 2008). The first use of large-scale mammalian cell culture was for vaccine development in the 1950s, while the first modern biotechnology product manufactured using mammalian cells, recombinant insulin, was approved in 1982. Since then, around 100 biopharmaceutical products (including recombinant hormones, growth factors, blood factors, monoclonal antibody based products, interferons, therapeutic enzymes, and recombinant vaccines) have gained approval in US and 60% - 70% of them are produced using mammalian cell culture (Langdom, 2008; Walsh, 2010). The most widely used mammalian cell lines to express recombinant based products are Chinese Hamster Ovary (CHO) cells, mouse myeloma NSO cells, Baby Hamster Kidney (BHK) cells, Human Embryo Kidney (HEK-293) cells, and C127 cells (Langdom, 2008). Even though mammalian cell culture is more complicated, more expensive and time consuming compared to other expression platforms (e.g. microbial, insect or plant cell culture), it is an essential requirement for a wide range of biopharmaceuticals because mammalian cells have the unique ability to perform proper post-translational modifications and secrete bioactive glycoproteins (Langdom, 2008; Li, Vijayasankaran, Shen, Kiss, & Amanullah, 2010).

2.2 Recombinant protein expression by mammalian cells

Although varieties of mammalian cells are available, only some of them are commonly used as host systems for recombinant protein production. The selection of a host system is typically determined by its ability to grow in suspension (preferably in serum-free medium), its genetic stability, its low risk of accidental infection by potentially pathogenic viruses and its capability to deliver a bioactive product at a high production rate. Over the past two decades, Chinese Hamster Ovary (CHO) cells have been extensively used for the industrial production of biopharmaceutical

products, in particular glycoproteins. This expression platform has been enhanced using different strategies including genetic engineering, cellular engineering and metabolic engineering (Datta, Linhardt, & Sharfstein, 2013). CHO cells have become the predominant host used to produce recombinant proteins and are currently involved in the production of 70% of all therapeutic proteins (Jayapal, Wlaschin, Hu, & Yap, 2007).

The establishment of a cell line for manufacturing recombinant protein requires an expression vector construction and an efficient transfection method for either the transient or stable gene expression. Transient gene expression has been increasingly used over the past decade. Technological developments in transient transfection of CHO cells and its current status have been recently reviewed (Geisse & Voedisch, 2012). The main advantage of transient expression systems is the short development time; usually significant amounts of product can be produced within several days. Thus, they have lower development costs compared to stable expression systems and are well suited to fulfill the needs of basic research and preclinical studies (Matasci, Hacker, Baldi, & Wurm, 2008). But due to difficulty in scaling up transient expression into bioreactor systems, stable expression is preferred for the industrial production of larger quantities of protein.

A lot of efforts have also been made to improve the host cells characteristics using various cellular engineering approaches, for instance to achieve better control over product glycosylation (Go et al., 2013; Seth, Hossler, Yee, & Hu, 2006), decreasing programmed cell death by overexpression of anti-apoptotic genes (Elmore, 2007; Mohan, Kim, Koo, & Lee, 2008) or reducing waste accumulation (Jeong et al., 2001; S. H. Kim & Lee, 2007; Lim et al., 2010), just to name a few of the most significant ones. Another interesting avenue of research that is gaining increased interest is focused on the development of inducible mammalian expression systems.

2.2.1 Inducible expression system

The primary advantage of inducible expression systems is the ability to effectively decouple cell growth and product formation, since the recombinant product expression can be biochemically controlled (S.S. Ozturk & Hu, 2005; Rita Costa, Elisa Rodrigues, Henriques, Azeredo, & Oliveira, 2010). This is particularly advantageous in the case where the recombinant product exhibits a certain cytotoxicity for host cells. Initially, expression systems involved inducers having pleiotropic effects on host cells, such as heat shock induction (Brown & Rush, 1990;

Burdon, 1986), heavy-metal induction (Heuchel et al., 1994; Schützendübel & Polle, 2002) or glucocorticoid induction (Aoyama & Chua, 1997; Heuchel et al., 1994). However, owing to the broad range of effects that they produced on the host cells and the typically high levels of basal expression that they exhibit, more efficient inducible promoter expression systems have been developed. The most widely used are based on the tetracycline (tet) (Forster et al., 1999; Gossen & Bujard, 1992), the streptogramin (Fussenegger et al., 2000), the ecdysone (Hoppe, Marban, & Johns, 2000; No et al., 1996) and, more recently, the cumate (Gaillet et al., 2010; Mullick et al., 2006) systems. All these systems consist of a regulatory plasmid and an expression plasmid. The former is used for repressor or trans-activator expression, while the latter includes the regulated promoter linked to the gene product of interest. Its expression is then controlled by the addition (or removal) of an inducer compound to the culture medium, which regulates the activity of the repressor (or activator) (Rita Costa et al., 2010).

From a process development point of view, the use of an inducible expression system is attractive in that it provides the unique flexibility for defining operating conditions that are specific to the growth and production phases respectively (Panda, 2003). Several studies have been conducted dealing with inducible expression in yeasts (Holmes, Darby, Wilks, Smith, & Bill, 2009) and mostly bacterial systems (Choi, Keum, & Lee, 2006; Weuster-Botz, Altenbach-Rehm, & Arnold, 2001). In particular, it has been demonstrated that the process productivity can be dramatically increased by the selection of an appropriate induction time (Huber & Buchs, 2011) and by the implementation of a post-induction feeding strategy (Choi et al., 2006). But unlike for yeast and microbial systems, the literature devoted specifically to the optimization of processes involving mammalian inducible expression systems is still very sparse. Induction protocols are essentially defined by trial-and-error experiments for determining favorable operating conditions in terms of time of induction, concentration of inducer, culture medium, etc. Towards the goal of applying a more rational approach, the following section will review the most common methods/strategies for improving the productivity of mammalian cell cultures.

2.3 Culture strategies for the enhancement of productivity

In a cell culture process, the final product concentration is determined by the cell specific production rate, the biomass concentration and the culture longevity. Changes in any of these

variables will thus affect the required culture volume and production scale for a desired amount of antibody (P. W. Sauer, Burky, Wesson, Sternard, & Qu, 2000). Most of the culture strategies developed to date have been successful at increasing peak cell concentration and/or extending culture longevity, but some have also been found to improve cell-specific productivity. At the process level, significant enhancements were achieved by the development of culture modes allowing to reach high cell densities (i.e. fed-batch and perfusion cultures). Other common process strategies involve environmental perturbations to stimulate cell productivity. These aspects are reviewed in the following sections. Significant enhancements in cell culture performance were also due to improved expression vectors and host cell engineering, but these topics will not be covered here and have been recently reviewed in details by Dietmair *et al*. (Dietmair, Nielsen, & Timmins, 2011).

2.3.1 Cell culture modes

When mammalian cells are grown in batch mode, the maximum cell density and productivity are typically limited by the accumulation of metabolic by-products, mainly lactate and ammonia, or by the depletion of essential nutrients in the culture medium (Xie & Wang, 2006). Such limitation/inhibition can be alleviated, at least in part, using other modes of operation. Fed-batch is by far the most commonly employed culture mode for the industrial production of cell culture-based recombinant proteins. In typical fed-batch cultures, cells are supplied with a concentrated nutrient feed (either intermittently or continuously) without medium removal, thereby avoiding the early depletion of key medium components and allowing to maintain cell growth/viability over prolonged time. The development of an efficient feeding strategy involves a balance between different parameters such as the nature and concentrations of nutrients in the feed solution, the timing of nutrient additions and the rate of feeding (Jain & Kumar, 2008). This is not a trivial task due to the complexity of mammalian cell metabolism and the still limited knowledge about the intracellular regulating factors of product synthesis. The most frequent fed-batch protocols are designed to minimize the accumulation of lactate and ammonia (T. A. Bibila & D. K. Robinson, 1995). Many experimental studies on antibody production by mammalian cells have shown that maintaining low levels of glucose/glutamine can effectively reduce the so-called “overflow metabolism” and the ensuing production of waste metabolites (Helder J. Cruz,

Moreira, & Carrondo, 2000; Kurokawa, Park, Iijima, & Kobayashi, 1994; Jan Ljunggren & Häggström, 1994). However, the successful implementation of such strategy requires an efficient monitoring and control scheme to ensure that the main nutrients are not completely depleted from the culture environment. Moreover, maintaining low substrate concentrations can cause significant and undesired changes on the gene expression for glycosylation and impact the quality of secreted antibodies (Kochanowski et al., 2008; Wong, Wong, Goh, May, & Yap, 2010). Minimizing waste metabolite formation was also accomplished through substitutions of the main carbon sources in culture medium. For example, the simultaneous substitution of glucose by galactose and glutamine by glutamate in fed-batch cultures of CHO cells was shown to reduce significantly the generation of metabolic by-products, although the cell specific growth rate was slightly impaired by those substitutions (Altamirano, Paredes, Cairo, & Godia, 2000; Altamirano, Paredes, Illanes, Cairo, & Godia, 2004). Another rational approach that proved successful for fed-batch cultures involves feeding the cells with stoichiometric amount of concentrated nutrients. Cell requirements were derived from simple mass balance equations and, in the case of hybridoma cells, this led to substantial improvements in terms of cell growth and product yield compared to batch cultures (Liangzhi Xie & Daniel I. C. Wang, 1996).

While the majority of current industrial bioreactors are operated in fed-batch mode, a perfusion process can be more advantageous in some cases, for instance when the product of interest is unstable in the culture environment. In this mode of operation, a constant supply of nutrients and a concomitant removal of culture medium are performed at the same rate, while cells are retained inside the bioreactor through some filtering device placed inside the vessel (e.g. spin filter) or on the outflow (e.g. acoustic separator). The main advantage of the perfusion mode is that the cells are retained in a favorable biochemical environment (high nutrient and low waste concentrations), which allows to reach high cell densities while minimizing the residence time of the product (Dalm et al., 2007; O. Henry, Kamen, & Perrier, 2007). However, in this mode of operation, large volumes of fresh and spent media must be fed/harvested to/from the bioreactor and the product can be significantly diluted. Consequently, the main disadvantages of perfusion systems are the inherent complexity and costs of the production/purification steps (Chon & Zarbis-Papastoitsis, 2011; Mercille, Johnson, Lanthier, Kamen, & Massie, 2000). Nonetheless, viable cell concentrations of 1-5×10^7 cells/ml at 10 volumes/day dilution rate and product titres in

the range of several g/L are typically achieved with current perfusion technology, which is on average an order of magnitude greater than conventional batch processes (Woodside, Bowen, & Piret, 1998), but comparable to the performance of optimized fed-batch cultures.

The chemostat is another type of continuous mode, but without cell retention (Martens, de Gooijer, van der Velden-de Groot, Beuvery, & Tramper, 1993). Its operation is in general difficult and the cell concentrations achieved are very low due to the constant culture dilution. This mode is thus mostly employed in research to conduct metabolic studies of cells under defined steady-state culture conditions (H. P. Bonarius et al., 2001; Miller, Blanch, & Wilke, 1988). The semi-continuous (or repeated-batch) mode is an alternative form of operation, whereby a fraction of the culture volume is removed and replaced by fresh medium on a daily basis. This mode allows to approximate steady-state conditions, while preserving the relative simplicity of batch mode (Olivier Henry, Kwok, & Piret, 2008) and is thus relatively easy to perform at lab scale.

2.3.2 Environmental perturbations affecting cell productivity

Numerous strategies have been found to increase the cell specific productivity, typically by changing the culture environment through the addition of a specific compound (e.g. sodium butyrate, dimethyl sulphate, valproic acid) or by altering the physico-chemical conditions (e.g. mild hypothermia or hyper osmolality). It's interesting to note that most of these environmental perturbations have been associated with changes in metabolic and signalling pathways (O'Callaghan & James, 2008). For example, sodium butyrate addition has been shown in many instances to stimulate the production of recombinant proteins (Hendrick et al., 2001; McMurray-Beaulieu, Hisiger, Durand, Perrier, & Jolicoeur, 2009; Sunley & Butler, 2010). Up to 6 fold increase in antibody specific productivity was reported through the addition of sodium butyrate (Chun, Park, Chung, & Bang, 2003). However, in some cases this compound was also shown to induce cell growth or programmed cell death (F. Chen et al., 2011; Wang et al., 2004) and its use as a productivity enhancer must thus be assessed for each host cell system. It is also largely documented that operating cultures at lower temperature (usually between 30-33°C) during the production phase can have a positive impact on culture productivity, and this effect was observed with several cultivated mammalian cell systems (Fox, Patel, Yap, & Wang, 2004; Kou et al.,

2011; Sunley & Butler, 2010). For example, Yoon *et al*. reported that their CHO cell line exhibited lower specific growth rates (reduction of 30-63%) under mild hypothermic conditions, however, the cell specific productivity was enhanced greatly (4-25 fold) (Yoon, Hwang, & Lee, 2004). Although the mechanisms of the mild hypothermic response are not completely understood, it is believed that cell growth usually arrest in G0/1 phase of the cell cycle, resulting in an extension of viable cell lifetime (O'Callaghan & James, 2008). Hyperosmotic stress also induces cell cycle arrest in G0/1 phase and often lead to increased cell-specific productivity (N. S. Kim & Lee, 2002; M. S. Lee, Kim, Kim, & Lee, 2003; Sun, Zhou, Liang, McNeeley, & Sharfstein, 2004). Some strategies can be used in combination, such as the report on combining osmotic and temperature shifts to achieve increase of interferon production (Han, Koo, & Lee, 2009). It is interesting to point out that reported increases in productivity are often correlated with decreases in the proliferation rate (Dinnis & James, 2005).

2.3.3 Challenges in cell culture process enhancement

Over the last two decades, together with improvements of expression vectors and host cell engineering, optimization of culture media and cultivation processes have led to about a five-fold increase in cell densities, a three-fold enhancement in culture longevity and a 100-fold increase in product concentration (Dietmair et al., 2011). While many of the approaches described previously have shown to be practically effective for increasing product yields, most of these studies also underscore that more comprehensive analysis and mechanistic understanding of cell metabolism is necessary to assess and eventually control rationally how mammalian cells respond to environmental perturbations and process conditions. To this day, bioprocess optimization is often largely based on trial-and-error experiments. This is notably the case when developing fed-batch protocols, since cellular growth and protein expression are two complex metabolic functions, and it is not yet well understood how these two functions and nutritional requirements are related. Further characterization of the underlying limiting metabolic factors is thus needed to allow for the rational development of adapted feeding strategies in fed-batch processes. To maximize final product concentration, it appears that a suitable trade-off must sometimes be found between the levels of gene expression and cell growth (Dinnis & James, 2005). Therefore, elucidating the alterations in central carbon metabolism caused by recombinant protein production is

instrumental for the establishment and optimization of a productive mammalian cell expression platform. This has led to extensive studies on cell metabolism and the development of comprehensive metabolic models, as reviewed in the next section.

2.4 Metabolic characterization of mammalian cells

2.4.1 Theoretical aspects of mathematical approaches

Mathematical approaches have a crucial importance for quantitatively characterizing cell physiology under relevant process conditions. Cell metabolism consists of highly interconnected metabolic pathways that involve thousands of intracellular reactions catalyzed by enzymes. The rates of the intracellular biochemical reactions are defined as the metabolic fluxes. Together with intracellular metabolite pools, metabolic fluxes are considered to represent the minimal information needed for describing cell physiology and metabolism under a set of environmental conditions (G. Stephanopoulos, 1999). Different mathematical modeling methods have been developed for describing cellular functions, either individual function (Single Cell Method, SCM) or the function of overall (Population Balance Model, PBM) cellular processes (Sidoli, Mantlaris, & Asprey, 2004). In traditional metabolic studies, models were formulated based only on extracellular metabolites (such as nutrients and products) and biomass concentration (Sanderson, Phillips, & Barford, 1996). Often, these unstructured models have a narrow range of applicability and fail to predict cellular behaviour under many relevant process conditions (Gombert & Nielsen, 2000). Advances in analytical methods have allowed the development of more structured models. Moreover, the vast increase in computing power and speed made possible to solve large and highly non-linear models.

A mathematical model able to describe the cellular metabolism is a fundamental tool in metabolic engineering. These models can be stoichiometric, whereby a set of algebraic equations is used to describe the intracellular reactions and can be used to simulate metabolic fluxes at steady-state. Kinetic models on the other hand are usually based on rate laws for biochemical reactions and can provide a dynamic description of cell metabolism. Up to now, stoichiometric models have had more widespread applications when dealing with large metabolic networks. While kinetic models can be powerful tools for studying the dynamics of metabolic and biosynthetic pathways (Baughman, Huang, Sharfstein, & Martin, 2010; Ghorbaniaghdam, Henry, & Jolicoeur, 2013),

the typical lack of relevant enzymatic kinetic and intracellular concentration data often constitutes a severe limitation for their development, validation and use. With the stochiometric approach, which is usually simply based on steady-state mass balances, there is no need to consider intracellular metabolite concentrations and kinetic parameters. Various intracellular processes can be specified within stoichiometric models, thereby allowing for example to account for the metabolic requirements and energetic cost for recombinant protein production (Sheikh, Förster, & Nielsen, 2005).

2.4.2 Stoichiometric models and metabolic flux analysis

Because of their relative ease of application, stoichiometric models of metabolic networks are now widely used tools in metabolic engineering (Boghigian et al., 2010). They are at the heart of "metabolic flux analysis", a technique which aims at quantifying the actual rates of intracellular reactions occurring inside a cell. The stoichiometry of a network is defined in a "m" by "n" dimensional matrix, which is called the stoichiometric matrix ("S"). Here, "m" is the number of internal metabolites and "n" is the number of intracellular reactions (fluxes). Each entry in the matrix corresponds to the stoichiometric coefficient of the m^{th} metabolite participating in the n^{th} reaction. Since most metabolites participate in only a small number of reactions, the stoichiometric matrix is typically sparse, meaning that most of the entries are zero (Boghigian et al., 2010).

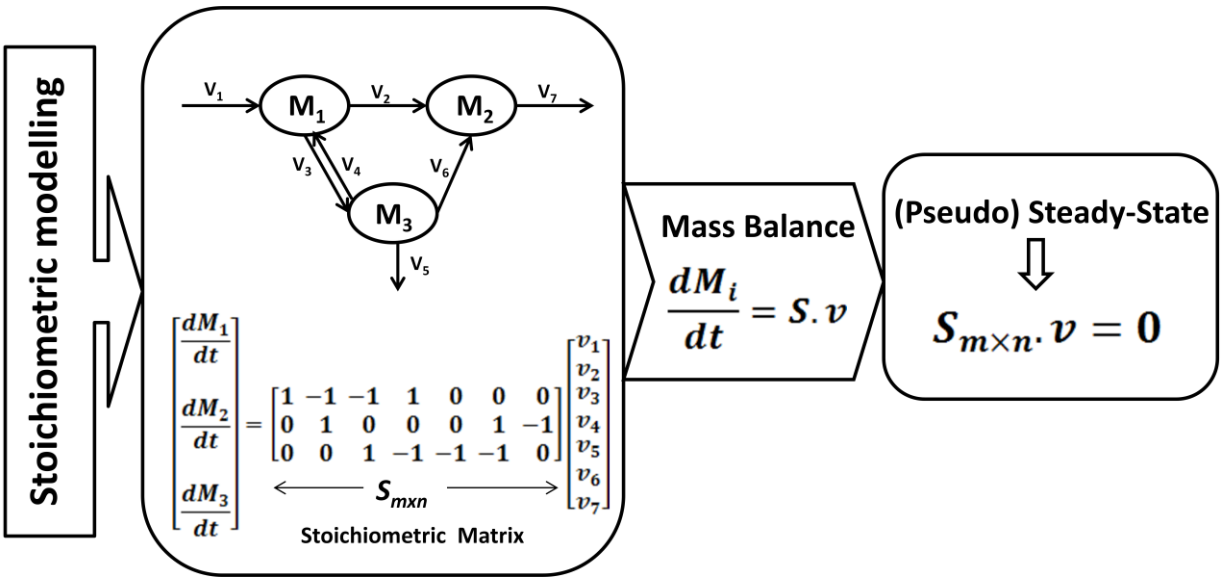

Figure 2-1: Principle of stoichiometric models

Figure 2-1 illustrates this concept for a very simple example network. Studies are mainly carried out under the assumption of metabolic steady-state, which is a prerequisite for stationary metabolic flux analysis and implies that there is no significant accumulation of internal metabolites in the system (G. Stephanopoulos, 1999). Thus, a system of linear equations is obtained in the form:

$S_{m \times n}.V=0$

It should be emphasized that, in practice, true steady state conditions do not need to be reached. In most cases, fluxes are calculated during the exponential growth phase of the cells. During this phase, if a dramatic transient does not occur, the so-called pseudo-steady state assumption has been found to hold reasonably well (Niklas & Heinzle, 2012; Sidorenko, Wahl, Dauner, Genzel, & Reichl, 2008).

Depending on the number of linearly independent metabolite balances (r), given by the rank of matrix S, and the number of reactions (n), three scenarios are possible (K. Lee, Berthiaume, Stephanopoulos, & Yamush, 1999):

1- If r = n, the system is determined. These systems usually have a unique solution and are algebraically and computationally the simplest.
2- If r > n, the system is over-determined. Fluxes can be calculated by a least squares regression. Redundant equations can also be used to validate data and model consistency.

3- If r < n, the system in under-determined with "n-r" degrees of freedom. An infinite number of solutions exist for these systems. Only a subset of fluxes can be directly calculated.

In most biochemical networks, the number of unknown fluxes exceeds the number of independent equations (underdetermined system) (Boghigian et al., 2010). This happens due to the lack of measurements and the presence of parallel metabolic pathways (e.g. the pentose phosphate pathway or the malate shunt), cyclic pathways and bidirectional reaction steps (H.P. Bonarius, Schmid, & Tramper, 1997; Wiechert, 2001). A unique flux distribution cannot be computed in this case, unless additional constraints or model assumptions are considered. Several approaches have been proposed to address this issue. Although some of the fluxes may be calculable, it will result in a limited and incomplete picture of cell metabolism (Klamt & Schuster, 2002). Bonarius et al. (H.P. Bonarius et al., 1997) reviewed several strategies involving theoretical assumptions or constraints that can be used to solve underdetermined network: mass balances of cofactors and co-metabolites (e.g. ATP and NADH), objective functions solved by linear optimization (e.g. minimizing the consumption of ATP) and irreversibility of reactions. However, validation of these assumptions has been repeatedly called into question (Fischer & Sauer, 2005; F. Llaneras & Pico, 2008; Wiechert, 2001).

A better approach is to fully resolve metabolic networks using additional independent data derived from labeling experiments with tracers, as described in the following section.

2.4.3 Metabolic flux analysis with isotopic tracers

The traditional use of isotopic tracer experiments in metabolic studies goes back to 1940-1960s, when such experiments were used for the structural identification of biochemical reactions (U. Sauer, 2006). For decades, this approach involved the use of radioactive tracers (e.g. ^{14}C) and they was intensively used for the evaluation of metabolic fluxes during the 1980s (Blum & Stein, 1982). Since then, radioactive tracers have been replaced for the most part by stable isotopes (e.g. ^{13}C-labeling). Isotopic tracer experiments have become a powerful technique to analyse metabolic networks, owing to advances in nuclear magnetic resonance (NMR) and mass spectrometry (MS) technologies, along with the development of efficient computational

algorithms (Crown & Antoniewicz, 2013). The main differences between radioisotopes and stable isotopes are related to the output of the measurement methods for evaluating the enrichment. For radioisotopes, the results of isotopic enrichment measurement are reported in terms of specific activity (or dpm/mol). Only the total labeling data is available and there is no information regarding the relative amount of labeled or unlabeled molecules in a sample. Thus, only one balance equation may be written for the total radioactivity. In contrast, more experimental data can be derived from stable isotopic experiments (Kelleher, 2001). For example, mass spectrometry measurements can provide the relative amount of each mass isotopomer and a balance equation can thus be written for the fractional abundance of each of them. Accordingly, metabolic flux analysis based on stable isotopic experiments, so called "^{13}C-metabolic flux analysis, can allow to investigate the metabolism on a more global level than radioisotope experiments (Zupke & Stephanopoulos, 1995).

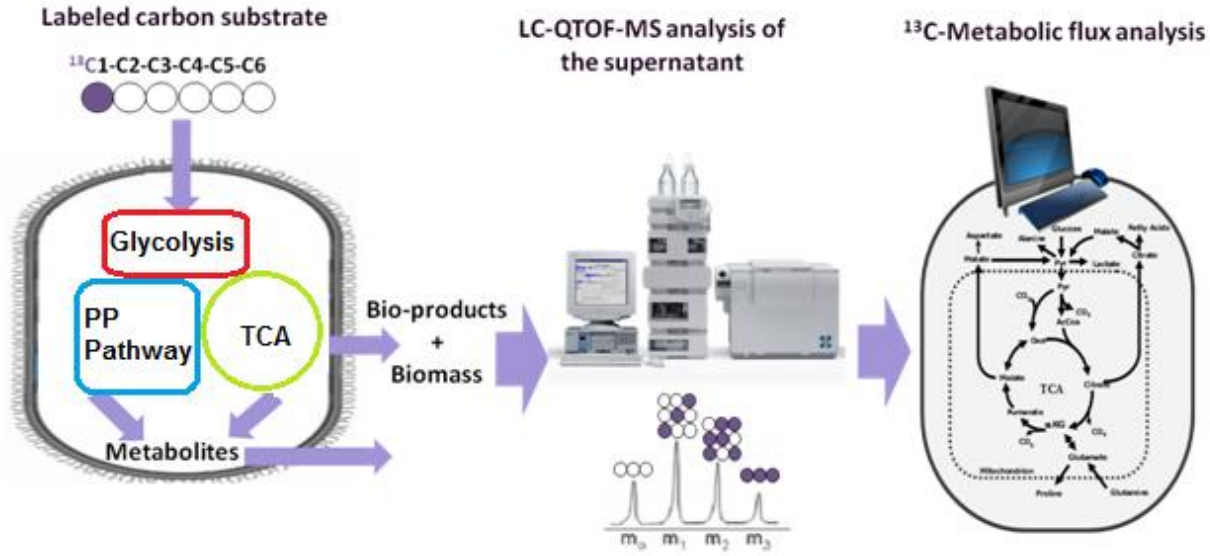

Figure 2-2: Typical procedure for isotopic tracer experiments and flux analysis

With ^{13}C-metabolic flux analysis, additional constraints for intracellular flux estimation can be provided through the use of ^{13}C-labeled substrates and subsequent measurement of isotope integration into intracellular or extracellular metabolite pools. An overview of how labeling experiments are typically performed is depicted in Figure 2-2. In such experiment, cells in culture

are fed with medium containing one or several specifically labeled substrates. Upon being consumed by the cells, the labeled carbon is then distributed throughout the metabolic network. Techniques based on Mass spectrometry (MS) or nuclear magnetic resonance (NMR) spectrometry can then be used to measure the level of isotope enrichment in different metabolites. The resulting enrichment data, in combination with extracellular flux measurements, can be used together with stoichiometric balancing to compute the intracellular fluxes for the system. In principle, this technique enables the quantification of certain metabolic fluxes which cannot be estimated solely from extracellular rate measurements and mass balancing. This is notably the case for parallel pathways, cyclic and reversible pathways. However, these pathways can be observed with isotopic tracers since they will give rise to distinct isotopomer distribution patterns (an isotopomer is a metabolite with a specific ^{13}C-labeling pattern) (Christensen & Nielsen, 2000b). Since the method is based on carbon balancing, flux estimation does not rely on energy and/or redox balance assumptions. The energy and redox balances can however be assessed from the resulting flux distribution obtained via 13C-MFA (Quek, Wittmann, Nielsen, & Kromer, 2009; Wittmann, 2002).

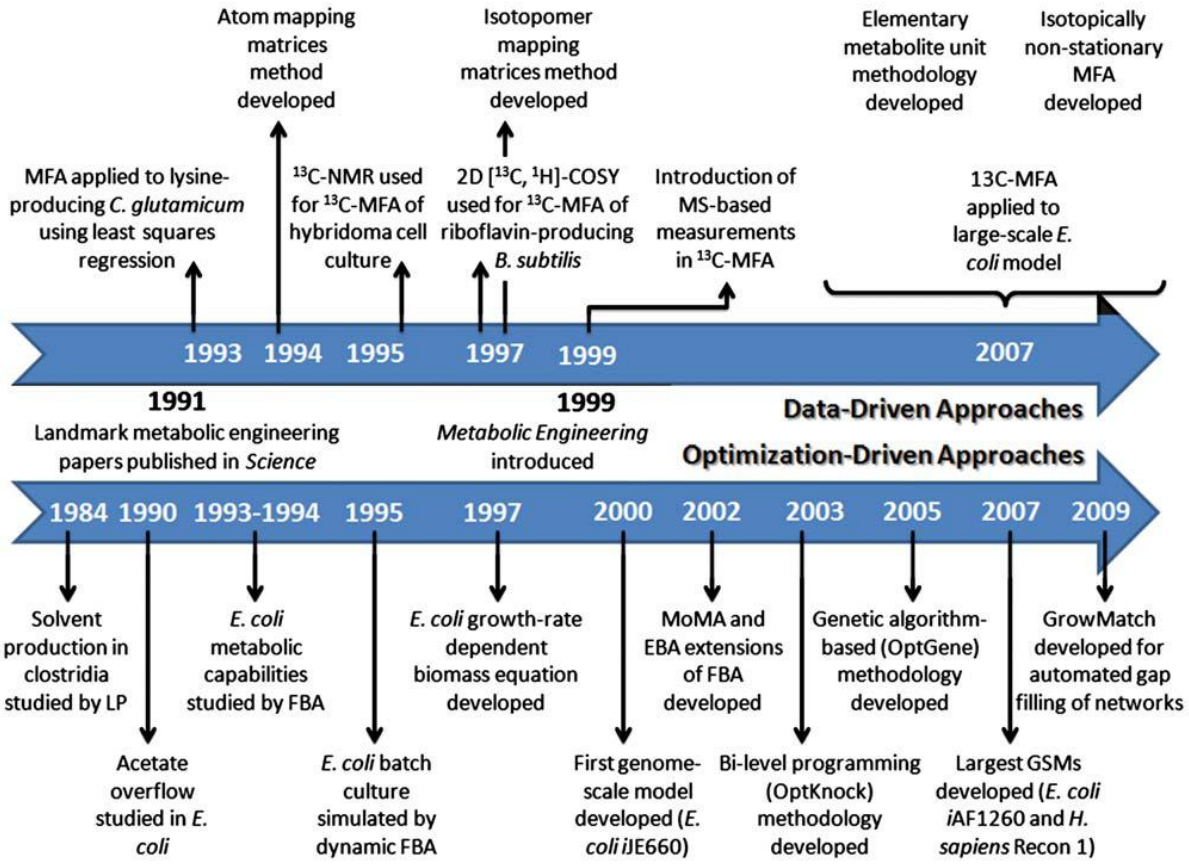

Figure 2-3: Major technical and computational advances in the development of ^{13}C-MFA. Figure taken from (Boghigian et al., 2010).

Until recently, ^{13}C-metabolic flux analysis has been predominantly used to estimate intracellular fluxes in the central carbon metabolism of microorganisms such as bacteria (Al Zaid Siddiquee, Arauzo-Bravo, & Shimizu, 2004; Schaub, Mauch, & Reuss, 2007; Schmidt, Nielsen, & Villadsen, 1999) and yeasts (Costenoble et al., 2007; Kleijn et al., 2007; W. A. van Winden et al., 2005). Labeling experiments are facilitated from the fact that these organisms can grow in defined medium containing a single carbon source. These studies were conducted during both steady-state and pseudo-steady-state conditions by simultaneous metabolite and isotopomer balancing.

Because ^{13}C-MFA offers a huge potential for rational process design, it has recently found increasing applications in metabolic studies of mammalian cells. However, one of the major challenge for the application of this method to mammalian cells lies in the relative complexity of

the culture media, which contain multiple carbon sources (e.g. glucose, amino acids, lipids). As a result, the 13C-labeled tracer can be significantly diluted due to the presence of unlabeled carbon sources, making the determination of reliable enrichment data difficult. Nonetheless, in the last decade, several isotopic tracer studies were conducted to obtain flux distributions in many relevant mammalian cell lines, such as Hybridoma cells (H. P. Bonarius et al., 1996; H. P. Bonarius et al., 2001; H. P. Bonarius, Timmerarends, de Gooijer, & Tramper, 1998; Paredes, Sanfeliu, Cardenas, Cairó, & Gòdia, 1998; Zupke & Stephanopoulos, 1995), Chinese Hamster Ovary cells (CHO) (Woo Suk Ahn & Antoniewicz, 2011; Deshpande, Yang, & Heinzle, 2009; C. Goudar et al., 2010; Mohan et al., 2008; Sengupta, Rose, & Morgan, 2011; Zamorano, Vande Wouwer, & Bastin, 2009; Zamorano, Wouwer, & Bastin, 2010), hepatic cells (Hofmann et al., 2008; Maier, Hofmann, Reuss, & Mauch, 2008) and Human Embryonic Kidney 293 cells (HEK 293) (Olivier Henry & Durocher, 2011; Olivier Henry, Jolicoeur, & Kamen, 2010). The experimental and computational aspects associated with ^{13}C-metabolic flux analysis when applied in the context of mammalian cell cultures are reviewed in the following sections.

2.5 Technical aspects of ^{13}C-metabolic flux analysis

2.5.1 Labeling experiments

Several studies were focused on improving isotope labeling strategies/protocols to allow for a reliable estimation of intracellular fluxes. Typically, ^{13}C-labeled substrates are fed to the cells until the labeled carbon is distributed throughout the metabolic network. Then, the ^{13}C labeling patterns of certain metabolites are measured using modern analytical techniques such as high-resolution NMR spectroscopy (C. Goudar et al., 2010; P. G. Henry et al., 2006; Mancuso, Sharfstein, Tucker, Clark, & Blanch, 1994; Shen et al., 1999; Simpson & Constantinidis, 2007; W. van Winden, Schipper, Verheijen, & Heijnen, 2001; Zupke & Stephanopoulos, 1995) or mass spectrometry (MS) (Maciek R Antoniewicz, Joanne K Kelleher, & Gregory Stephanopoulos, 2007; H. P. Bonarius et al., 2001; Olivier Henry et al., 2010; Rühl et al., 2012; Wittmann, 2007). The design of labeling experiments is a crucial step in ^{13}C-MFA in order to estimate the fluxes of interest with good confidence. Flux identifiability and accuracy depend on 1) the metabolic network structure 2) the specific labeled substrate(s) used and 3) the nature and number of

available labeling measurements. The first step is usually to select an appropriate labeled substrate (e.g. 100 % U-^{13}C-glucose) or a mixture of specifically labeled substrates (e.g. 50 % 1-^{13}C and 50 % U-^{13}C glucose). Studies have proposed different approaches to guide the selection of an optimal tracer or combination of tracers (Crown, Ahn, & Antoniewicz, 2012; Libourel, Gehan, & Shachar-Hill, 2007; Metallo, Walther, & Stephanopoulos, 2009). Depending on whether a whole metabolic profile or specific fluxes are targeted, some tracers will be more suited than others. ^{13}C-labeled glucose and glutamine are the most common tracers used for ^{13}C-MFA of mammalian cells, as they are usually the two main carbon sources in culture medium. Through simulations of a representative mammalian cell network, it was for example demonstrated that the TCA cycle fluxes can be well estimated using uniformly labeled glutamine, whereas 1,2-^{13}C glucose can provide precise estimates for the pentose phosphate pathway (Metallo et al., 2009). However, these results were obtained for a given flux distribution, which is a priori unknown when conducting an isotopic tracer study, and for a given set of available measurements. Without prior knowledge, proper tracer selection has to be done through an iterative process based on the quality and quantity of measurements available.

Typically, not all the fluxes in a network can be reliably estimated with a single experiment (P.F. Suthers et al., 2007). Thus, depending on the metabolic pathway structure, different labeling experiments will be best appropriate (Niklas & Heinzle, 2012). An isotopic labeling experiment can be performed in a single culture (using a single tracer or a mixture of tracers), but can also be performed in multiple parallel cultures, each having specifically labeled substrates. Provided that each culture can be maintained in a similar physiological state, the data extracted from all the parallel cultures can then be combined to infer a single representative metabolic flux distribution. Henry *et al.* used four parallel experiments using three glucose tracers (1-, 6- and U-^{13}C glucose) and one glutamine tracer (U-^{13}C glutamine) and by analyzing only the resulting mass isotopomer distributions of extracellular lactate, they managed to elucidate and quantify all the main intracellular fluxes of HEK-293 cells (Olivier Henry et al., 2010). Recently, the technical and theoretical advantages of parallel labeling experiments have been reviewed by Crown and Antoniewicz (Crown & Antoniewicz, 2013).

2.5.2 Metabolic model construction

The mammalian cell metabolism consists of thousands of known enzyme-catalyzed reactions. However, setting up of fully mechanistic models to describe cellular metabolism is usually not practical and most models employed in metabolic investigations are based on several simplifications (e.g. lumping of reactions). In a first step, a metabolic network should be constructed by adding piece by piece relevant biochemical reactions based on information derived from the literature. Many metabolic models have been proposed for the primary metabolism of several mammalian cells. As an example, a metabolic network of the central carbon metabolism of CHO cells is presented in Figure 2-4. This model has been constructed from both classical biochemistry text books and previously published stochiometric models (Altamirano et al., 2001; C. Goudar et al., 2010; Quek, Dietmair, Krömer, & Nielsen, 2010; Zamorano et al., 2010). In general, metabolic models of mammalian cells consider the following pathways:

Glycolysis and lactate production (reactions 1-6)

Glycolysis involves several enzyme-catalyzed reactions that convert glucose to pyruvate and usually constitutes a major source of energy for cultivated mammalian cells due to the high glucose uptake rate. Because of the large decline of net free energy, this is essentially an irreversible pathway. The overall reaction of glycolysis is:

$$Glucose + 2NAD^{+} + 2ADP + 2P_i \rightarrow 2Pyruvate + 2NADH + 2H^{+} + 2ATP$$

So the aerobic glycolysis generates 2 mol of ATP and 2 mol of NADH per mol of glucose consumed. Then, in the respiratory chain, NADH will release energy in the form of ATP.

Pentose-phosphate pathway (reactions 7-10)

This pathway contains an oxidative branch (reaction 7) and a non-oxidative branch (reaction 8-10). The oxidative branch of pentose phosphate pathway (ox-PPP) is mainly responsible for producing the building blocks for nucleotides synthesis. This pathway also generates cytosolic NADPH in mammalian cells, through converting glucose-6-phosphate to ribulose-5-phosphate. Besides, the non-oxidative pentose phosphate pathway (non-ox-PPP) links the pentose phosphate pathway to glycolysis through the reactions from xylulose-5-phosphate (X5P) to

glyceraldehydes-3-phosphate (GAP) and fructose-6-phosphate (F6P). In fact, non-ox-PPP consists of a series of many reversible reactions (transaldolase and transketolase reactions) which operate near equilibrium. The split between ox-PPP and non-ox-PPP part cannot be determined from extracellular rate measurements alone. In conventional metabolic flux analysis studies, it is usually assumed that the PPP flux will exactly meet the requirements for nucleotides synthesis (Niklas & Heinzle, 2012), that is, the transaldolase and transketolase activity is ignored and only ox-PPP is considered (Martens, 2007). However, it is possible to quantify fluxes through the PPP with ^{13}C-tracers and such questionable assumption is therefore not required.

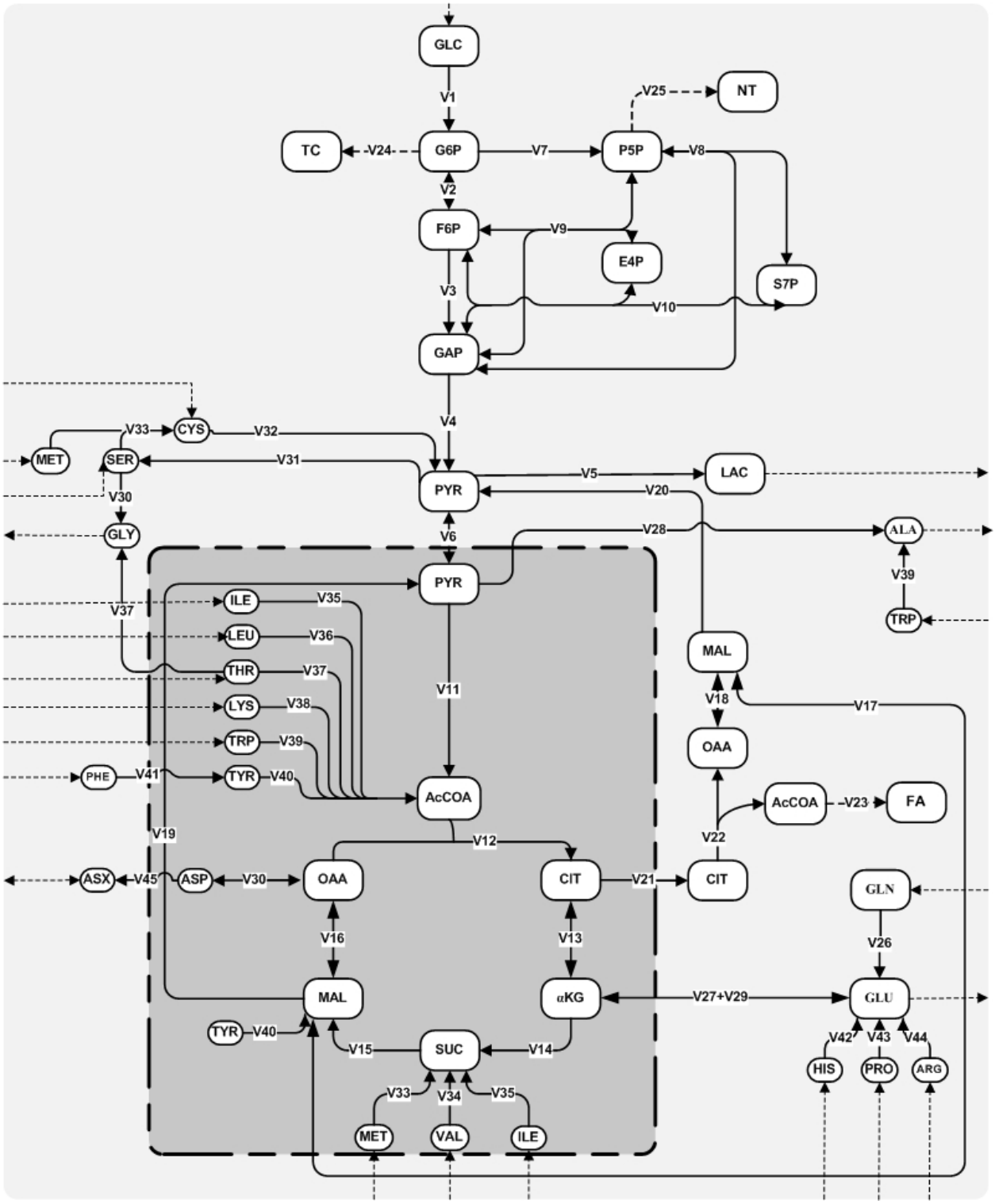

Figure 2-4: a schematic metabolic network model for the central carbon metabolism of CHO cells

Tricarboxylic acid (TCA) cycle (reactions 11-16)

Pyruvate produced during glycolysis is transported into mitochondria and is then converted into acetyl-CoA. The pyruvate dehydrogenase complex (PDC) catalyzes the irreversible conversion of pyruvate to acetyl-CoA and CO_2 (reaction 11). PDC is actually a complex of three distinct enzymes: pyruvate dehydrogenase, dihydrolipoly transacetylase, and dihydrolipoly dehydrogenase. Acetyl-CoA then enters the TCA cycle, which is a major source of energy for cells. The net reaction of TCA cycle is:

$$\text{Acetyl CoA} + 3\,\text{NAD}^+ + \text{FAD} + \text{GDP} + \text{P}_\text{i} + 2\text{H}_2\text{O} \rightarrow 2\text{CO}_2 + 3\text{NADH} + \text{FADH}_2 + \text{GTP} + 2\text{H}^+ + \text{CoA}$$

In fact, only one ATP is produced per cycle, but the large formation of ATP happens in the respiratory chain where the NADH and $FADH_2$ are oxidized in the electron-transport chain Besides ATP generation, TCA cycle also supplies intermediates required for the synthesis of biomass (e.g. citrate for lipid synthesis).

Amino acid metabolism (reactions 26-45)

Essential amino acids cannot be synthesized in mammalian cells and they must be supplied in the culture medium. Therefore, their catabolism is important to consider in metabolic studies. Mammalian cells can synthesize non-essential amino acids that can be involved in both anabolic and catabolic pathways. Among all amino acids, glutamine is usually the most consumed.

2.5.3 Flux estimation from labeling measurements

Metabolic fluxes are calculated from measured labelling data according to the general procedure outlined in Figure 2-5. Whereas conventional MFA involves mass balance equations for each metabolite in a system, ^{13}C-MFA relies on simultaneous metabolite and isotopomer balances and involve consequently a large number of equations. Moreover, labeling data are nonlinear functions of the fluxes making the approach even more complex. As a result, there have been several studies devoted to the development of systematic procedures and computational

algorithms to efficiently estimate flux distribution from labeling data obtained via NMR or mass spectrometry.

One of the first such modeling contributions was proposed by Zupke and Stephanopoulos (Zupke & Stephanopoulos, 1994) who introduced the elegant concept of "Atom Mapping Matrices" (AMMs), which can be used to compute ^{13}C enrichments of metabolites from a known flux distribution and a given input labeled substrate. In their method, for each enzymatic reaction, an AMM is constructed to track the transfer of carbon atoms from reactants to products. The first application of this general approach was carried out to characterize the metabolism of Hybridoma cells with *in vivo* ^{13}C NMR data (Zupke & Stephanopoulos, 1995). The first extensive labeling data set comprising more than 25 ^{1}H NMR measurements was generated and analyzed by Marx *et al.* (Marx, de Graaf, Wiechert, Eggeling, & Sahm, 1996). subsequent studies performed by Wiechert *et al.* (Wiechert & de Graaf, 1997; Wiechert, Siefke, de Graaf, & Marx, 1997) presented detailed treatment of flux estimation with improved measurements obtained from ^{1}H NMR experiments and they also discussed the statistical analysis of the resulting estimates. Follstad and Stephanopoulos (Follstad & Stephanopoulos, 1998) were able to analyze the effects of reversible reactions on the distribution of ^{13}C carbons using the AMM technique.

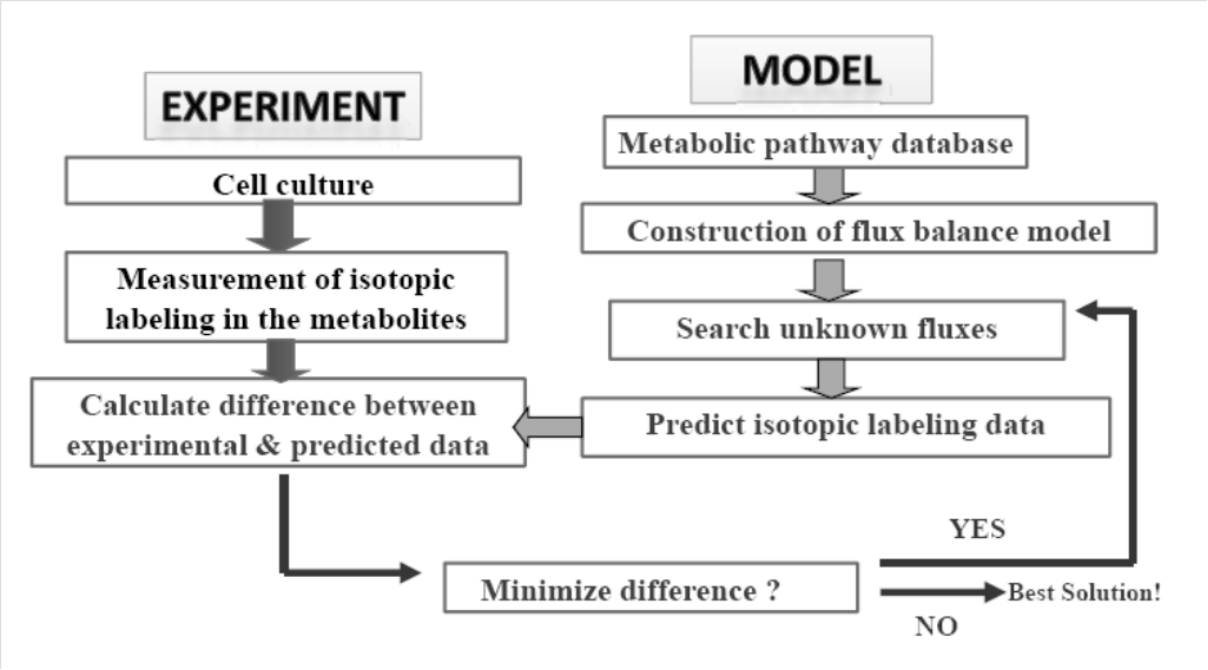

Figure 2-5: General procedure for ^{13}C-based metabolic flux analysis

Around the same time, the concept of isotopomer balancing was gaining increasing recognition in the field. A metabolite with "n" carbon atoms will have "$2^{n"}$ isotopomers. While the formerly ^{1}H NMR-based experiments only allowed the measurement of "n" enrichments per metabolite molecule, the measurement of isotopomers, through wisely planned ^{13}C NMR experiments, could provide up to 2^n measurements per molecule, therefore enormously increasing the amount of raw data to estimate intracellular fluxes. Schmidt e*t al.* (Schmidt, Carlsen, Nielsen, & Villadsen, 1997) extended the concept of AMMs to "Isotopomer Mapping Matrices" (IMMs) and developed a SIMULINK module that could automatically generate isotopomer balances. With the use of IMMs, it is possible to formulate efficiently all isotopomer mass balances for each metabolite by means of "Isotopomer Distribution Vectors" (IDVs) and to calculate the fraction of each metabolite present in a specific isotope form. Isotopomer analysis is inherently much more complicated. As an illustrative example, considering two metabolites A and B with "n" and "m" number of carbons respectively (A is a substrate and B is a product), the size of IMM (A→B) is $2^m \times 2^n$ while the size of the AMM(A→B) is m×n. Klapa *et al*. (Klapa, Park, Sinskey, & Stephanopoulos, 1999) illustrated the technique of isotopomer enumeration and balancing,

wherein only physically detectable isotopomers were balanced. This technique is advantageous in experiments using specifically labelled substrates (e.g. 1-^{13}C glucose or 2-^{13}C pyruvate) present in large percentages (90% and above), so that the natural abundance of ^{13}C becomes negligible in the analysis. They applied this technique to analyze the TCA cycle in mammalian cells and developed the analytical formulas that can be used to evaluate fluxes from NMR data. With this approach, they were able to detect the presence or absence of glyoxylate shunt activity. A subsequent study discussed practical application of this work when applied to E. *coli* and labeling data gathered from mammals (S. M. Park, Klapa, Sinskey, & Stephanopoulos, 1999). The IMM approach was also used in conjunction with GC-MS data for studying the central carbon metabolism of *Penicillium* by Christensen and Nielsen (Christensen & Nielsen, 2000a).

Although it could provide useful results, the IMM approach is cumbersome and isotopomer balances must be solved with an iterative scheme. To cope with these limitations, the cumomer (cumulative isotopomer) concept was soon after introduced by Wiechert *et al*. (Wiechert, Mollney, Isermann, Wurzel, & de Graaf, 1999). Compared to the isotopomer balancing approach, the main advantage of this method is that intracellular fluxes are calculated by solving in cascade a set of linear equations. Thus, the concept of cumomer provides a much more efficient way to estimate fluxes, compared to the earlier iterative method which was computationally expensive, particularly for systems involving near-equilibrium reversible reactions. In a sequel paper, Mollney *et al.* (Mollney, Wiechert, Kownatzki, & de Graaf, 1999) analyzed the identifiability of the fluxes and detailed the procedures for the optimal design of carbon labeling experiments, taking into account various errors that arise in the raw labeling data. These procedures were incorporated into a carbon labeling evaluation software released in 2001 (Wiechert, 2001). Petersen *et al.* (Petersen et al., 2000) used this software and were able to successfully demonstrate a significant futile cycle in *Corynebacterium glutamicum*.

The "Elementary Metabolite Unit" (EMU) is a recent model framework that was also developed to improve the efficiency of flux estimation (M.R. Antoniewicz, J.K. Kelleher, & G. Stephanopoulos, 2007). This approach consists in a powerful decomposition algorithm that only retains the relevant carbon transitions for the available measured mass distribution data. The functional units (or EMUs) resulting from the decomposition form the basis for describing the links between metabolic fluxes and labeling data. Since it is not required to simulate all possible isotopomers with the EMU framework, it yields a significant reduction in computational time for

flux determination and also for the evaluation of the associated confidence intervals (P. F. Suthers, Chang, & Maranas, 2010).

2.5.4 Stationary and instationary ^{13}C-MFA

^{13}C-MFA can also be categorized into stationary and non-stationary approaches. In the stationary case, experiments must be designed in such a way that both isotopic and metabolic steady-states are achieved prior to sampling for mass spectrometry analysis. With cultivated mammalians cells under balanced-growth, it was shown that such conditions are attained within several hours (usually 4 to 6h) after tracer addition in the culture medium, but the dynamics of labeling can vary among different metabolites.

Wiechert and his co-workers proposed an instationary (or transient) metabolic flux analysis, whereby the labeling time-courses of metabolites are considered for flux estimation (Noh et al., 2007; Noh, Wahl, & Wiechert, 2006; Noh & Wiechert, 2006; Wiechert & Noh, 2005). The non-stationary method requires to perform repeated sampling over time, whereas the stationary method only requires a single measurement performed under metabolic and isotopic steady-states (Morgan & Rhodes, 2002). Since the intracellular pools are typically very small, it is expected that equilibration is reached relatively fast and consequently the experiments can be very short. Moreover, the amount of costly labelled substrate can be reduced with this approach and, if enough experimental labeling data are available, instationary analysis also allows the estimation of intracellular pool sizes. But, as expected, the experimental, computational and mathematical difficulties for the transient case are much greater than for the steady-state case (Noh et al., 2007). Recently, Noh *et al.* successfully applied instationary ^{13}C-MFA for the analysis of *E. coli* cultures and discussed various aspects related to the experimental design (sampling intervals, feed label composition), the sensitivity analysis and the computational methods for the transient case (Noh et al., 2007; Noh et al., 2006; Noh & Wiechert, 2006). Hofmann and Maier demonstrated the application of this approach to study the metabolism of hepatic cells (Hofmann et al., 2008; Maier et al., 2008). They described an experimental set up to quantify the extra- and intracellular metabolite concentrations and also detailed methods allowing the measurements of mass isotopomer fractions by GC-MS and LC-MS. However, they did not consider the metabolism of all amino acids in their analysis. More recently, Ahn and Antonirewicz have reviewed the novel techniques available for dynamic metabolic flux analysis and outlined the

challenges that still need to be solved in the case of mammalian cells (W. S. Ahn & Antoniewicz, 2012), which are essentially the slow labeling dynamics and the compartmentalization of cell metabolism.

2.6 Application of metabolic flux analysis in CHO cell cultures

As mentioned previously, among all mammalian cells, Chinese Hamster Ovary (CHO) cells are the most popular host system for the industrial production of recombinant proteins. It is thus not surprising that they have received a lot of attention and have been the subject of many comprehensive metabolic studies. This section provides a review of the main studies in which classical MFA and ^{13}C-MFA were employed for CHO cell characterization and process improvements.

2.6.1 Metabolic flux analysis of CHO cells

In the past two decades, metabolic flux analysis has become an established tool and the primary approach to study in details mammalian cell metabolism. One of the first effort to perform such comprehensive characterization of CHO cells metabolism was carried out by Nyberg *et al.* (Nyberg, Balcarcel, Follstad, Stephanopoulos, & Wang, 1999). They employed metabolic flux analysis to validate the consistency of extracellular measurements and found that, with complex hydrolysate-containing media, the contribution of amino acids originating from the peptides is significant and must be taken into account when analysing the cell needs. They also investigated the relationship between cell metabolism and glycosylation site occupancy heterogeneity in different glucose and glutamine limited steady-state cultures (Nyberg, Balcarcel, Follstad, Stephanopoulos, & Wang, 2000). They found that glycosylation correlated with TCA cycle activity, but not with glycolysis. A similar study was performed recently and also revealed possible links between protein glycosylation and the primary metabolism of CHO cells (Burleigh et al., 2011).

MFA studies were also conducted with the goal of helping the rational design of enhanced medium formulations. In particular, the identification of suitable substrates that can generate less

lactate and ammonia was investigated by several groups. Altamirano *et al.* have characterized by MFA the effects of substituting glutamine by glutamate and found that glutamate-based medium promoted a more efficient utilization of glucose and nitrogen sources (Altamirano et al., 2001). Several experimental observations confirmed that lactate can be re-metabolized by CHO cells (Luo et al., 2012; Tsao et al., 2005; Zagari, Jordan, Stettler, Broly, & Wurm, 2013). To better understand the factors which can cause the metabolic shift to lactate consumption, comparative metabolic flux analysis were performed in culture media containing different combinations of glucose and galactose (Altamirano, Illanes, Becerra, Cairo, & Godia, 2006; Wilkens, Altamirano, & Gerdtzen, 2011). These studies suggested that the metabolic shift happens when an insufficient amount of pyruvate is produced to support energy requirements properly. Comparative flux balance analysis performed before and after the metabolic switch revealed that lactate consuming cells exhibit an energy efficiency that is much greater than lactate producing cells (Martinez et al., 2013). Along the same line, results derived from MFA also revealed that AKT1 signaling, which is a major mechanism in regulation of cellular metabolism according to cells growth needs, plays a key role in facilitating the metabolic shift to lactate consumption (Mulukutla, Gramer, & Hu, 2012). In a recent study, Xing *et al*. (Xing et al., 2011) also demonstrated the application of MFA to support the optimization of medium and feed solution compositions. They first identified the limiting amino acids and those that were in excess by flux balance analysis, and this allowed them to define balanced amino acid compositions to be used for the fed-batch cultivation of CHO cells. The quasi real time application of metabolic flux analysis was also discussed (C. Goudar et al., 2006), opening up the possibility to use this technique as a powerful monitoring tool for industrial cell cultures.

Other studies were concerned with computational aspects of classical metabolic flux analysis. Llaneras and Picó (Francisco Llaneras, Pic, amp, & Jes, 2007) and Zamorano *et al.* (Zamorano et al., 2009) introduced a detailed extension of MFA to determine intervals for non-calculable fluxes in an underdetermined network of CHO cells. Using a detailed metabolic network of more than 100 reactions, Zamorano et al. (Zamorano et al., 2010) demonstrated that for a well-posed system, the size of flux intervals can be significantly reduced by the addition of more extracellular measurements, except in the case of parallel pathways. Besides, Goudar et al. proposed a method to determine error propagation from extracellular measurements into the

estimated fluxes for high cell density CHO cell perfusion culture (Chetan T. Goudar, Biener, Konstantinov, & Piret, 2009).

2.6.2 ^{13}C-Metabolic flux analysis of CHO cells

Due to the inherent limitations of classical MFA, in particular the inability of this approach for estimating certain key intracellular fluxes, recent and emerging studies are now increasingly focused on the application of ^{13}C metabolic flux analysis for refining CHO cell characterization. Using a mixture of isotopic tracers (10% U-^{13}C glucose, 40% 1-^{13}C glucose and the remaining 50% unlabeled glucose) and 2D (^{13}C,^{1}H) COSY NMR analysis allowed to characterize the physiological state of CHO cells in high cell density perfusion cultures (C. Goudar et al., 2010). This study demonstrated a relatively good agreement between glycolytic and TCA flux estimates derived using respectively MFA and ^{13}C-MFA. However, the pentose phosphate pathway and anaplerotic fluxes could only be estimated with the aid of isotopic tracers. Ahn and Antoniewicz performed comparative studies of CHO cell metabolism during the exponential and stationary phases (Woo Suk Ahn & Antoniewicz, 2011, 2013). These studies highlighted a significant flux rewiring in the transition from exponential growth to the stationary phase. The latter was characterized by a reduced glycolytic activity, a switch to lactate consumption and an increase in the oxidative pentose phosphate pathway flux. More importantly, they demonstrated the invalidity of some assumptions frequently employed in classical MFA, that is the non-negligible activity of oxidative PPP and pyruvate carboxylase fluxes in CHO cells. Another group also worked on characterizing the metabolism of CHO cell during non-growth phase, where most of antibody production usually takes place (Sengupta et al., 2011). They observed marked differences compared to flux distributions determined during the growth phase, mostly in terms of the portion of glucose oxidized through PPP and also in the fluxes around pyruvate node. By performing ^{13}C-MFA at various stages of a fed-batch cultures, it was recently reported that cell growth is correlated with high glycolytic fluxes, whereas high antibody production seems associated with a high oxidative state (Templeton, Dean, Reddy, & Young, 2013).

Although ^{13}C-MFA has yielded valuable insights into the cellular metabolism, this technique can still be considered in its infancy when applied to mammalian cell cultures. But because it provides more reliable estimates of intracellular fluxes, it can be considered one of the most useful tool to support the analysis and rational optimization of cell culture processes.

CHAPTER 3 METHODOLOGY

3.1 Cell line and culture conditions

All experiments were performed using the recombinant CHO cell line, CHO-CUM2, which was kindly provided by Viropro International 120 Inc. (Montreal, Canada). This cell line stably expresses the reverse cumate transactivator described in (Mullick et al., 2006) and produces a human anti-CD20 monoclonal antibody. These cells were also adapted to serum-free suspension culture. Seed cultures were grown in a serum- and protein-free chemically defined medium HyClone SFM4CHO (Thermo Scientific, UT). The medium was supplemented with 30mM of glucose and 5mM of glutamine. T25 flasks (Corning, USA) were used to maintain cells at 37C in humid atmosphere of 5% CO_2. The cultures were diluted 2 or 3 times per week to keep the cells in their exponential phase of growth. After two months of maintenance, new vials of frozen cells were thawed.

For the experiments, the cultures were initially seeded at 0.2-0.5 × 10^6 cells/ml into shake flasks of 125 ml. 1 μg/mL cumate was added to each flask to trigger the protein expression and, if required, the temperature was shifted to sub-physiological temperature (30-32°C) for the duration of the production phase. Supernatants were collected by centrifugation at 300 g for 5 min and samples were stored at -80^{0}C for subsequent analysis.

3.2 Analytical methods

3.2.1 Determination of cell density and viability

Cell numbers and viability were determined by mixing the cell suspension with Trypan blue (sigma) and counted on a hemacytometer. 25µl of Trypan blue 0.4% was added to 100µl of cell sample. A small volume of the prepared mixture was dispensed onto a hemacytometer. Total number of unstained and stained cells were counted under an inverted microscope (10× objective).

The cell concentration in the sample was obtained by:

$$[cells/ml] = \sum(4 \text{ counts}) \times 3125 \times \text{dilution factor}$$

And cell viability was given by:

$$Viability\ (\%) = \frac{Live\ cells}{Live\ cells\ +\ Dead\ cells} \times 100$$

3.2.2 Analysis glucose, lactate and glutamine concentrations

The glucose, glutamine, and lactate concentrations in supernatants were measured using a dual-channel immobilized oxidase enzyme biochemistry analyzer (2700 SELECT, YSI Inc. Life Sciences, Yellow Springs, OH, USA), using calibration buffers provided by the manufacturer.

3.2.3 Analysis of amino acids using LC/MS

Extracellular amino acid concentrations were determined on an Agilent 1290HPLC system (Agilent technologies, Quebec, Canada) coupled to an Agilent 6460 triple quadruple mass spectrometer (Agilent technologies, Quebec, Canada). The underivatized amino acids were separated by a 2.1x150mm ZICTM-Hilic column (3.5um, 200A, PEEK) (Merck SeQuant) and 2.1x20mm ZICTM-Hilic guard column (5um, 200A, PEEK) (Merck SeQuant) at a temperature of 35^{o}C and at an injection volume of 5uL. The mobile phase buffer contained 20mM $HCOONH_4$

at pH 4. The mobile phase A was 10% of the mobile phase buffer in water, and the mobile phase B was 10% of the mobile phase buffer in ACN. The mobile phase B linearly decreased from 90% to 35% in 19 min, then was increased to 90% in one min and hold at 90% for 15 min at a flow rate of 0.1ml/min.

3.2.4 Analysis of ^{13}C-labeling patterns

The ^{13}C fractional enrichment of lactate and amino acids in the samples was measured on an Agilent 1100 series LC-MSTOF (Agilent technologies, Quebec, Canada). First, 200µL of supernatant samples were deproteinized by adding 1mL cold acetone (-20°C) and then were vortexed strongly. After centrifugation at 20,000g for 5 min, the solutions were filtered and evaporated in vacuo. After that, 400 µL of water was added to the samples. The analysis was done in negative electrospray mode without derivatization using a Kinetex HILIC Phenomenex column, 100 x 4.6mm and 2.6um particle size. The eluants used were 5mM ammonium formate (in water) and acetonitrile containing 0.1% formic acid. The gradient was in HILIC mode and went from 90% to 50% ACN with a total run time of 20 minutes.

Organic acids were analyzed on a UPLC-MS/MS (Agilent, Quebec, Canada) equipped with a 1290 infinity binary pump, an autosampler, a column controller and a 6460A triple quad mass spectrometer. 20uL of supernatant sample were filtered through a 0.22 µm PTFE filter (Millipore, Ontario, Canada) before injection. Organic acids were separated on a Hypercarb column (100*2.1 mm, 5 µm) and a Hypercarb pre-column (2.1*10, 5 µm) (Thermo Fisher, Ontario, Canada) with mobile phase A: 20mM ammonium acetate at pH 7.5, and mobile phase B: 10 % (v/v) methanol in water at a flow rate of 0.3 mL/min. The mobile phase gradient was: 10% A from 0 to 5 min, linear gradient from 10 to 20% A from 5 to 10 min, linear gradient from 20 to 100% A from 10 to 20 min, 100% A from 20 to 30 min, linear gradient from 100 to 10% A from 30 to 32 min and, finally, 10% A from 32 to 40 min. The negative electrospray ionization model was selected for the analysis with an Agilent Jet Stream source. The mass spectrometer operation conditions were set as follows: gas temperature 300°C, gas flow rate 7L/min, nebulizer pressure 40 psi, sheath gas temperature 300°C, sheath gas flow 12L/min and capillary voltage -3.5kv.

3.2.5 Quantification of Monoclonal antibody

Monoclonal antibody titer was measured by enzyme-linked immunosorbent assay (ELISA). First, a goat anti-human IgG1 (H+L) solution (Jackson ImmunoResearch) diluted to 2.5 µg/ml in 50mM sodium carbonate (Fischer Scientific) was added to 96-well plates (Costar) and incubated at 4°C overnight. Then, blocking non-specific sites was carried out by adding PBS solution containing 1% casein. After incubation for 1h at 37°C, either samples or standards diluted in PBS-casein were added in triplicate and incubated for 1h at 37°C. The wells were then incubated with 1/10,000 diluted peroxidase-conjugated affinipure fragment Goat anti-human IgG (Jackson ImmunoResearch) for 1h at 37°C. After each of the previous steps, the wells were washed three times (PBS with 1% w/v Tween 20). Finally, the reaction was revealed by 3,3′,5,5′-Tetramethylbenzidine (TMB) (Sigma) and stopped after 10-15 minutes by adding 1N hydrochloric acid. The absorbance at 450 nm was measured using a Victor^3 V microplate reader (Perkin-Elmer).

Cell specific productivities were determined from ELISA data by using the slopes when the integral viable cell concentration (IVCC) in 10^6cells-day/mL was plotted against the antibody concentration (mg/L). The IVCC was calculated using the following equation (P. W. Sauer et al., 2000):

$$IVCC = IVCC_0 + \int_{t_1}^{t_n} Cdt \cong IVCC_0 + \sum_{i=1}^{n} (\frac{C_i - C_{i-1}}{2})(t_i - t_{i-1})$$

Where, t_i and C_i are time (day) and viable cell concentration (10^6cells/mL) at point i, respectively.

3.3 Calculation of specific nutrition uptake rates and specific metabolite production rates

The following logistic equations were used to fit the viable cell density, nutrient and product concentration profiles in batch cultures (Olivier Henry et al., 2008). All parameters in the

equations are non-negative. The cell specific rates are then easily calculated as these equations are analytically differentiable (Chetan T Goudar, Joeris, Konstantinov, & Piret, 2005).

For viable cell density:

$$X(t) = \frac{x_1}{e^{x_2 t} + x_3 e^{-x_4 t}}$$

For nutrient concentration profiles:

$$S(t) = \frac{s_1}{e^{s_2 t} + s_3} + s_4$$

For lactate production:

$$P(t) = \frac{p_1}{e^{p_2 t} + p_3 e^{-p_4 t}}$$

For fed-batch cultures, cell specific rates were derived from the following balance equations:

$$\frac{d[X]}{dt} = \mu X - \frac{F}{V} X$$

$$\frac{d[S]}{dt} = -q_S X + \frac{F}{V}(S_{in} - S)$$

$$\frac{d[LAC]}{dt} = q_{LAC} X - \frac{F}{V} P$$

where F is the feed rate, V is the culture volume and q_i denotes the specific uptake/production rates.

Since glutamine spontaneously degrades to form ammonia, the glutamine decomposition rate constant (k) has been evaluated under the experimental conditions used in this work, without cells. Then, the actual glutamine specific uptake rate was determined using:

$$\frac{d[Gln]}{dt} = -k[Gln] - q_{GLn} X + \frac{F}{V}([Gln_{in}] - [Gln])$$

3.4 Calculation of biosynthetic rates

For the purpose of studying central carbon metabolism, the biomass composition of proteins, DNA, RNA, lipids and carbohydrates is needed for the flux analysis. For CHO cells, biomass compositions can be found in the literature. The drain of metabolites for biomass synthesis was collected from previous reports (Table 3-1) (Martens, 2007; Sheikh et al., 2005). The average biomass composition was assumed to be 74.2% protein, 1.6% DNA, 6.1% RNA, 10.1% lipids and 5.04% carbohydrates, based on published data (Quek et al., 2010; Sheikh et al., 2005). the average molecular weight of biomass was calculated to be 135 g/mol and a dry cell weight was assumed to be 350 pg/cell for CHO cells (Woo Suk Ahn & Antoniewicz, 2011; Altamirano et al., 2001). The average amino acid composition of biomass protein is shown in Table 3-2. In our metabolic model, individual fluxes of biomass were lumped into a general biomass reaction.

Table 3-1: Average biomass composition

Metabolite	mmol/gDW	Metabolite	mmol/gDW
dAMP	0.0148	Cholesterol	0.0182
dCMP	0.0099	Phosphatidylcholine	0.0695
dGMP	0.0099	Phosphatidylethanolamine	0.0263
dTMP	0.0148	Phosphatidylinositol	0.0095
AMP	0.033	Phosphatidylserine	0.0026
CMP	0.0551	Phosphatidylglycerol	0.0013
GMP	0.0624	Diphosphatidylglycerol	0.0028
UMP	0.033	Sphingomyelin	0.0084
glycogen	0.28	Amino acids	in Table 2

For different compounds of biomass, we have the following equation:

$$\frac{dX_{comp}}{dt} = r_x - \mu X_{comp}$$

where X is the mass fraction of a component on a dry basis. As it was shown that there is little heterogeneity in composition among different CHO cell lines (Selvarasu et al., 2012), we

assumed insignificant potential variations of cellular composition. So, the biosynthetic rates were obtained by the macromolecular composition of cells and from the growth rate.

Amino acid requirements for MAb biosynthesis were predicted based on published average IgG1 composition (Quek et al., 2010) (Table3-2). The molecular weight of IgG1 was calculated to be 126 kg/mol.

Table 3-2 : Amino acid (AA) composition of biomass and IgG1

AA	Biomass (mmol AA/g cell)	MAb (mol AA/mol MAB)
Gln	0.322	0.03999
PRo	0.313	0.07173
Val	0.416	0.08568
Leu	0.564	0.06296
Lys	0.570	0.06084
Met	0.138	0.01277
Thr	0.386	0.10560
Ile	0.324	0.03293
His	0.143	0.02293
Arg	0.377	0.02261
Phe	0.219	0.04153
Tyr	0.182	0.02875
Cys	0.145	0.02517
Ser	0.430	0.01064
Glu	0.386	0.05181
Ala	0.600	0.05847
Gly	0.538	0.06601
ASP	0.359	0.03654
TRP	0.044	0.02240
ASN	0.288	0.04487

3.5 Calculation of intracellular fluxes

We have developed Matlab-based algorithms to perform steady-state ^{13}C-MFA using mass isotopomer distribution data. As illustrated in Figure 3-1, the program consists of three parts. The first part automatically generates the metabolite and isotopomer balance models from a text-file containing the list of biochemical reactions and the corresponding carbon transitions. The code is an implementation of the elementary metabolite unit network decomposition method (M.R. Antoniewicz et al., 2007). This method allows to retain the minimum information required to simulate the available labeling data within a metabolic network based on the atom transitions of all the biochemical reactions. Typically, the decomposition will reduced the number of equations by at least one order of magnitude.

Figure 3-1 : Workflow of the algorithm

In the second part, a constrained nonlinear least-squares regression (Figure 3-2) is performed using the built-in Matlab function fmincon to minimize the sum of weighted squared residuals (WSR) between measured (x_i^{meas}) and simulated variables (x_i^{sim}):

$$\min_{[\text{free fluxes}]}(WSR = \sum_{i=1}^{n}[(x_i^{sim} - x_i^{meas})^T . cov_i^{-1} . \left(x_i^{sim} - x_i^{meas}\right) \ ])$$

cov_i^{-1} is the inverse of covariance matrix, and "i" is the number of parallel experiments. The minimization is repeated a minimum of ten times with random (but feasible) initial estimates of the free fluxes (the dimension of the free flux vector equals the degrees of freedom in the system) to ensure the attainment of a global optimal solution.

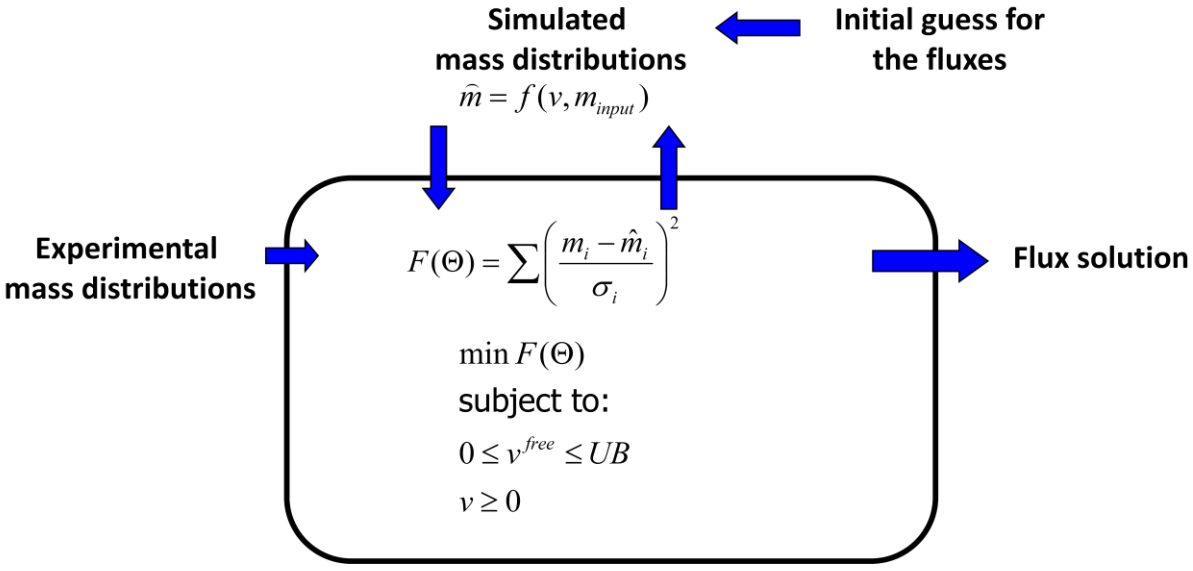

Figure 3-2: Algorithm for intracellular flux estimation based on weighted least-squares parameter estimation

Finally, nonlinear confidence intervals for the flux were determined based on the sensitivity of the WSR to flux variations using the method developed by Antoniewicz et al. (Antoniewicz, Kelleher, & Stephanopoulos, 2006). Although more computationally intensive, this approach was shown to yield a more accurate estimate of flux uncertainty compared to local estimates of the standard deviations.

3.6 Statistical evaluation of the fit

Since obtaining a set of fluxes that minimizes the difference between measured and simulated data does not guarantee that the model is adequate, validation of the fit was performed based on a chi-square goodness-of-fit test. The minimized variance-weighted sum of squared residuals (WSR) is assumed to follow a chi-square distribution with the number of degrees of freedom defined as the difference between the number of independent measurements and the number of unknown free fluxes. The resulting WSR must be between $\chi^2_{\alpha/2}(df)$ and $\chi^2_{1-\alpha/2}(df)$. Outside this range, there is either a lack of fit or over fitting. Individual residuals were also verified to be linearly distributed using a normal probability plot (using the function normplot in Matlab).

CHAPTER 4 PROBING THE METABOLISM OF AN INDUCIBLE MAMMALIAN EXPRESSION SYSTEM USING EXTRACELLULAR ISOTOPOMER ANALYSIS

4.1 Presentation of the article

This section contains an article entitled "***Probing the metabolism of an inducible mammalian expression system using extracellular isotopomer analysis***". This work has been published in "**Journal of Biotechnology**" on April 2013 (Volume 164, Issue 4, Pages 469–478). In this manuscript, we quantitatively assess the metabolic load of recombinant protein production on the primary metabolism of CHO cells using an efficient inducible expression system. A comparative ^{13}C-metabolic flux analysis was conducted, whereby cells were grown in parallel semi-continuous cultures containing various labeled glucose and glutamine tracers. This approach allowed us to obtain reliable estimates for the main intracellular fluxes, including pathways that cannot be observed from external rate measurements (e.g. the pentose phosphate pathway). To the best of our knowledge, this is the first time that a comprehensive isotopic tracer study is conducted to evaluate the impact exerted by heterologous protein expression in mammalian cells. Our analysis also provides the first detailed metabolic flux map for CHO cells under mild hypothermic conditions.

4.2 Probing the metabolism of an inducible mammalian expression system using extracellular isotopomer analysis

Zahra Sheikoleslami[1], Mario Jolicoeur[1], Olivier Henry[*]

[1]Département de Génie Chimique, École Polytechnique de Montréal,

C.P. 6079, Succ. Centre-ville, Montréal, Québec, Canada, H3C 3A7

(Published in Journal of Biotechnology, http://dx.doi.org/10.1016/j.jbiotec.2013.01.025)

*Correspondence to:

Olivier Henry

Chemical Engineering Department

École Polytechnique de Montréal

C.P. 6079, Succ. Centre-ville,

Montréal, Québec, Canada, H3C 3A7

Tel: 1-514-340-4711 (2191)

Fax: 1-514-340-4159

Email: olivier.henry@polymtl.ca

4.2.1 Abstract

In an effort to quantitatively assess the impact of recombinant protein expression on the primary metabolism of mammalian cells in culture, we have employed an efficient inducible expression system and conducted a comparative study of the intracellular flux map distribution with and without the induction of recombinant protein synthesis. Cells were grown in parallel semi-continuous cultures with various singly and uniformly labelled substrates and the resulting mass isotopomer distributions of lactate and extracellular amino acids were measured by mass spectrometry. These distributions were used to quantify the main intracellular fluxes. The analysis revealed that, under mild hypothermic conditions, the onset of protein expression is correlated with small but significant changes in several key pathways related to ATP and NADPH formation. More specifically, we observed that induced cells exhibit a more efficient utilization of glucose, characterized by an increased flux of pyruvate into the TCA cycle. In contrast, the catabolic rates of most amino acids remained relatively unaffected. Such analysis is instrumental to guide the identification of robust biomarkers of productivity, as well as the development of medium formulations optimized for recombinant protein production.

Keywords: CHO cells, inducible expression, ^{13}C-metabolic flux analysis, recombinant protein

4.2.2 Introduction

Mammalian cells continue to be the preferred expression system for the production of valuable therapeutic proteins and vaccines, which require specific post-translational modifications that cannot be performed in other microorganisms. Monoclonal antibodies (MAb) produced by mammalian cell culture form the most important group of new biopharmaceuticals approved or under development and their market is expected to grow significantly in the next few years (Walsh, 2010). In order to meet the growing demand for MAb, there is a continuing need to develop robust, cost-effective and efficient cell culture processes. Conventional process development for mammalian cell culture MAb platforms has been conducted mainly by experimental and especially trial-and-error methods (Baughman et al., 2010). Despite significant advances in the field of cell culture technology, the establishment of an optimal set of process conditions remains mostly cell line-specific. Typically, improvements in product titers have been essentially achieved through an increase of the cumulative integrated viable cell density, but factors limiting the cell specific productivity of mammalian cells are still poorly understood (Meleady et al., 2011). Efforts to further enhance processes have thus rapidly underscored the need for better characterization and control of the complex mammalian cell metabolism in culture. In particular, compared to parental cells, recombinant cells typically exhibit reduced specific growth rates and increased nutrient utilization (Yallop, Nørby, Jensen, Reinbach, & Svendsen, 2003). Assessing and analysing the impact of recombinant protein expression on the cells' central metabolism is thus of utmost importance for the establishment and optimization of a productive mammalian cell expression platform.

To this end, quantification of metabolic fluxes can provide critical insights into the fundamental processes of biological systems and allow the identification of possible metabolic bottlenecks (Boghigian et al., 2010; Metallo et al., 2009; J. H. Park, Lee, Kim, & Kim, 2008). In turn, such information has proven to be invaluable to enable the targeted optimization of cell culture processes. Many comprehensive metabolic models have now been developed for the most relevant industrial cell lines such as CHO, BHK, HEK-293 and hybridoma cells (Niklas & Heinzle, 2012). However, a complete and accurate determination of the flux distribution in mammalian cell networks is generally impossible to obtain from routine measurements and

simple metabolite balancing, due to the typically large number of biochemical reactions involved on the one hand, and the existence of reversible, cyclic and parallel pathways on the other hand. To cope with this problem and alleviate the need to resort to questionable assumptions or constraints, additional independent information can be derived with the use of isotopic tracers. ^{13}C-metabolic flux analysis (^{13}C-MFA) has recently been increasingly applied to mammalian systems in order to obtain a more detailed and accurate description of cellular physiology. The technique is based on culturing cells with specific ^{13}C-labeled substrates and subsequently measuring the label distribution in the network's metabolites using either mass spectroscopy (Woo Suk Ahn & Antoniewicz, 2011; H. P. Bonarius et al., 2001; Hofmann et al., 2008; Metallo et al., 2009; Niklas, Sandig, & Heinzle, 2011; Sengupta et al., 2011) or NMR analysis (H. P. Bonarius et al., 2001; C. Goudar et al., 2010; Mancuso, Sharfstein, Fernandez, Clark, & Blanch, 1998). However, these approaches are experimentally challenging; they typically require the reliable and accurate determination of the mass distributions of several free intracellular metabolites, which necessitates careful and labor-intensive extraction/analysis procedures. Moreover, to ensure the achievement of proper metabolic and isotopic steady-states, such experiments are preferably carried out in a chemostat, which requires the setup of a complex culture system. Recent studies emphasized that adequate (pseudo-)steady conditions may be difficult to achieve in typical batch/fed-batch cultures (Deshpande et al., 2009). While transient isotopic studies can be performed (Woo Suk Ahn & Antoniewicz, 2011; Maier et al., 2008; J.D. Young, Walther, Antoniewicz, Yoo, & Stephanopoulos, 2007), they are even more experimentally/computationally demanding since, in addition to mass isotopomer distributions, the intracellular pool concentrations must either be accurately measured or estimated along with the unknown fluxes.

In the current contribution, we demonstrate that reliable estimates can be obtained for several key intracellular fluxes using an approach that alleviates the need for a complex chemostat setup and the difficulties inherent in the extraction/analysis of intracellular metabolites. Cells were grown in parallel semi-continuous cultures containing various labeled glucose and glutamine tracers and only the resulting mass isotopomer distributions of extracellular metabolites (three excreted amino acids and lactate) were measured by LC-QTOF MS. The semi-continuous (or repeated batch) mode provides a simple and flexible operation with good approximation of

(pseudo)steady-state conditions (Olivier Henry et al., 2008). This method was used to analyze the central carbon metabolism of a mammalian cell line in relation with cellular productivity. To this end, we have employed a CHO cell line that has been engineered with an inducible expression system called the "cumate gene-switch" (Gaillet et al., 2007; Mullick et al., 2006). These cells are capable of robust growth in serum-free and protein-free suspension cultures and, upon addition of a non-toxic small molecule (cumate) in the culture medium, they start to express a recombinant antibody. Comparing the metabolism of the induced and non-induced cells using ^{13}C-MFA allowed investigating the effect of the onset of protein expression on the primary metabolism of the cells. Confidence intervals for the evaluated fluxes were calculated to properly judge the significance of the observed similarities/differences. Such analysis is invaluable for the rational development of improved cell culture processes on both the metabolic and process scales (Boghigian et al., 2010).

4.2.3 Materials and methods

4.2.3.1 Cell lines, medium and culture conditions

The study was performed using an industrially relevant recombinant CHO cell line provided by Viropro International Inc. (Montreal, Canada) and producing a human anti-CD20 monoclonal antibody. The cell line was derived from CHO-Cum2 cells, which stably express the reverse cumate transactivator described in Mullick et al. (Mullick et al., 2006). Cells were grown in a costumed chemically-defined SFM4CHO medium (Hyclone). Prior to culturing the cells, the medium was supplemented with 4mM glutamine (Hyclone), 25mM glucose (Sigma), and 0.05mg/ml dextran sulphate (Mw: 500000, Amersham Pharmacia Biotech). ^{13}C labelling experiments were conducted by growing the cells in parallel shake-flask cultures containing respectively unlabeled, 1-^{13}C, 6-^{13}C, U-$^{13}C_6$ glucose (Cambridge Isotopes, all at 99 % purity) and U-$^{13}C_5$ glutamine (Cambridge Isotopes, 97-99 % purity). This selection of tracers was motivated by their great impact on the identifiability and accuracy of intracellular flux estimates (Metallo et al., 2009). To ensure that all cells were in a similar physiological state, they were initially seeded at 0.5×10^6 cells/ml into a single Erlenmeyer flask at 37°C in humid atmosphere of 5% CO_2. Following an incubation period of 48 hours, this culture was distributed into 10 shake-flasks with a working volume of 10 mL. 1 µg/mL cumate was added to half of the flasks to trigger protein expression, while the remaining flasks were kept as controls (non-induced cells). Induced and non-induced cells were thus each cultured with unlabeled and labeled substrates. It should also be emphasized that cumate was shown to have no noticeable effect on mammalian cells growth and morphology at concentrations up to 200 µg/mL (Mullick et al., 2006). Since mildly hypothermic conditions were previously shown to improve protein production (Gaillet et al., 2010), the temperature was shifted to 32°C at the time of induction. The cultures were run in semi-continuous mode, whereby a fixed culture volume (approximately 25% to 35%) was replaced by fresh medium on a daily basis so as to maintain pseudo-constant cell and nutrient concentrations. Upon reaching pseudo-steady conditions and prior to tracer addition, cells were centrifuged so as to minimize the dilution effect caused by the accumulation of unlabeled extracellular metabolites. Cells were resuspended using the specific label-containing media and feeding was resumed for a minimum of three days to ensure the achievement of an isotopic pseudo-steady state. The control

cultures containing naturally labeled substrates were handled similarly, that is the cell centrifugation step and the temperature shift were also performed.

4.2.3.2 Analytical methods

Cell numbers and viability were determined by mixing the cell suspension with trypan blue (sigma) and counting on a hemocytometer. The culture samples were centrifuged at 300 x g for 5min to separate cells and the supernatant. The supernatant was frozen at -20°C for subsequent analysis. The glucose, glutamine, and lactate concentrations in supernatants were measured with a YSI 2700 biochemistry analyzer (Yellow Springs, OH). Monoclonal antibody concentration was quantified using an enzyme-linked immunosorbent assay. First, a goat anti-human IgG1 (H+L) solution (Jackson ImmunoResearch) diluted to 2.5 µg/ml in 50mM sodium carbonate (Fischer Scientific) was added to 96-well plates (Costar) and incubated at 4°C overnight. Then, blocking non-specific sites was carried out by adding PBS solution containing 1% casein. After incubation for 1h at 37°C, either samples or standards diluted in PBS-casein were added in triplicate and incubated for 1h at 37°C. The wells were then incubated with 1/10,000 diluted peroxidise-conjugated affinipure fragment Goat anti-human IgG (Jackson ImmunoResearch) for 1h at 37°C. After each of the previous steps, the wells were washed three times (PBS with 1% w/v Tween 20). Finally, the reaction was revealed by 3,3′,5,5′-Tetramethylbenzidine (TMB) (Sigma) and stopped after 15-20 minutes by adding 1N hydrochloric acid. The absorbance at 450 nm was measured using a Victor^3 V microplate reader (Perkin-Elmer).

^{13}C fractional enrichment of lactate, alanine, glutamate and aspartate in the samples was measured on an Agilent 1100 series LC-MSTOF (Agilent technologies, Quebec, Canada). The analysis was done in negative electrospray mode without derivatization using a Kinetex HILIC Phenomenex column, 100 x 4.6mm and 2.6um particle size. The eluants used were 5mM ammonium formate (in water) and acetonitrile containing 0.1% formic acid. The gradient was in HILIC mode and went from 90% to 50% ACN with a total run time of 20 minutes. The analysis of amino acid concentrations was performed on an Agilent 1290HPLC system (Agilent technologies, Quebec, Canada) coupled to an Agilent 6460 triple quadruple mass spectrometer

(Agilent technologies, Quebec, Canada). The underivatized amino acids were separated by a 2.1x150mm ZICTM-Hilic column (3.5um, 200A, PEEK) (Merck SeQuant) and 2.1x20mm ZICTM-Hilic guard column (5um, 200A, PEEK) (Merck SeQuant) at column temperature of 35^{o}C and injection volume of 5uL. The mobile phase buffer contained 20mM $HCOONH_4$ at pH 4. The mobile phase A was 10% of the mobile phase buffer in water, and the mobile phase B was 10% of the mobile phase buffer in ACN. The mobile phase B linearly decreased from 90% to 35% in 19min, then was increased to 90% in one min and hold at 90% for 15min at a flow rate of 0.1ml/min.

4.2.3.3 Metabolic Network and intracellular flux calculation

The metabolic model employed in this study was developed through an iterative process based on previous reports on mammalian cells (Woo Suk Ahn & Antoniewicz, 2011; C. Goudar et al., 2010; Olivier Henry et al., 2010; Martens, 2007) and the information derived from the labelling experiments. The metabolic network consists of 68 biochemical reactions, including glycolysis, the pentose phosphate pathway, the Krebs Cycle, the catabolism of 20 amino acids and anaplerotic reactions (Table A). The model is also taking into account compartmentation between mitochondria and the cytosol. To account for biosynthetic requirements, the model includes simplified reactions for the biomass and antibody synthesis, which were established from published average biomass/product composition data (R. P. Nolan & Lee, 2012; Quek et al., 2010) and assuming a dry cell weight of 350 pg/cell for CHO cells (Woo Suk Ahn & Antoniewicz, 2011; Altamirano et al., 2001). As it was shown that there is little heterogeneity in composition among different CHO cell lines (Selvarasu et al., 2012), any potential variations of cellular composition are not expected to be significant. Biosynthetic rates were thus determined based on this average composition and the average molecular weights of its constituents, as well as the measured cell specific growth rates (George Stephanopoulos, Aristidou, & Nielsen, 1998). A constant cell size was assumed in all experiments, since the semi-continuous mode of operation allowed to maintain the cells under balanced exponential growth conditions (Sadettin S Ozturk & Palsson, 1991; Quek et al., 2010). Crude estimates using a hemacytometer yielded average cell diameters of 13.8±1.8 and 14.4±1.9 μm for non-induced and induced cells, respectively. Ribose-5-phosphate, Ribulose 5-phosphate, and Xylulose 5-phosphate were

combined into one single pool (P5P) and, assuming near equilibrium conditions, fructose-6-phosphate and fructose-1,6-biphosphate were also lumped together. All reversible reactions considered in the network were separated into forward and backward fluxes and were constrained to be non-negative. For the transport of metabolites between compartments, it is assumed that citrate is co-transported with malate via the citrate/malate shuttle, pyruvate transport occurs via the pyruvate carrier, malate is transported via the dicarboxylate carrier and aspartate is transferred via the glutamate/aspartate shuttle. Cofactor balances were not included in the model. Furthermore, it was assumed that all carbon dioxide reincorporated into the system was unlabeled, since cultures were grown under humid air containing 5% unlabeled CO_2 and since the medium also contained unlabeled bicarbonate as a buffer. Succinate and fumarate were combined into a single pool and the scrambling of ^{13}C-labels was taken into account. The incorporation of unlabeled carbon into the TCA resulting from the oxidation of fatty acids was considered negligible.

Cell specific nutrient uptake and metabolite production rates were calculated from concentration measurements by taking into account the daily medium exchange rate, as described in Henry et al.(Olivier Henry et al., 2008). The glutamine uptake rate was corrected to account for the spontaneous degradation of this substrate, assuming first order hydrolysis kinetics ($k=0.048\ d^{-1}$). To calculate the intracellular fluxes from measured consumption/production rates and the mass distribution data, we employed the elementary metabolite unit network decomposition method (Maciek R Antoniewicz et al., 2007; Quek et al., 2009; P. F. Suthers et al., 2010), based on the carbon transitions listed in Table A (Appendix). For each of the two conditions under investigation (induced and non-induced cells), we determined the set of intracellular fluxes minimizing the weighted sum of squared residuals (WSSR) between the vectors of simulated and experimental values:

$$\min_{\text{free fluxes}}\left(WSSR=\sum\nolimits_{1}^{n}\left[\left(x_i^{sim}-x_i^{meas}\right)^T \operatorname{cov}_i^{-1}\left(x_i^{sim}-x_i^{meas}\right)\right]\right)$$

where cov_i^{-1} is the inverse of the covariance matrix and n is the number of cultures performed with distinct isotopic tracers. Algorithms for generating metabolite/isotopomer balances, flux estimation and statistical evaluations of the fit were implemented in the Matlab environment. The

nonlinear least-squares regression was performed using the fmincon() function for constrained optimization. The minimization was repeated ten times with random initial estimates of free fluxes to ensure the attainment of a global optimal. Validation of the fit was performed based on a standard chi-square goodness-of-fit test and 95 % confidence intervals for the intracellular fluxes were evaluated using the method outlined in Antoniewicz et al. (Antoniewicz et al., 2006). For statistical comparison between corresponding fluxes of two groups (induced and non-induced cultures), unpaired two-tailed Student's t-tests were performed.

4.2.4 Results

4.2.4.1 Kinetics of growth and substrate utilization

Cells were grown in semi-continuous mode to meet the requirements for metabolic and isotopic pseudo-steady states. The time profiles of viable cell concentrations for the cultures performed with and without cumate addition are shown in Figure 4-1A. For each case, the data presented are the average and standard deviation from five parallel cultures. The apparent growth rates for the non-induced and the induced cultures were determined to be 0.36 (d^{-1}) and 0.33 (d^{-1}), respectively. To allow reliable intracellular flux estimation, all the parallel cultures performed with distinct labelled substrates had to be maintained in a similar physiological state. In order to check the similarity between the five cultures of each series and to assess whether metabolic pseudo-steady state conditions were attained, the main specific consumption and production rates were compared at 48h and 72h following tracer addition. These cell specific rates were evaluated from the measured concentrations, the medium exchange rate and the known fresh medium composition as described in Henry et al. (2008). As evident from the standard deviations shown in Figure 4-1B, good consistency among the parallel cultures within each set was observed. Moreover, the specific rates evaluated respectively at 48 and 72h showed no significant time-dependent variation in cellular growth and only marginal reductions (< 5 %) in glucose uptake and lactate production, indicating that reasonable metabolic (pseudo) steady-state conditions were achieved.

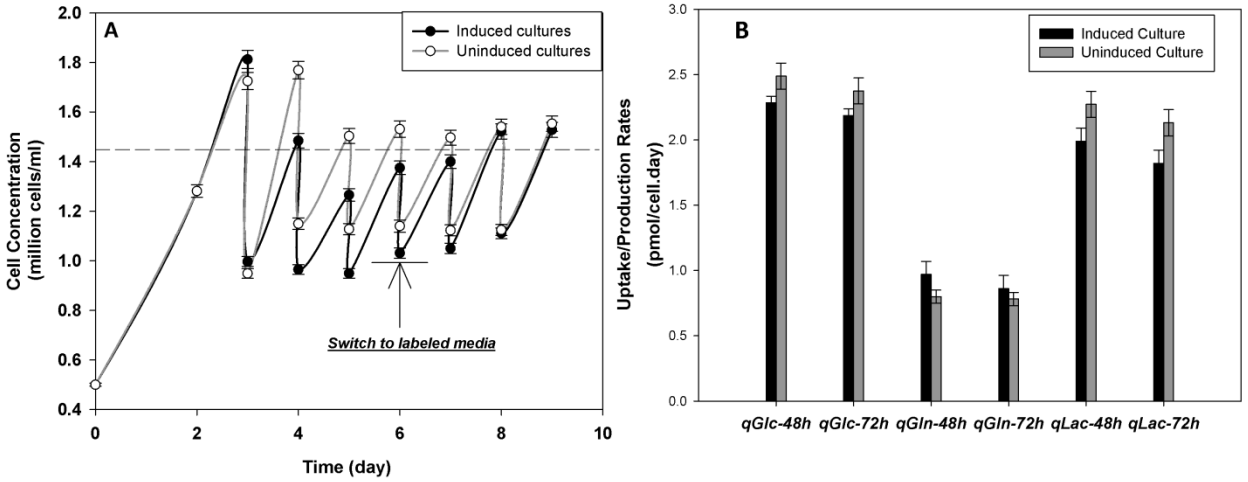

Figure 4-1:Time profile of the average viable cell density for induced and non-induced cells in semi-continuous cultures. Labeled substrates were introduced at day 6 and the cultures were maintained for three subsequent days (A); comparison of glucose and glutamine consumption and lactate production rates for induced and non-induced cells at 48 and 72h post tracer addition (B). Standard deviations were computed from five parallel cultures in each set

The measured cell specific consumption/production rates of amino acids 72h following tracer addition are reported in Table 4-1. A net production of alanine, glutamate, aspartate, and glycine was observed, while all other amino acids were consumed by the cells. When comparing the cultures with and without cumate addition, we observed that the glutamine uptake rate was slightly enhanced (~14%) for the induced cells, while there was a concomitant decrease in glucose uptake rate (~8%). The molar ratio of lactate production on glucose consumption was also slightly reduced (0.86 vs 0.8). Interestingly, these yields of lactate on glucose are both noticeably lower than the typical values reported for mammalian cells in cultures under non-limiting glucose concentrations ($Y_{Lac/Glc} \cong 1\text{-}2$), suggesting that this cell line exhibits an efficient carbon metabolism, irrespective of the induction of recombinant protein expression. The measured cell specific antibody productivity for the cultures supplemented with cumate was 13.7 pg/cell.d, whereas it was ~1 pg/cell.d in the case of non-induced cells, as a result of minor leaky expression. As shown in Table 4-1, the burden imposed by the synthesis of an extra protein was

not accompanied by a clear trend in the consumption patterns of essential and non-essential amino acids.

4.2.4.2 ^{13}C-label incorporation into extracellular metabolites

Labeled-carbon incorporation into extracellular lactate and amino acids was measured by LC-MS TOF analysis. The isotopomer mass distribution of each labeled substrate was also determined experimentally to confirm their level of purity. Clear signs of ^{13}C-enrichment were detected in the isotopomer mass distributions of lactate, aspartate, alanine and glutamate (Figure 4-2 and 4-3), while all other extracellular amino acids exhibited patterns corresponding to their natural labelling. This result was consistent with the observed net specific rates of amino acids utilization (Table 4-1). The fresh medium did not contain any lactate, alanine or glutamate, thus their measured mass distributions were directly indicative of their enrichment. However, the medium contained low initial levels of aspartate, effectively diluting the labelling of this amino acid. Although produced, glycine was omitted from the analysis due to excessive tracer dilution, as this amino acids was present in the fresh medium and is mainly synthesized from unlabeled serine. Mass isotopomer distributions measured after 48h and 72h following the switch to label containing medium were compared to ensure the achievement of an adequate isotopic steady state. The results obtained for the non-induced and the induced cells are shown in Figure 4-2 and Figure 4-3, respectively. Considering the measurement errors involved (about 1-2 %), there were no significant time-dependent differences, indicating that these metabolites had achieved constant ^{13}C-labeling within three days. Although some studies reported that stable labelling pattern in mammalian cells can be obtained after an incubation of only 4 to 6h with an isotopic tracer (Metallo et al., 2009), others have shown that some metabolites, particularly TCA intermediates, may require longer periods of time (Woo Suk Ahn & Antoniewicz, 2011; Maier et al., 2008; Sengupta et al., 2011).

Table 4-1: Measured cell specific uptake/production rates (in pmol/cell.d) at 72h after tracer addition

Compound	**Non-induced cells**	**Induced cells**
Glucose	-2.38 ±0.12	-2.19 ±0.11
Lactate	2.11 ±0.11	1.82 ±0.09
Glutamine	-0.82 ±0.04	-0.94 ±0.09
Phenylalanine	-0.05 ± 0.01	-0.06 ± 0.01
Threonine	-0.07 ± 0.01	-0.07 ± 0.01
Isoleucine	-0.06 ± 0.01	-0.07 ± 0.01
Leucine	-0.11 ± 0.01	-0.11 ± 0.01
Methionine	-0.04 ± 0.01	-0.04 ± 0.01
Tyrosine	-0.04 ± 0.01	-0.04 ± 0.01
Valine	-0.10 ± 0.01	-0.10 ± 0.01
Proline	-0.16 ± 0.02	-0.10 ± 0.01
Serine	-0.22 ± 0.02	-0.28 ± 0.03
Asparagine	-0.22 ± 0.02	-0.38 ± 0.04
Cysteine	-0.05 ± 0.01	-0.04 ± 0.01
Arginine	-0.12 ± 0.01	-0.12 ± 0.01
Lysine	-0.11 ± 0.01	-0.13 ± 0.01
Histidine	-0.04 ± 0.01	-0.04 ± 0.01
Glutamate	0.07 ± 0.01	0.06 ± 0.02
Alanine	0.26 ± 0.03	0.23 ± 0.02
Aspartate	0.03 ± 0.01	0.04 ± 0.01
Glycine	0.28 ± 0.03	0.18 ± 0.02

Direct inspection of the mass distribution data provided early useful insights for the development and validation of the metabolic model. For example, the mass isotopomer distribution of glutamate in cultures grown with uniformly labeled glutamine clearly suggested that a significant portion of this metabolite originated from other carbon source(s) than glutamine. Indeed, glutamate ^{13}C-enrichment was detected in all the cultures grown with labeled glucose. The reverse glutamate dehydrogenase and transaminase reactions were thus important to consider in

the metabolic analysis. It could also be observed that alanine and lactate, which are both mainly produced from pyruvate, exhibited similar but nonetheless distinct labelling patterns. This observation reinforced the importance of considering the effect of compartmentation, i.e. the presence of distinct pyruvate pools in the cytosol and the mitochondria (Peuhkurinen, Hiltunen, & Hassinen, 1983). In our work, the best agreement between simulated and experimental labelling data was obtained by considering that some alanine is derived from mitochondrial pyruvate, while lactate is generated from cytosolic pyruvate. While cytosolic pyruvate is mainly derived from glucose, mitochondrial pyruvate contains more label originating from glutamine. A similar assumption was employed by Walther et al. (Walther, Metallo, Zhang, & Stephanopoulos, 2012) for describing the distinct labelling pattern of lactate and alanine in their analysis of a mammalian cell line.

4.2.4.3 ^{13}C metabolic flux analysis

The mass isotopomer distribution data from the samples collected 72h after tracer addition were used to conduct a ^{13}C-Metabolic flux analysis. The isotope model contains 15 free fluxes and, combining the labelling data from all parallel cultures, 60 independent mass spectrometry measurements were available. Thus, the minimum and maximum allowed values for the WSSR were 30.6 and 61.7, respectively (chi-square threshold at 95% level of confidence with 45 degrees of freedom) (Antoniewicz et al., 2006). We found an acceptable agreement between predicted and measured mass distribution data with WSSR values of 47.1 and 58.5 for non-induced and induced cells, respectively. Comparisons of the fit between simulated and measured isotopomer data are shown in Figure 4-2 and Figure 4-3. Standard-deviation weighted residuals were also verified to be reasonably normally distributed as shown in the normal probability plots (Figure 4-2 and 4-3). The calculated intracellular flux distributions under both induced and non-induced conditions are shown in Figure 4-4. The associated 95 % confidence intervals, from which the median and standard error values were evaluated (Jamey D Young, Shastri, Stephanopoulos, & Morgan, 2011), are included as Supplementary Material (Table 4-3). For some exchange fluxes, the associated confidence intervals equal or exceed the feasible range of values and these fluxes can thus be considered not observable with the tracers employed and the available MS data. However, relatively narrow confidence intervals could be obtained for most of

the corresponding net fluxes, thereby allowing to reveal some differences in the metabolism of induced and non-induced cells. The onset of protein expression was notably correlated with a reduction in glycolytic fluxes, a concomitant decrease in pentose phosphate pathway fluxes, while TCA fluxes from citrate to malate were found to be slightly enhanced. However, most anaplerotic reactions involving amino acids remained largely unaffected. These metabolic observations are further elaborated in the next section.

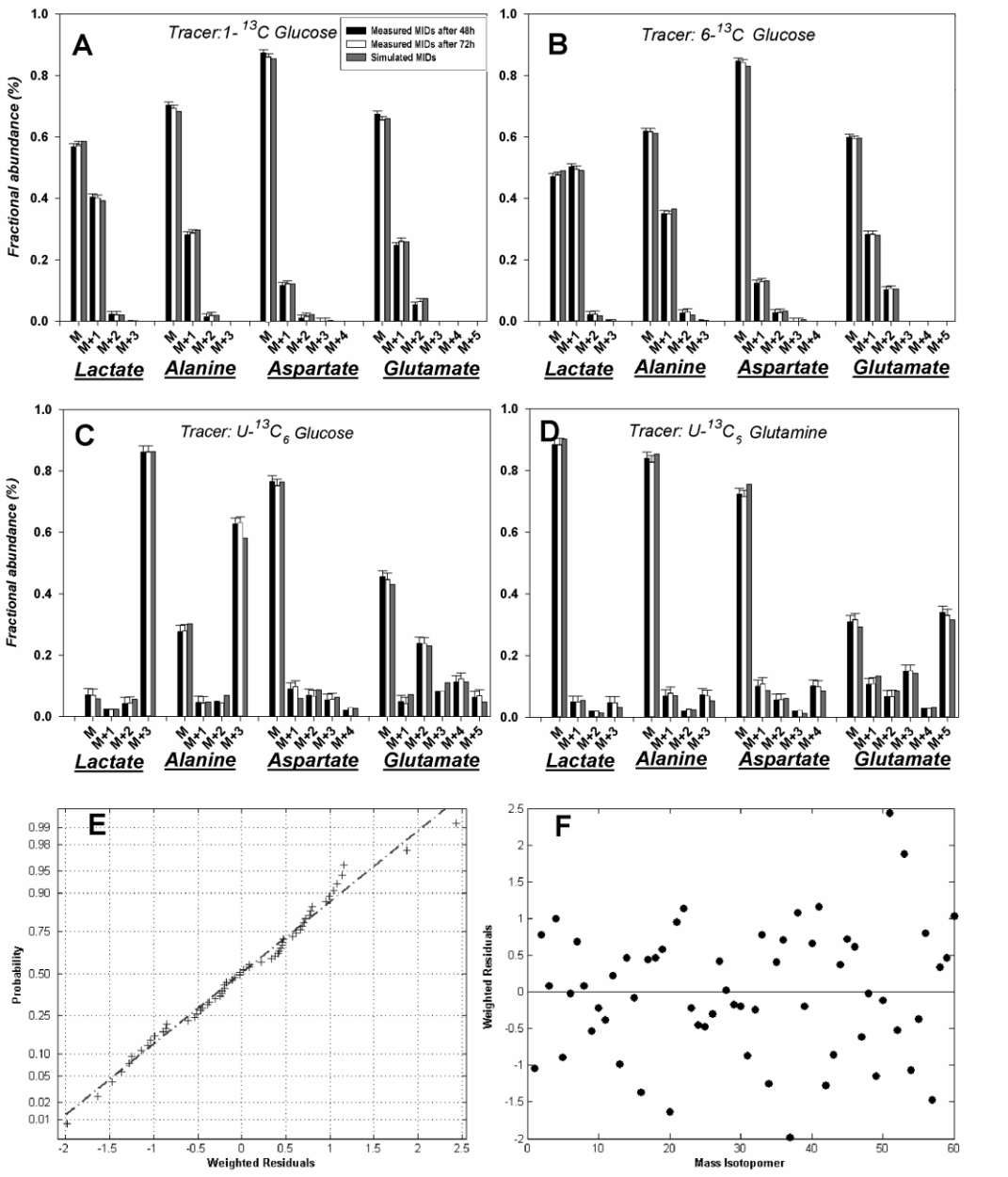

Figure 4-2: Measured (at 48 and 72h) and fitted (at 72h) mass distributions of lactate, alanine, aspartate, and glutamate in non-induced cells grown in 1-^{13}C glucose (A), 6-^{13}C glucose (B), U-$^{13}C_6$ glucose (C) and U-$^{13}C_5$ glutamine (D); normal probability plot indicating an approximately normal distribution of the residuals (E); Standard-deviation weighted residuals (F)

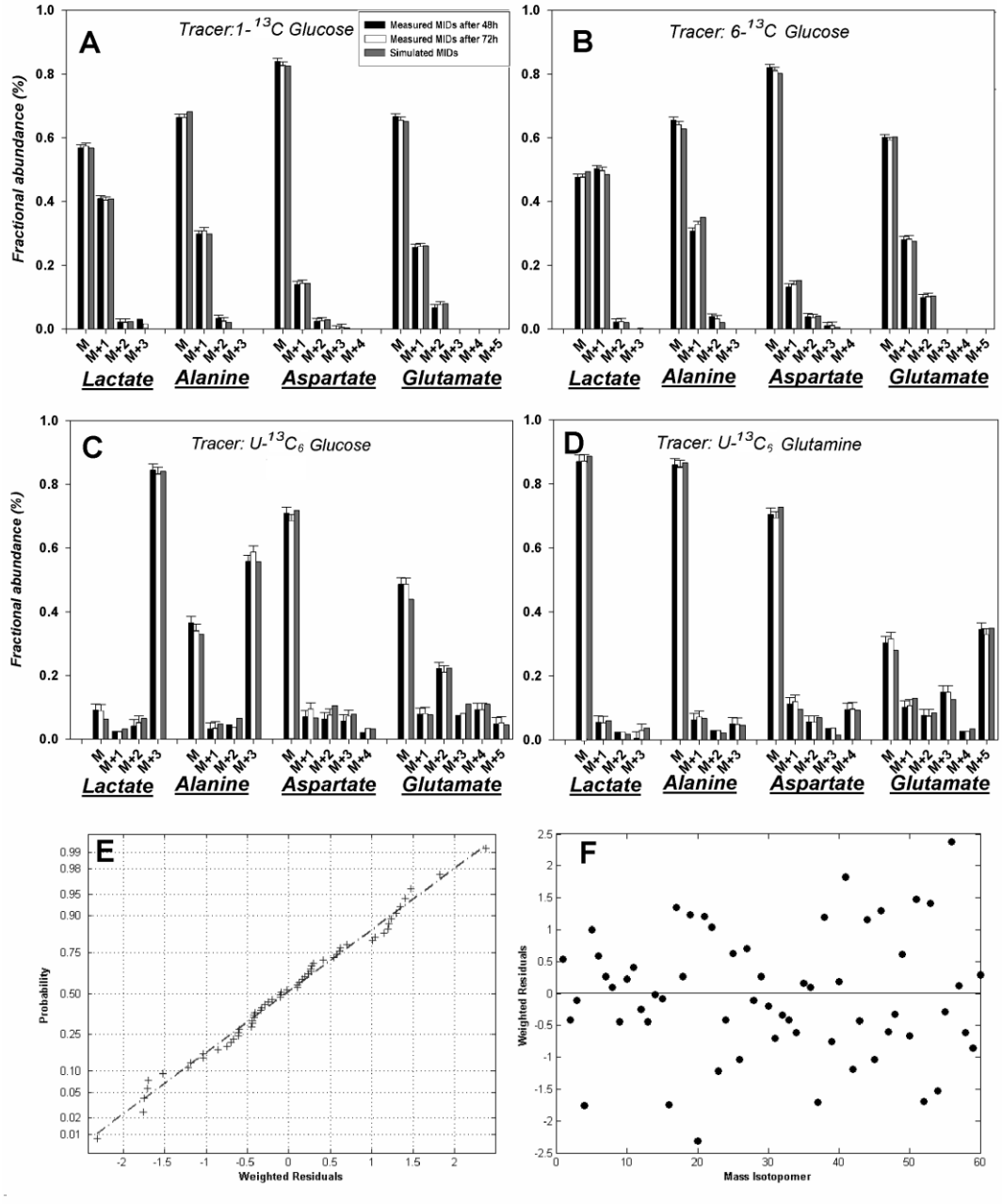

Figure 4-3: Measured (at 48 and 72h) and fitted (at 72h) mass distributions of lactate, alanine, aspartate, and glutamate in induced cells grown in 1-^{13}C glucose (A), 6-^{13}C glucose (B), U-$^{13}C_6$ glucose (C) and U-$^{13}C_5$ glutamine (D); normal probability plot indicating an approximately normal distribution of the residuals (E); Standard-deviation weighted residuals (F)

4.2.5 Discussion

Compared to parental cell lines, recombinant mammalian cell lines generally exhibit reduced growth rates and increased substrate utilization (Yallop et al., 2003), most likely to meet the specific energy and biosynthetic demands related to protein synthesis and related posttranslational modifications. Recent studies performed on yeasts and bacteria have characterized the metabolic response to the overproduction of recombinant protein and revealed significant redirections of intracellular carbon fluxes towards energy formation (Heyland, Blank, & Schmid, 2011; Heyland, Fu, Blank, & Schmid, 2011). The identification of potential metabolic burdens is critical to further enhance protein production in any expression system. Towards this goal and in an effort to analyse the impact of protein expression on the primary metabolism of mammalian cells in culture, we have employed an efficient inducible expression system and conducted a comparative study of the intracellular flux map distribution with or without the induction of recombinant protein synthesis.

Under non-limiting glucose concentrations, cultivated mammalian cells typically display high glycolytic rates relative to TCA fluxes, thereby converting the majority of glucose consumed into lactate. In our study, the onset of protein expression was not accompanied by statistically significant changes in the reactions catalyzed by hexokinase and phosphoglucose isomerase, but we observed a significant decrease in the G6P dehydrogenase reaction, which generates ribose-5-phosphate and NADPH (Figure 4-4). The former is an important building block for nucleotides, while the latter is essential for reductive processes, most notably the biosynthesis of fatty acids. Without cumate addition, we observed that the cells channelled 20 % of the glucose consumed toward the pentose phosphate pathway, while this value was reduced to 13 % when the cells were induced. Both values were within the range commonly reported for mammalian cells in culture (Altamirano et al., 2006; H. P. Bonarius et al., 2001), although some studies have measured up to 40% (C. Goudar et al., 2010; Sengupta et al., 2011). The decrease in the pentose phosphate pathway flux observed in cultures grown with cumate was concomitant with the slight reduction in specific growth rate, therefore related, at least in part, to reduced biosynthetic needs.

Whether the cells were induced or not, the flux distribution around the pyruvate branch point showed that a high proportion of pyruvate originated from glycolysis (75 to 78 %), while 21 to

24% came from the conversion of malate via malic enzyme, and a minor fraction was derived from the degradation of amino acids such as cysteine or serine. Furthermore, 49 to 58 % of the pyruvate pool was channelled into the TCA cycle, while only 35-40 % was converted into lactate. Therefore, irrespective of the recombinant protein expression, the cell line under study exhibited a highly efficient nutrient utilization, even under high residual glucose concentrations (glucose was maintained in the range of 12 to 16 mM in the semi-continuous cultures). The fraction of pyruvate entering the TCA in our study was noticeably higher than values previously reported for other CHO cell lines (Altamirano et al., 2001; C. Goudar et al., 2010), presumably related in part to the fact that our experiments were performed under mild hypothermic conditions. However, recent characterization during the stationary phase revealed that CHO cells can produce very little lactate (Sengupta et al., 2011) or even exhibit a net consumption rate of this metabolite (Woo Suk Ahn & Antoniewicz, 2011). We observed similar trends for lactate kinetics when cells were grown in batch mode (data not shown).

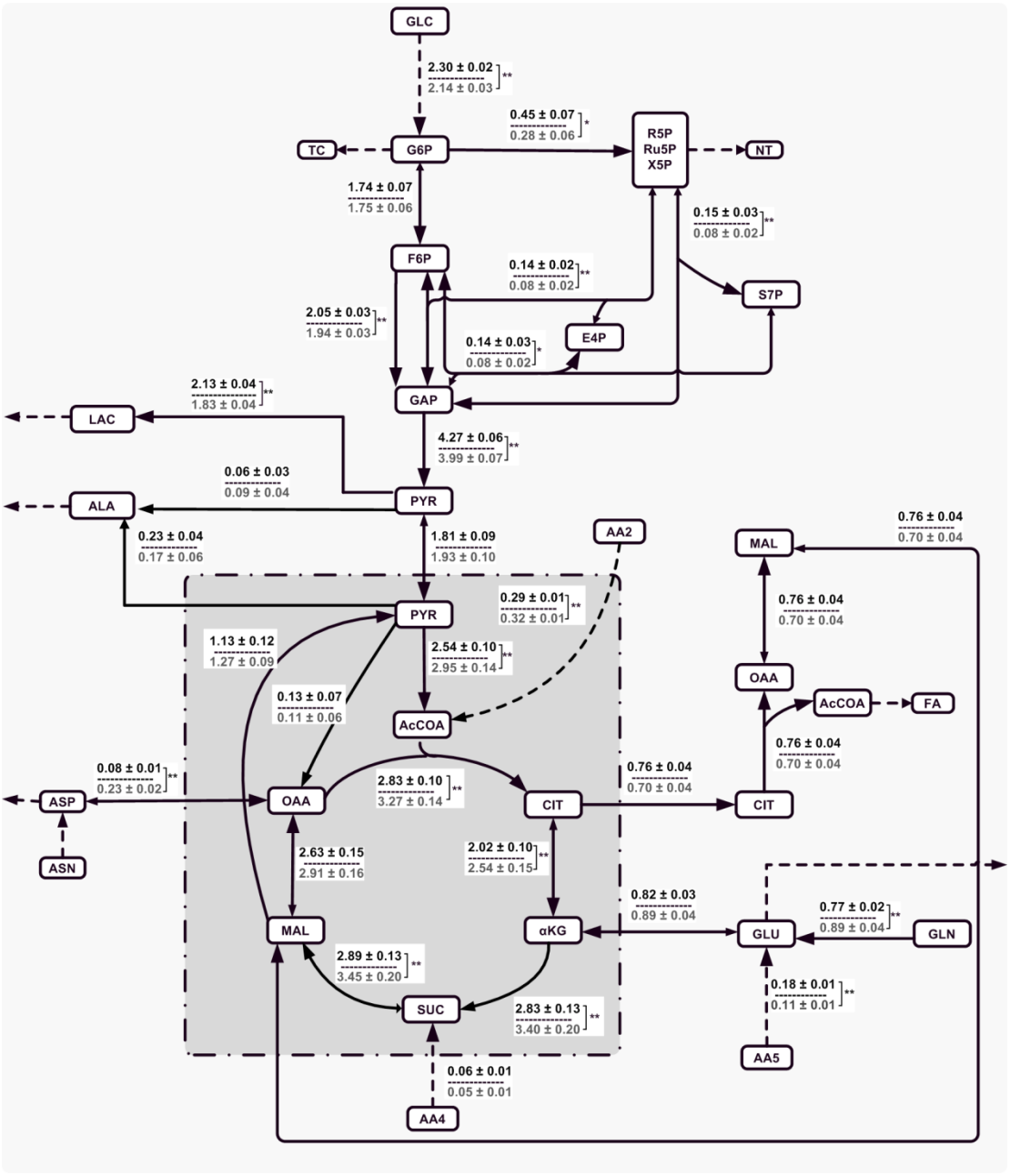

Figure 4-4: Metabolic flux map for non-induced (top values) and induced (bottom values) cells. The values are the median of the 95% flux confidence interval and standard errors were calculated from the upper and lower bounds of the 95 % confidence intervals. In the case of reversible reactions, the values correspond to the estimated net fluxes. * and ** indicate significance at $p<0.1$ and $p<0.05$, respectively. Abbreviations: AA2= Leu, Lys, Ile, Tyr, Trp, and Thr; AA4= Val, Met, and Ile; AA5= His, Arg, and Pro.

Induced cells also exhibited a small but statistically significant increase (16 %) in the flux through pyruvate dehydrogenase (Figure 4-4). However, both induced and non-induced cells did not exhibit a significant flux via the pyruvate carboxylase, a common observation for cultivated mammalian cells (Quek et al., 2010). As a result of the increased entry of pyruvate via pyruvate dehydrogenase, an increase in the average TCA cycle fluxes was observed (Figure 4-4), presumably to support the additional production of energy required for protein synthesis and related cellular processes. From the resulting flux distributions and assuming a P/O ratio of 2.5 for $NADH_m$ and 1.5 for $FADH_{2m}$, it is evaluated that cells derived 90 % of the total ATP production from the TCA cycle. Assuming a stoichiometry of 3.78 mol of ATP per mol of biomass and 4 mol of ATP per mol of antibody (Ryan P Nolan & Lee, 2011; L. Xie & D. I. Wang, 1996), the energy requirements for biomass and recombinant protein synthesis account respectively for only 10 % and a mere 1 % of the estimated ATP production rate. It is therefore unlikely that energy is the main factor limiting recombinant protein expression in cultivated cells.

While we estimated a greater pyruvate recycling (i.e. pyruvate derived from TCA intermediates) via malic enzyme in the case of the induced cells, the observed differences are within the confidence intervals and cannot be considered significantly different with the data in hand. Together with the pentose phosphate pathway, malic enzyme constitutes a major route for the generation of NADPH. In the metabolic network considered herein, the main NADPH requirements are associated with the synthesis of fatty acids, nucleic acids and alanine. From the obtained flux distributions, the NADPH produced by the pentose phosphate pathway accounted for 0.9 and 0.6 pmol/cell-d for non-induced and induced cells, respectively. On the other hand, malic enzyme provided approximately 1.1 and 1.3 pmol/cell-d, respectively. Interestingly, the slightly greater contribution of malic enzyme observed in the case of the induced cells seemed to compensate for the reduction in NADPH synthesis via the pentose phosphate pathway. While our data suggested that NAPDH synthesis was relatively evenly distributed between the two pathways, contribution of the pentose phosphate pathway in the range of 18 to 90% of the total NADPH production have been reported in the literature for cultivated CHO cells (Altamirano et al., 2006; Altamirano et al., 2001; C. Goudar et al., 2010), hybridoma cells (H. P. Bonarius et al., 2001; Dalm et al., 2007), and HEK cells (Olivier Henry & Durocher, 2011).

Glutamine was the main amino acid consumed by the cells, albeit at a rate significantly lower than glucose. The latter was the main carbon source for the TCA cycle (51-53 %), but glutamine also contributed a significant amount (38-40 %). The combined catabolism of all other amino acids thus represented a small, but non-negligible fraction (7-11%) of the total carbon entering the TCA cycle as either acetyl-CoA, malate, α-ketoglutarate or oxaloacetate. Interestingly, induced and non-induced cells exhibited very similar catabolic rates for the amino acids. It appears thus that the varying anabolic needs for cell growth and recombinant protein synthesis did not significantly impact the contribution of amino acids towards energy production. Indeed, while the growth rate reduction exhibited by induced cells decreases the amino acid requirements for biomass synthesis by approximately 8 %, the onset of recombinant protein formation increases the biosynthetic demand for amino acids, on average by 9 to 15 %, as can been inferred from Table 4-4 in Supplementary Materials. As a result, the total anabolic demand for protein synthesis, in terms of amino acids and energy, is not expected to differ significantly between induced and non-induced cells. Consequently, the increased TCA cycle fluxes noted in the former cannot be attributed solely to the biosynthesis of the recombinant product, but can presumably be linked in part to the energetic costs associated with other protein processing events (e.g. folding, modification, secretion), may serve to compensate the reduced energy produced through glycolysis or support different maintenance energy requirements altogether.

The induction of recombinant protein expression by the addition of cumate is thus associated with small, yet detectable changes in the primary metabolism of the cells. However, although recombinant protein production causes an increase load on the cells, it should be emphasized that the augmentation of total cellular protein resulting from MAb production is estimated to be at most approximately 15%, considering the measured specific productivity and assuming a protein dry cell weight of 240 pg/cell. Moreover, the production capacity is thought to be not limited at the anabolic level, but rather at the folding and assembly stages (Dinnis et al., 2006). Taken together, this may explain the relatively modest changes observed in the intracellular flux distribution. Despite the small magnitude of these changes, our results nonetheless provide a quantitative indication that recombinant protein expression is positively correlated with an increased flux through pyruvate dehydrogenase and a corresponding increase in TCA cycle fluxes.

Our study also demonstrated that the use of multiple isotopic tracers in parallel semi-continuous cultures, combined with isotopomer analysis of extracellular metabolites, allows to obtain reliable estimates of the main intracellular fluxes. Semi-continuous cultures retain the technical simplicity of batch mode, while maintaining the cells under balanced growth conditions over a sufficiently long time to ensure the achievement of pseudo-steady isotopic and metabolic states. Additionally, by varying the daily exchange rate, this mode of operation could allow in principle to run experiments under different apparent growth rates, similar to classical kinetic studies performed in continuous cultures. While repeated feeding with expensive label-containing media may appear prohibitive, this is balanced by the fact that cultures can easily be performed at fairly small scale (even well plates), in contrast to chemostat. The main drawbacks of this approach are related to the uncontrolled culture conditions (with respect to pH and pO_2), as well as the necessity to conduct several cultures in parallel and ensure that they remain in a comparable physiological state.

4.2.6 Conclusion

The use of an efficient inducible mammalian expression system combined to a relatively straightforward experimental approach allowed us to characterize the primary metabolism of CHO cells in relation with their specific productivity. The main intracellular fluxes were quantified with relatively narrow confidence intervals, thereby allowing to decipher metabolic changes related to the onset of recombinant protein expression. Our study notably revealed small but significant variations in a number of key pathways related to ATP and NADPH formation, including the pentose phosphate pathway, the malic enzyme and the TCA cycle. When expressing the recombinant antibody, cells exhibited a more efficient utilization of glucose with comparatively more carbon incorporated into the TCA cycle. Characterizing the primary metabolism of other cells exhibiting different productivities may confirm the observed trends in our study and further guide the identification of reliable physiological markers and desirable metabolic states for production. In turn, this can provide a rational basis for maximizing the productivity through the selection of an appropriate induction time and the design of an efficient feeding strategy pre- and post-induction.

Acknowledgments

The authors wish to acknowledge Dr. Alexandra Furtos from Université de Montréal for ^{13}C QTOF-LCMS analysis, Jingkui Chen from Ecole Polytechnique for amino acids analysis, as well as Dr. Patrick Benoist and Dr. Patrick Daoust of Viropro Internal Inc. (Montreal, Canada) for providing the cell line employed in this study.

Table 4-2: Biochemical network and atom transition

Reaction	*Carbon Transition*
Glycolysis	
GLC → G6P	abcdef = abcdef
G6P ↔ F6P	abcdef = abcdef
F6P → 2 GAP	abcdef = cba + def
GAP → PYR	abc = abc
PYR → LAC	abc = abc
PYR ↔ PYRm	abc = abc
PPP	
G6P → P5P + CO_2	abcdef = bcdef + a
2P5P ↔ S7P + GAP	abcde + fghij = abfghij + cde
P5P + E4P ↔ F6P + GAP	abcde + fghi = abfghi + cde
S7P + GAP ↔ F6P + E4P	abcdefg + hij = abchij + defg
TCA	
PYRm → AcCOAm + CO_2	abc = bc + a
AcCOAm + OAAm → CITm	ab + cdef = fedbac
CITm ↔ aKGm + CO_2	abcdef = abcde + f
aKGm → SUCm + CO_2	abcde = bcde + a
SUCm → 0.5 MALm + 0.5 MALm	abcd = 0.5 abcd + 0.5 dcba
MALm ↔ OAAm	abcd = abcd
MALm ↔ MAL	abcd = abcd
OAA ↔ MAL	abcd = abcd
MALm → PYRm + CO_2	abcd = abc + d
PYRm + CO_2 → OAAm	abc + d = abcd
CITm + MAL → CIT + MALm	abcdef + ghij = abcdef + ghij
CIT → AcCOAc + OAA	abcdef = ed + fcba
Amino acid reactions	
GLN → GLU	abcde = abcde

GLU ↔ aKGm	`abcde = abcde`
PYRm → ALA	`abc = abc`
PYR → ALA	`abc = abc`
ASP + aKGm ↔ OAAm + GLU	`abcd + efghi = abcd + efghi`
SER → GLY + C	`abc = ab + c`
PYR → SER	`abc = abc`
CYS → PYR	`abc = abc`
MET + SER → SUCm + CYS + C	
MET → MET1 + C	`abcde = abcd + e`
MET1 + SER → MET2 + CYS	`abcd + efg = abcd + efg`
MET2 + CO_2*in →* CO_2 *+ SUCm*	`abcd + e = a + bcde`
VAL → SUCm + CO_2	
VAL + CO_2*in → SUCm + VAL2*	`abcde + f = decf + ab`
VAL2 → CO_2 *+* CO_2	`ab = a + b`
ILE → AcCOAm + SUCm	
ILE + CO_2*in →* CO_2 *+ ILE1*	`abcdef + g = a + debfcg`
ILE1 → AcCOAm + SUCm	`abcdef = ab + cdef`
LEU → 3AcCOAm	
LEU + CO_2*in → LEU1 + LEU2*	`abcdef + g = age + bcdf`
LEU1 → CO_2 *+ AcCOAm*	`abc = a + bc`
LEU2 → AcCOAm + AcCOAm	`abcd = ab + cd`
THR → AcCOAm + GLY	`abcd = ab + cd`
LYS → 2AcCOAm + 2 CO_2	
LYS → LYS1 + LYS2	`abcdef = af + bcde`
LYS1 → CO_2 *+* CO_2	`ab = a + b`
LYS2 → AcCOAm + AcCOAm	`abcd = ab + cd`
TRP → ALA + 2AcCOAm + 4 CO_2	
TRP → TRP1 + TRP2A	`abcdefghijk = abcd + efghijk`
TRP1 → ALA + CO_2	`abcd = abc + d`

TRP2A → TRP2 + TRP3	abcdefg = abcd + efg
TRP2 → AcCOAm + AcCOAm	abcd = ab + cd
TRP3 → CO_2 + CO_2 + CO_2	abc = a + b + c
TYR → 2AcCOAm + MALm + CO_2	
TYR → TYR1 + TYR2	abcdefghi = abcde + fghi
TYR1 → MALm + CO_2	abcde = bcde + a
TYR2 → AcCOAm + AcCOAm	abcd = ab + cd
PHE → TYR	abcdefghi = abcdefghi
HIS → GLU	abcde = abcde
PRO → GLU	abcde = abcde
ARG → GLU	abcde = abcde
ASN → ASP	abcd = abcd
Transport	
GLC ex → GLC	abcdef = abcdef
GLN ex → GLN	abcde = abcde
PRO ex → PRO	abcde = abcde
VAL ex → VAL	abcde = abcde
LEU ex → LEU	abcdef = abcdef
LYS ex → LYS	abcdef = abcdef
MET ex → MET	abcde = abcde
THR ex → THR	abcd = abcd
ILE ex → ILE	abcdef = abcdef
HIS ex → HIS	abcde = abcde
ARG ex → ARG	abcde = abcde
PHE ex → PHE	abcdefghi = abcdefghi
TYR ex → TYR	abcdefghi = abcdefghi
CYS ex → CYS	abc = abc
SER ex → SER	abc = abc
TRP ex → TRP	abcdefghijk = abcdefghijk

ASN ex → ASN	`abcd = abcd`
LAC → LAC ex	`abc = abc`
GLU → GLUex	`abcde = abcde`
ALA → ALA ex	`abc = abc`
GLY → GLY ex	`ab = ab`
ASP → ASP ex	`abcd = abcd`

Biomass Reaction

0.912 Protein + 0.0315 P5P + 0.0379 G6P + 0.317 AcCOAc → BIOMASS

Recombinant Product Synthesis

0.059 ALA + 0.023 ARG + 0.045 ASN + 0.037 ASP + 0.025 CYS + 0.040 GLN + 0.052 GLU + 0.066 GLY + 0.023 HIS + 0.033 ILE + 0.063 LEU + 0.061 LYS + 0.013 MET + 0.042 PHE + 0.072 PRO + 0.011 SER + 0.106 THR + 0.022 TRP + 0.029 TYR + 0.086 VAL → ANTIBODY

Cellular Protein Synthesis

0.081 ALA + 0.051 ARG + 0.039 ASN + 0.049 ASP + 0.020 CYS + 0.044 GLN + 0.052 GLU + 0.073 GLY + 0.019 HIS + 0.044 ILE + 0.076 LEU + 0.077 LYS + 0.019 MET + 0.030 PHE + 0.042 PRO + 0.058 SER + 0.052 THR + 0.006 TRP + 0.025 TYR + 0.056 VAL → PROTEIN

4.3 Supplementary data

Table 4-3: Estimated intracellular fluxes (pmol/cell.d) in non-induced and induced cells

		Non-induced cells			*Induced cells*		
Reaction		***Optimal Flux***	***95 % C.I.***	***Median Value***	***Optimal Flux***	***95 % C.I.***	***Median Value***
GLC → G6P		2.26	[2.26 , 2.34]	2.30	2.08	[2.08 , 2.20]	2.14
G6P ↔ F6P	net	1.76	[1.61 , 1.86]	1.74	1.76	[1.62 , 1.87]	1.75
	exch	12.00	[0.00 , inf]	-	12.00	[0.00 , inf]	-
F6P → 2 GAP		2.03	[1.99 , 2.11]	2.05	1.92	[1.88 , 1.99]	1.94
GAP → PYR		4.20	[4.15, 4.39]	4.27	3.91	[3.86 , 4.13]	3.99
PYR → LAC		2.20	[1.90 , 2.31]	2.13	1.88	[1.64 , 2.00]	1.83
PYR ↔ PYRm	net	1.80	[1.63 , 1.99]	1.81	1.88	[1.74 , 2.13]	1.93
	exch	3.55	[1.81 , 7.01]	-	3.84	[2.12 , 9.12]	-
G6P → P5P + CO_2		0.44	[0.31 , 0.59]	0.45	0.27	[0.16 , 0.41]	0.28
2P5P ↔ S7P + GAP	net	0.14	[0.10 , 0.19]	0.15	0.08	[0.04 , 0.11]	0.08
	exch	0.55	[0.00 , inf]	-	0.34	[0.00 , inf]	-
P5P + E4P ↔ F6P + GAP	net	0.14	[0.10 , 0.18]	0.14	0.08	[0.04 , 0.11]	0.08
	exch	0.00	[0.00 , inf]	-	0.00	[0.00 , inf]	-
S7P + GAP ↔ F6P + E4P	net	0.14	[0.09 , 0.19]	0.14	0.08	[0.04 , 0.12]	0.08
	exch	2.69	[0.00 , inf]	-	12.00	[0.00 , inf]	-
PYRm → AcCOAm + CO_2		2.49	[2.36 , 2.73]	2.54	2.88	[2.68 , 3.22]	2.95
PYRm + CO_2 → OAAm		0.05	[0.00 , 0.27]	0.13	0.08	[0.00 , 0.22]	0.11
AcCOAm + OAAm → CITm		2.79	[2.64 , 3.03]	2.83	3.21	[3.00 , 3.54]	3.27
CITm ↔ aKGm + CO_2	net	1.98	[1.81 , 2.22]	2.02	2.48	[2.24 , 2.83]	2.54
	exch	0.00	[0.00 , 1.54]	-	0.00	[0.00 , 5.00]	-
aKGm → SUCm + CO_2		2.80	[2.58 , 3.08]	2.83	3.34	[3.01 , 3.79]	3.40

SUCm → 0.5MALm + 0.5MALm	net	2.85	[2.64 , 3.13]	2.89	3.40	[3.07 , 3.83]	3.45
	exch	0.00	[0.00 , inf]	-	12.00	[0.00 , inf]	-
MALm↔ OAAm	net	2.66	[2.33 , 2.93]	2.63	2.90	[2.59 , 3.23]	2.91
	exch	0.00	[0.00 , inf]	-	0.00	[0.00 , inf]	-
MAL ↔ MALm	net	0.81	[0.68 , 0.84]	0.76	0.73	[0.63 , 0.77]	0.70
	exch	0.95	[0.68 , inf]	-	7.40	[0.63 , inf]	-
OAA ↔ MAL	net	0.81	[0.68 , 0.84]	0.76	0.73	[0.63 , 0.77]	0.70
	exch	0.41	[0.00 , inf]	-	2.09	[0.00 , inf]	-
CITm → CIT		0.81	[0.68 , 0.84]	0.76	0.73	[0.63 , 0.77]	0.70
CIT → ACCOA + OAA		0.81	[0.68 , 0.84]	0.76	0.73	[0.63 , 0.77]	0.70
MALm → PYRm + CO_2		1.03	[0.91 , 1.36]	1.13	1.25	[1.09 , 1.45]	1.27
GLN → GLU		0.78	[0.73 , 0.81]	0.77	0.88	[0.82 , 0.97]	0.89
GLU ↔ αKG	net	0.82	[0.75 , 0.88]	0.82	0.86	[0.80 , 0.97]	0.89
	exch	8.10	[5.10 , 13.42]	-	4.80	[3.36 , 5.77]	-
PYR → ALA		0.00	[0.00 , 0.12]	0.06	0.08	[0.00 , 0.17]	0.09
PYRm → ALA		0.28	[0.15 , 0.32]	0.23	0.16	[0.06 , 0.28]	0.17
ASP + αKG ↔ OAA + GLU	net	0.08	[0.06 , 0.11]	0.08	0.23	[0.19 , 0.27]	0.23
	exch	0.10	[0.08 , 0.12]	-	0.26	[0.20 , 0.31]	-

Table 4-4: Amino acids requirements for biomass and product synthesis (in pmol/cell.d).

Rates were calculated from average biomass/antibody compositions and the measured cell specific growth/production rates. Due to the very low basal expression of non-induced cells, the requirements for antibody synthesis were neglected.

	Non-induced cells		**Induced cells**	
	Biomass	**Product**	**Biomass**	**Product**
Ala	0.076	---	0.069	0.006
Arg	0.048	---	0.044	0.002
Asn	0.036	---	0.033	0.005
Asp	0.045	---	0.041	0.004
Cys	0.018	---	0.017	0.003
Gln	0.041	---	0.037	0.004
Glu	0.049	---	0.045	0.006
Gly	0.068	---	0.062	0.007
His	0.018	---	0.017	0.002
Ile	0.041	---	0.037	0.004
Leu	0.071	---	0.065	0.007
Lys	0.072	---	0.066	0.007
Met	0.017	---	0.016	0.001
Phe	0.028	---	0.025	0.005
Pro	0.039	---	0.036	0.008
Ser	0.054	---	0.050	0.001
Thr	0.049	---	0.045	0.011
Trp	0.006	---	0.005	0.002
Tyr	0.023	---	0.021	0.003
Val	0.052	---	0.048	0.009

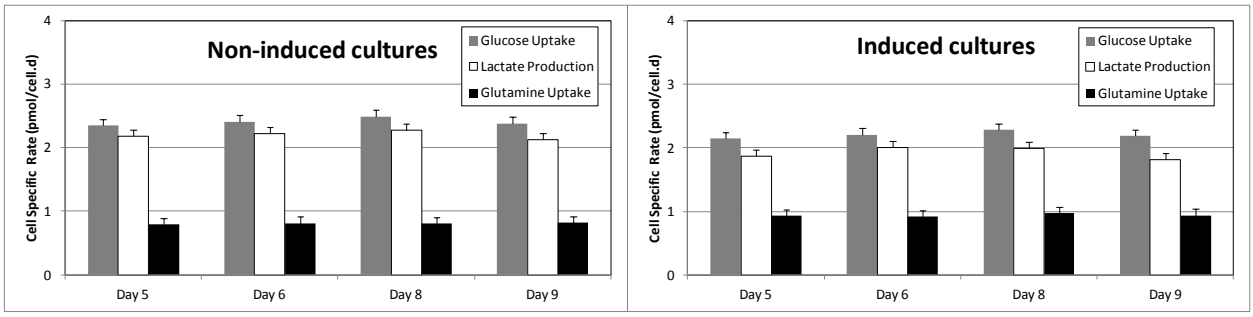

Figure 4-5: Measured cell specific uptake/production rates (in pmol/cell.d) during semi-continuous cultures of induced and non-induced CHO cells.

From day 3, a fixed culture volume was replaced by fresh medium on a daily basis so as to maintain pseudo-constant cell and nutrient concentrations. The switch to label containing medium was performed on Day 6. Thus, days 8 and 9 correspond to 48 and 72h post tracer addition, respectively.

CHAPTER 5 THE IMPACT OF THE TIMING OF INDUCTION ON THE METABOLISM AND PRODUCTIVITY OF CHO CELLS IN CULTURE

5.1 Presentation of the article

This section contains the article entitled "***The impact of the timing of induction on the metabolism and productivity of CHO cells in culture***" which was published in "**Biochemical Engineering Journal**" (Volume 79, 2013, Pages 162–171). In this study, we demonstrate that, in a biphasic process, cell growth and recombinant protein expression during the production phase are largely determined by the time, and the prevailing cell concentration, at which the induction is performed. It is shown that the potential benefit of inducing a culture with a high cell concentration is negated by a significant drop in cell specific productivity, most likely related to a reduced availability of nutrients or waste metabolite accumulation. An isotopic tracer experiment was conducted to assess the metabolic differences between culture induced at respectively low and high cell densities. The resulting intracellular flux maps were compared in an effort to identify metabolic fluxes that are correlated to cell specific growth or productivity.

Compared with the previous chapter, the labeling experiments carried out in this study were performed with fewer labeled substrates, based on simulation work indicating that using 1-^{13}C glucose and U-^{13}C glutamine would be the most efficient combination to provide reliable flux estimates.

5.2 The Impact of the Timing of Induction on the Metabolism and Productivity of CHO Cells in Culture

Zahra Sheikholeslami[1], Mario Jolicoeur[1], Olivier Henry[1*]

[1]Département de Génie Chimique, École Polytechnique de Montréal,

C.P. 6079, Succ. Centre-ville, Montréal, Québec, Canada, H3C 3A7

*Correspondence to:

Olivier Henry

Chemical Engineering Department

École Polytechnique de Montréal

C.P. 6079, Succ. Centre-ville,

Montréal, Québec, Canada, H3C 3A7

Tel: 1-514-340-4711 (2191)

Fax: 1-514-340-4159

Email: olivier.henry@polymtl.ca

5.2.1 Abstract

Efficient inducible mammalian expression systems are becoming increasingly available and are particularly attractive from a process optimization point of view in that they allow decoupling the growth and production phases. In biphasic processes, the timing of induction is one of the most critical factors to consider for maximizing the productivity, since it will affect both the cumulative biomass concentration and the cell specific productivity. In an effort to assess how these two factors must be balanced for optimal productivity, we have performed a metabolic characterization of CHO cells expressing a recombinant antibody and harboring an efficient inducible expression system. Cells taken at different stages of growth were transferred and induced in fresh medium at their corresponding cell densities, and the kinetics of growth, nutrient consumption and product formation were compared during the production phase. Low cell density inductions achieved lower maximum cell concentrations, but exhibited higher cell specific productivity and greater culture longevity, and ultimately led to increased final product titers. To gain more physiological insights into the observed differences, ^{13}C metabolic flux analysis was performed to characterize and compare the metabolism of cells induced at respectively low and high cell concentrations. A number of key intracellular fluxes were found to be affected by the cell density and the corresponding availability of nutrients during the induction phase. While glucose utilization efficiency is increased in high cell density induction, thereby reducing the specific lactate production rate, it appears to be compensating for the decreased catabolic rates of amino acids. The comprehensive metabolic characterization performed in this work can help guide the development of an efficient feeding strategy pre- and post-induction.

Keywords: Inducible expression, ^{13}C-metabolic flux analysis, CHO cell cultures

5.2.2 Introduction

Nowadays, two thirds of the top selling biopharmaceutical products are manufactured using mammalian cell systems, and CHO cells in particular remain the dominant expression platform in industry (Walsh, 2010). The fact that these cells have the ability to synthesize proteins with human-like posttranslational modifications makes them the most suitable host system for many valuable biotherapeutics. Due to the increasing demand for biologics, the pressure to reduce the cost associated with process development and the need to shorten the time to market, continuous efforts have been made in mammalian cell technologies to maximize both the yields and product quality. This has been mostly achieved through the design of enhanced expression vectors, improved medium formulations and the application of fed-batch strategies supporting high cell densities as well as extending culture time (Butler & Meneses-Acosta, 2012; Dietmair et al., 2011; Lim et al., 2010; O'Callaghan & James, 2008).

In recent years, there has been also a growing interest in the development of inducible mammalian expression systems, such as the widely used tetracycline- (Gossen & Bujard, 1992) and ecdysone-regulated expression platforms (No et al., 1996). In these systems, expression of the transgene of interest is typically initiated upon the addition of a regulating compound to culture medium (Rita Costa et al., 2010). The use of inducible expression systems is particularly advantageous in the case of recombinant products which have known cytotoxic effects on the host cells, since the production can be triggered once cells have been grown to sufficiently high cell densities. More generally, the ability to decouple the growth and production phases allows one to perform biphasic cultivations, which are particularly attractive from a process optimization point of view in that they permit to define specific operating conditions that are optimal for each phase (Trummer et al., 2006b). Indeed, the cell specific productivity of mammalian cells is usually non-growth associated (Li et al., 2010) and is sometimes reported to be inversely correlated with their proliferation rate (Al-Rubeai, Emery, Chalder, & Jan, 1992; F. W. Lee, Elias, Todd, & Kompala, 1998). Moreover, cells can presumably be grown more rapidly before induction as they do not have the extra metabolic load associated with recombinant protein expression (Lipscomb, Mowry, & Kompala, 2004). Such metabolic burden was demonstrated in yeast and bacteria (Glick, 1995; Heyland, Blank, et al., 2011; Heyland, Fu, Blank, & Schmid,

2010). Although recombinant proteins account for a lower fraction of total cellular proteins in the case of mammalian cells (typically below 10 to 15 %), recombinant cell lines also exhibit signs of increased metabolic load, in the form of reduced cellular growth and altered rates of nutrient utilization (Kuystermans, Krampe, Swiderek, & Al-Rubeai, 2007; Yallop et al., 2003), presumably due to the energy being diverted towards product synthesis. Many studies have also reported notable increases in cell specific productivity and culture longevity when the production phase is performed at a lower culture temperature (typically 30 to 32 °C), related to the ensuing reduction or arrest of cell growth (Fogolin, Wagner, Etcheverrigaray, & Kratje, 2004; Kaufmann, Mazur, Fussenegger, & Bailey, 1999; Kaufmann et al., 2001; Kumar, Gammell, Meleady, Henry, & Clynes, 2008; Trummer et al., 2006a).

In the development of an efficient biphasic process, the timing of induction is one of the most crucial factors to optimize, as the final product yield will ultimately be determined by both the cumulative viable cell density and the cell specific productivity. These two factors must be carefully balanced, as they depend and impact on the culture environment, most notably substrate and toxic by-product concentrations. Indeed, the benefits of performing the induction at high cell concentrations can be partly or wholly negated by a reduction in cell specific productivity or a shorter duration of the production phase, as a result of decreased nutrient availability and/or waste metabolite accumulation. In particular, lactate and ammonia are well known inhibitors of both cellular growth and productivity, with adverse effects typically reported for lactate concentrations above 20 mM and ammonia levels as low as 2-3 mM (H. J. Cruz, Freitas, Alves, Moreira, & Carrondo, 2000; Glacken, 1986; S.S. Ozturk, Riley, & Palsson, 1992). It is thus instrumental to characterize how the conditions at induction will affect the cell's physiological state and the ensuing process productivity. While mammalian inducible expression platforms are becoming more and more available, comprehensive metabolic studies are still missing and needed to allow the rational optimization of biphasic cultures.

Towards this goal, the main objective of this work was to quantitatively assess the impact of different cell densities at induction on the primary metabolism and specific productivity of CHO cells in culture. To this end, we have employed a recombinant cell line harboring a cumate-inducible expression system (Mullick et al., 2006) that exhibits very low basal expression levels

in the repressed state and high expression upon induction with cumate, a small non-toxic molecule. Cells taken from the same batch culture at different stages of growth were re-suspended and induced in fresh medium, and the kinetics of growth, nutrient consumption and product formation were compared during the production phase. To gain more insights into the observed changes, two culture conditions corresponding to low and high cell density induction were further characterized by ^{13}C-metabolic flux analysis, whereby induced cells were grown in parallel cultures containing a mixture of ^{13}C-labeled tracers and the resulting mass isotopomer distributions of extracellular metabolites secreted by the cells (amino and organic acids) were measured by LC-QTOF-MS. The main intracellular fluxes were calculated along with confidence intervals and this allowed to analyze the cell metabolism in relation with the prevailing culture conditions and the measured cellular productivities. Such analysis is needed to guide the rational development of biphasic processes, in particular to support the design of a balanced and efficient feeding protocol post-induction.

5.2.3 Materials and Methods

5.2.3.1 Cell lines, medium and culture conditions

A recombinant CHO cell line, CHO-CUM2, was obtained from Viropro International Inc. (Montreal, Canada). The cell line stably expresses the reverse cumate transactivator described in Mullick et al. (Mullick et al., 2006) and produces a recombinant human anti-CD20 monoclonal antibody. In our study, we employed a custom serum- and protein-free, chemically defined SFM4CHO medium (Hyclone). This basal medium did not contain any glucose and glutamine, so as to facilitate the metabolic characterization and the isotopic tracer study described below. Before culturing the cells, the fresh medium was supplemented with 5mM glutamine (Hyclone), 30mM glucose (Sigma), and 0.05mg/ml dextran sulphate (Mw: 500000, Amersham Pharmacia Biotech). [1-^{13}C] glucose (99%) and [U-$^{13}C_5$] glutamine (98%) were purchased from Cambridge Isotope Laboratories (Andover, MA). Glucose and glutamine tracers were dissolved in deionized water at 650mM and 200mM, respectively, as a stock solution.

For the growth phase, recombinant cells were inoculated at 0.2×10^6 cells/mL in a 250 mL Erlenmeyer flask and grown in suspension with unlabeled substrates at 37°C in a 5% CO_2 and

95% humid atmosphere. From this batch culture, cells were harvested for four consecutive days (at 24, 48, 72 and 96h), centrifuged and re-suspended in fresh medium. All culture conditions were performed in duplicate 125 mL flasks. Harvested cells were not diluted and the inductions were thus carried out at increasing cell densities from day 1 to day 4. The medium exchange was performed so as to avoid early nutrient limitations, especially for high cell density cultures, while also minimizing isotopic tracer dilution effects caused by the presence of residual unlabeled glucose/glutamine and by the previous accumulation of unlabeled extracellular metabolites. In cultures seeded with cells harvested on day 2 and day 3, the inductions were done in medium containing [1-^{13}C] glucose and [U-^{13}C] glutamine. 1 µg/mL cumate was added to each flask to trigger the protein expression and the temperature was shifted from 37°C to 30°C for the duration of the production phase. Supernatants were collected by centrifugation at 300 g for 5 min and samples were stored at -80°C for subsequent analysis.

5.2.3.2 Quantification of cell density and metabolites

Samples from cell cultures were taken daily and monitored for viable cell density. When the cell density was high, samples were diluted with phosphate-buffered saline (PBS). Culture samples were mixed with trypan blue and cell numbers were counted using a hemacytometer and a standard light microscope. Glucose, lactate, and glutamine concentrations were measured off-line using a YSI 2700 Biochemistry Analyser (Yellow Springs, OH). Extracellular amino acid concentrations were determined on an Agilent 1290HPLC system (Agilent technologies, Quebec, Canada) coupled to an Agilent 6460 triple quadruple mass spectrometer (Agilent technologies, Quebec, Canada). The underivatized amino acids were separated by a 2.1x150mm ZICTM-Hilic column (3.5um, 200A, PEEK) (Merck SeQuant) and 2.1x20mm ZICTM-Hilic guard column (5um, 200A, PEEK) (Merck SeQuant) at a temperature of 35^{o}C and at an injection volume of 5uL. The mobile phase buffer contained 20mM $HCOONH_4$ at pH 4. The mobile phase A was 10% of the mobile phase buffer in water, and the mobile phase B was 10% of the mobile phase buffer in ACN. The mobile phase B linearly decreased from 90% to 35% in 19min, then was increased to 90% in one min and hold at 90% for 15min at a flow rate of 0.1ml/min.

5.2.3.3 Analysis of ^{13}C-labeling patterns

The ^{13}C fractional enrichment of lactate, aspartate, alanine and glutamate in the samples was measured on an Agilent 1100 series LC-MSTOF (Agilent technologies, Quebec, Canada). First, 200µL of supernatant samples were deproteinized by adding 1mL cold acetone (-20^0 C) and then were vortexed strongly. After centrifugation at 20,000g for 5 min, the solutions were filtered and evaporated in vacuo. After that, 400 µL of water was added to the samples. The analysis was done in negative electrospray mode without derivatization using a Kinetex HILIC Phenomenex column, 100 x 4.6mm and 2.6um particle size. The eluants used were 5mM ammonium formate (in water) and acetonitrile containing 0.1% formic acid. The gradient was in HILIC mode and went from 90% to 50% ACN with a total run time of 20 minutes. The mass isotopomer distributions of α-ketoglutarate and succinate were analyzed on a UPLC-MS/MS (Agilent, Quebec, Canada) equipped with a 1290 infinity binary pump, an autosampler, a column controller and a 6460A triple quad mass spectrometer. 20uL of supernatant sample were filtered through a 0.22 µm PTFE filter (Millipore, Ontario, Canada) before injection. Organic acids were separated on a Hypercarb column (100*2.1 mm, 5 µm) and a Hypercarb pre-column (2.1*10, 5 µm) (Thermo Fisher, Ontario, Canada) with mobile phase A: 20mM ammonium acetate at pH 7.5, and mobile phase B: 10 % (v/v) methanol in water at a flow rate of 0.3 mL/min. The mobile phase gradient was: 10% A from 0 to 5 min, linear gradient from 10 to 20% A from 5 to 10 min, linear gradient from 20 to 100% A from 10 to 20 min, 100% A from 20 to 30 min, linear gradient from 100 to 10% A from 30 to 32 min and, finally, 10% A from 32 to 40 min. The negative electrospray ionization model was selected for the analysis with an Agilent Jet Stream source. The mass spectrometer operation conditions were set as follows: gas temperature 300^{o}C, gas flow rate 7L/min, nebulizer pressure 40 psi, sheath gas temperature 300^{o}C, sheath gas flow 12L/min and capillary voltage -3.5kv.

5.2.3.4 Quantification of monoclonal antibody

Monoclonal antibody titers were measured by an enzyme-linked immunosorbent assay (ELISA). First, a goat anti-human IgG1 (H+L) solution (Jackson ImmunoResearch) diluted to 2.5 µg/ml in

50mM sodium carbonate (Fischer Scientific) was added to 96-well plates (Costar) and incubated at 4°C overnight. Then, blocking of non-specific sites was carried out by adding a PBS solution containing 1% casein. After incubation for 1h at 37°C, either samples or standards diluted in PBS-casein were added in triplicate and incubated for 1h at 37°C. The wells were then incubated with 1/10,000 diluted peroxidase-conjugated AffiniPure gragment goat anti-human IgG (Jackson ImmunoResearch) for 1h at 37°C. After each of the previous steps, the wells were washed three times with PBS-Tween buffer (PBS, 1% Tween 20). Finally, the reaction was revealed by addition of 3,3′,5,5′-Tetramethylbenzidine (TMB) (Sigma) and stopped after 10-15 minutes by adding 1N hydrochloric acid. The absorbance at 450 nm was measured using a Victor^3 V microplate reader (Perkin-Elmer).

5.2.3.5 Determination of specific rates

To obtain reliable specific rate estimates, logistic equations were used to model the viable cell density, as well as nutrient and product concentration profiles (Chetan T Goudar et al., 2005; Olivier Henry et al., 2008). Glutamine uptake rates were corrected to account for the spontaneous decomposition of this substrate in the culture medium, which was experimentally determined under the culture conditions used in this work, yielding a first-order kinetic constant of 0.03 d^{-1}. Average antibody cell specific productivities were determined from the slopes when the integral of viable cell concentrations were plotted against the corresponding antibody concentrations (P. W. Sauer et al., 2000).

5.2.3.6 Metabolic network and intracellular flux evaluation

For intracellular flux analysis, a detailed metabolic network was constructed based on previous models for CHO cells (Woo Suk Ahn & Antoniewicz, 2011; Ghorbaniaghdam et al., 2013; C. Goudar et al., 2010; Zamorano et al., 2009). The metabolic network includes glycolysis, the oxidative and non-oxidative branches of the pentose phosphate pathway, the TCA cycle and anaplerotic reactions. Reversible reactions were separated into forward and backward fluxes

constrained to be non-negative. To account for biosynthetic requirements, the model includes simplified reactions for the biomass and antibody synthesis, which were established from published average biomass/production composition data (Quek et al., 2010) and by assuming a dry cell weight of 0.350 mg/10^6 for CHO cells (Woo Suk Ahn & Antoniewicz, 2011; Altamirano et al., 2001). A detailed list of the biochemical reactions and their corresponding C atom transitions can be found in Table A1 (Appendix A). The inputs used for flux estimation were the measured extracellular rates, as well as the labeling patterns of three secreted extracellular amino acids (aspartate, alanine and glutamate) and three extracellular organic acids (lactate, succinate and α-ketoglutarate). Standard assumptions related to ^{13}C analysis of mammalian cells were employed (Woo Suk Ahn & Antoniewicz, 2011; Metallo et al., 2009; Munger et al., 2008) and details are provided in the supplemental material. All calculations were performed in Matlab using the elementary metabolite unit network decomposition method (M.R. Antoniewicz et al., 2007). The constrained nonlinear least-squares regression was performed using the built-in function "fmincon" to minimize the sum of weighted squared residuals (WSR) between measured and simulated variables. The minimization was repeated ten times with random initial estimates of free fluxes to ensure the attainment of a global optimal solution. Validation of the fits was performed based on a standard chi-square goodness-of-fit test and 95 % confidence intervals for the intracellular fluxes were evaluated using the method outlined in Antoniewicz et al.(Antoniewicz et al., 2006). For statistical comparison of the corresponding fluxes obtained under two conditions (i.e. induction at low and high cell densities), unpaired two-tailed Student's t-tests were performed in Excel.

5.2.4 Results

In order to investigate and quantify the effects of induction conditions on the metabolism and productivity of CHO cells, cultures were induced in fresh medium and under mild-hypothermia conditions after being seeded with cells taken from a single uninduced batch culture at various stages of growth. The resulting induced cultures were analyzed at two levels. First, extracellular measurements were used to evaluate and compare the main kinetic rates of cellular growth, nutrient consumption, metabolite production and antibody formation post-induction. Second, a

more refined metabolic characterization was performed by quantifying the main intracellular fluxes with the aid of isotopic tracers and mass spectrometry measurements.

Table 5-1: Kinetics of growth and product formation for different induction times

Time of induction relative to growth phase	**Day 1**	**Day 2**	**Day 3**	**Day 4**
Cell density at induction (10^6cells/mL)	0.60±0.05	1.2±0.1	3.4±0.3	4.7±0.5
Cell specific growth rate post-induction (d^{-1})	0.35±0.05	0.25±0.04	0.17±0.02	0.18±0.03
Max. cell density post-induction (10^6cell/mL)	4.3±0.2	5.0±0.3	7.1±0.7	8.1±0.4
Final MAb concentration (mg/L)	136±20	157±24	81±12	63±9
Avg. cell specific productivity (pg/cell.d)	4.0±0.8	6.0±1.2	2.0±0.5	1.5±0.3

5.2.4.1 Impact of increasing cell densities at induction on cellular kinetics

The growth curve for the uninduced batch culture, which was run at 37°C, is shown in Figure 5-1A along with the different harvest points. The first two harvest points corresponded to relatively low densities (<1.2x106 cells/mL) with cells taken in their early exponential phase, while for the subsequent harvests, the cells were in their mid-exponential and early-stationary phases, respectively. Cell viability was nonetheless greater than 95 % in all the cultures which were induced to initiate the production phase. The resulting cell concentration profiles post-induction are shown in Figure 5-1B and the corresponding glucose, glutamine, lactate and antibody profiles are depicted in Figures 5-1C to 5-1F. The main kinetics of growth and product formation are summarized in Table 5-1 for all four induction conditions. Cultures induced at low cell densities exhibited relatively similar growth profiles (Figure 5-1B), reaching maximum cell densities of 4 to 5x106 cells/mL in 8 to 9 days, with average cell specific growth rates of 0.25 to 0.35 d-1 (see Supplementary Figure 5-5). The inductions performed at higher cell densities reached cell concentrations that were twice as high and the maxima were attained in 4 to 5 days, but exhibited

reduced specific growth rates (0.17 d-1 and 0.18 d-1, respectively) and cell viability started to decline rapidly after only 5 to 6 days post-induction. As shown in Figure 5-1F, the corresponding final MAb titers were significantly decreased in these cultures, reaching only 40 to 50 % of the maximum MAb concentrations achieved with lower cell densities at induction, albeit in a shorter time (6-7 days vs 11-13 days). The average cell specific antibody production rate was approximately 3-fold higher in low cell density cultures.

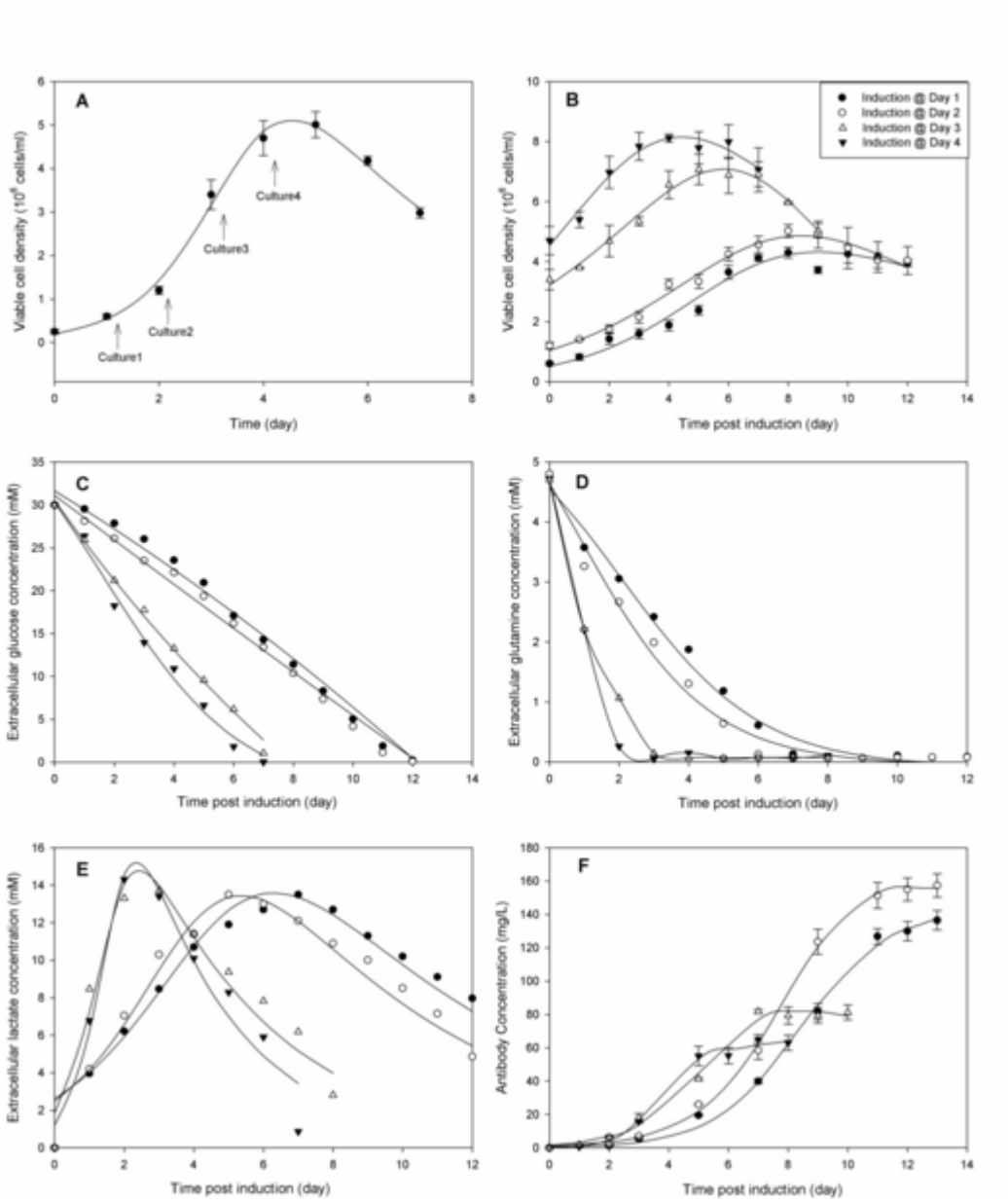

Figure 5-1: (A) Viable cell concentration profile during the growth phase at 37°C in a batch culture. Arrows indicate the times at which cells were harvested, re-suspended in fresh medium and induced at a temperature of 30°C. Viable cell density (B), glucose (C), glutamine (D), Lactate (E) and antibody concentration profiles post-induction.

Error bars represent the standard error of duplicate experiments. Open symbols correspond to culture conditions that were performed with isotopic tracers for conducting a comparative 13C-metabolic flux analysis.

Table 5-2 presents the cell specific uptake and metabolite secretion rates evaluated at 48h post-induction for all four conditions. As shown in Figure 5-1C, low residual concentrations of glucose were only observed at the end of the cultures, whereas glutamine was depleted 4 days post-induction in the cultures induced at high cell density. The cell specific glucose uptake and lactate production rates at 48h post-induction were both found to decrease with increasing cell density (Table 5-2). In addition, while the yield of lactate produced on glucose consumed was about 2 for low cell concentrations, this ratio decreased to 0.9 in higher cell density cultures. This is indicative of a significant change in nutrient utilization efficiency by the cells, most likely linked with the different prevailing culture conditions (e.g. the reduced nutrient availability). Moreover, in the high cell density cultures, lactate reached a maximum on day 2 or 3 and was consumed thereafter. As evident from Figure 5-1E, this metabolic shift seemed to coincide with the (near) depletion of glutamine in the culture environment. Greater cell specific glutamine uptake rates were also observed in cultures induced at low cell density and these rates decreased by up to 50 % for inductions at elevated cell concentrations. The utilization rates of other amino acids were also examined (Table 5-2) and, in all the cultures, most of them were consumed by the cells except for alanine, glycine, glutamate and aspartate that were found to be accumulated in the culture medium. When comparing the different induction conditions, the overall trend is a reduction of the amino acids uptake/secretion rates with increasing cell density at induction.

Even though all inductions were carried out in fresh medium (i.e. with similar initial nutrient levels), taken together, the measured kinetic rates clearly indicated that cells reached distinct metabolic states two days post-induction, depending on the prevailing cell density during production and presumably related to nutrient availability, toxic waste levels or cell age effects. In turn, these different physiological states impacted the overall productivity of the cultures, emphasizing the need to characterize the cell metabolism in relation with process conditions to further improve the yields.

Table 5-2: Cell specific uptake/secretion rates (in pmol/cell.d) measured 48h post-induction

	Low cell density inductions				**High cell density inductions**			
Time of induction	**Day 1**		**Day 2**		**Day 3**		**Day 4**	
Glucose	-1.50	±0.14	-1.36	±0.14	-1.16	±0.10	-1.00	±0.10
Lactate	3.02	±0.25	2.79	±0.28	1.07	±0.11	0.90	±0.10
Glutamine*	-0.40	±0.03	-0.45	±0.06	-0.28	±0.07	-0.20	±0.04
Phenylalanine	-0.01	±0.01	-0.01	±0.01	-0.01	±0.01	0.00	±0.01
Threonine	-0.05	±0.01	-0.03	±0.01	-0.01	±0.01	0.00	±0.01
Leucine/Ileucine	-0.21	±0.04	-0.20	±0.02	-0.08	±0.01	-0.06	±0.02
Methionine	-0.02	±0.01	-0.02	±0.01	-0.02	±0.01	-0.01	±0.01
Tyrosine	-0.02	±0.01	-0.01	±0.01	-0.02	±0.01	-0.02	±0.01
Valine	-0.04	±0.01	-0.03	±0.01	-0.03	±0.01	-0.01	±0.01
Proline	-0.06	±0.01	-0.05	±0.01	-0.02	±0.01	-0.02	±0.01
Alanine	0.15	±0.02	0.11	±0.03	0.17	±0.05	0.21	±0.03
Glycine	0.11	±0.01	0.05	±0.01	0.02	±0.01	0.10	±0.01
Serine	-0.11	±0.01	-0.07	±0.01	-0.08	±0.01	-0.09	±0.01
Asparagine	-0.47	±0.05	-0.24	±0.03	-0.13	±0.03	-0.19	±0.03
Glutamate	0.22	±0.04	0.15	±0.03	0.15	±0.05	0.10	±0.03
Aspartate	0.18	±0.02	0.10	±0.02	0.10	±0.03	0.00	±0.02
Arginine	-0.13	±0.02	-0.09	±0.01	-0.02	±0.01	-0.02	±0.01
Lysine	-0.03	±0.01	-0.08	±0.01	-0.02	±0.01	-0.03	±0.01
Histidine	-0.07	±0.01	-0.03	±0.01	-0.01	±0.01	-0.03	±0.01

* After correction for spontaneous decomposition.

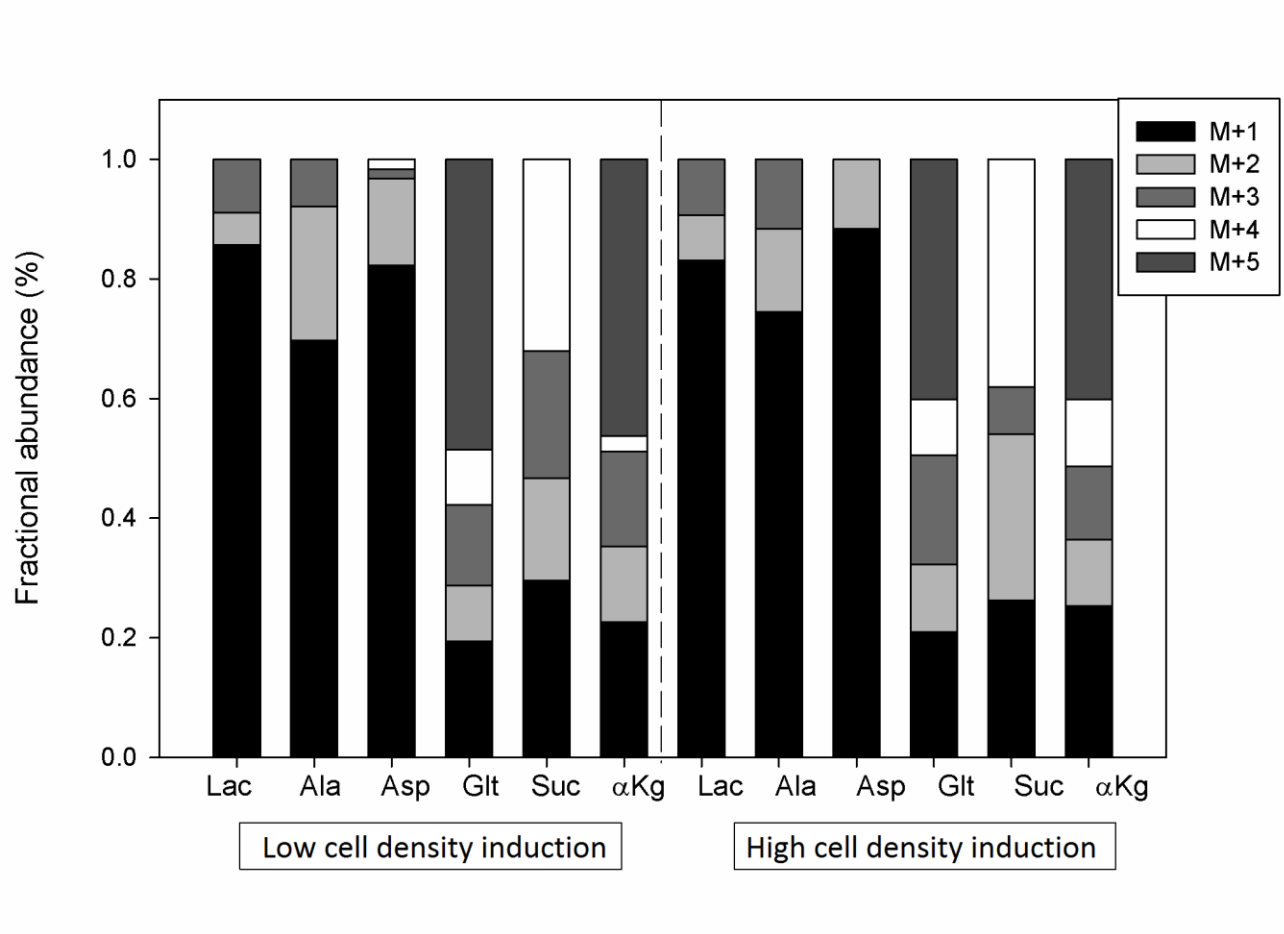

Figure 5-2: Fractional abundances of labeled mass isotopomers at 48h after inductions performed respectively at low and high cell densities, for the following metabolites: lactate, alanine, aspartate, glutamate, succinate and ketoglutarate. Cells were induced in fresh medium containing [1-^{13}C]- glucose and [U-$^{13}C_5$]- glutamine.

5.2.4.2 ^{13}C-metabolic flux analysis post-induction

As inferred from extracellular rate measurements, the metabolic activity of cells during the production phase is greatly affected by the cell density at induction. In order to shed more light into the underlying physiological changes, a comprehensive ^{13}C-metabolic flux analysis was performed to compare cultures induced respectively at low and high cell concentrations, corresponding to harvest points performed on day 2 and day 3 of the growth phase (Culture2 and Culture3 in Figure 5-1). For these two conditions, exponentially growing cells were transferred and induced into ^{13}C-tracer containing medium, and exponential growth was maintained for a minimum of 3 days post-induction, albeit at a lower rate due mainly to the temperature shift. At 48h post-induction, cell-free supernatant samples were collected and analyzed by mass spectrometry to measure the relative mass isotopomer distributions of six secreted metabolites, including three amino acids (alanine, aspartate and glutamate) and three organic acids (lactate, succinate and a-ketoglutarate). This period of time was chosen to ensure the attainment of pseudo-steady isotopic and metabolic state conditions, as well as to minimize isotopic tracer dilution effects from unlabeled biomass. Indeed, previous isotopic tracer studies conducted with mammalian cells have shown that isotopic steady-state conditions are typically attained within 24 hours (Olivier Henry & Durocher, 2011; Maier et al., 2008; Munger et al., 2008; Niklas et al., 2011). As shown in Figure 5-2 and consistent with the differences observed at the level of the cell kinetic rates (Table 5-2), cultures induced at low and high cell densities exhibited distinct labeling patterns for all the measured metabolites. These measured mass isotopomer distributions are reflective of the activity of the intracellular pathways and hence can provide both qualitative and quantitative information about cell metabolism. For example, the measured mass isotopomer distributions of alanine and lactate differed to some extent (Figure 5-2), even though both metabolites have pyruvate as their main precursor. Such apparent discrepancies can be due to tracer dilution from an unlabeled carbon source (e.g. free metabolites derived from protein or lipid turnover) or may suggest the presence of two distinct intracellular pools of pyruvate in the cytosol and the mitochondria (Peuhkurinen et al., 1983). The detection of fully labeled lactate, originating from [U-$^{13}C_5$] glutamine partial oxidation, was indicative of some pyruvate recycling from the TCA, e.g. via malic enzyme. Such information was thus taken into account in the development of the metabolic model (Table 5-3).

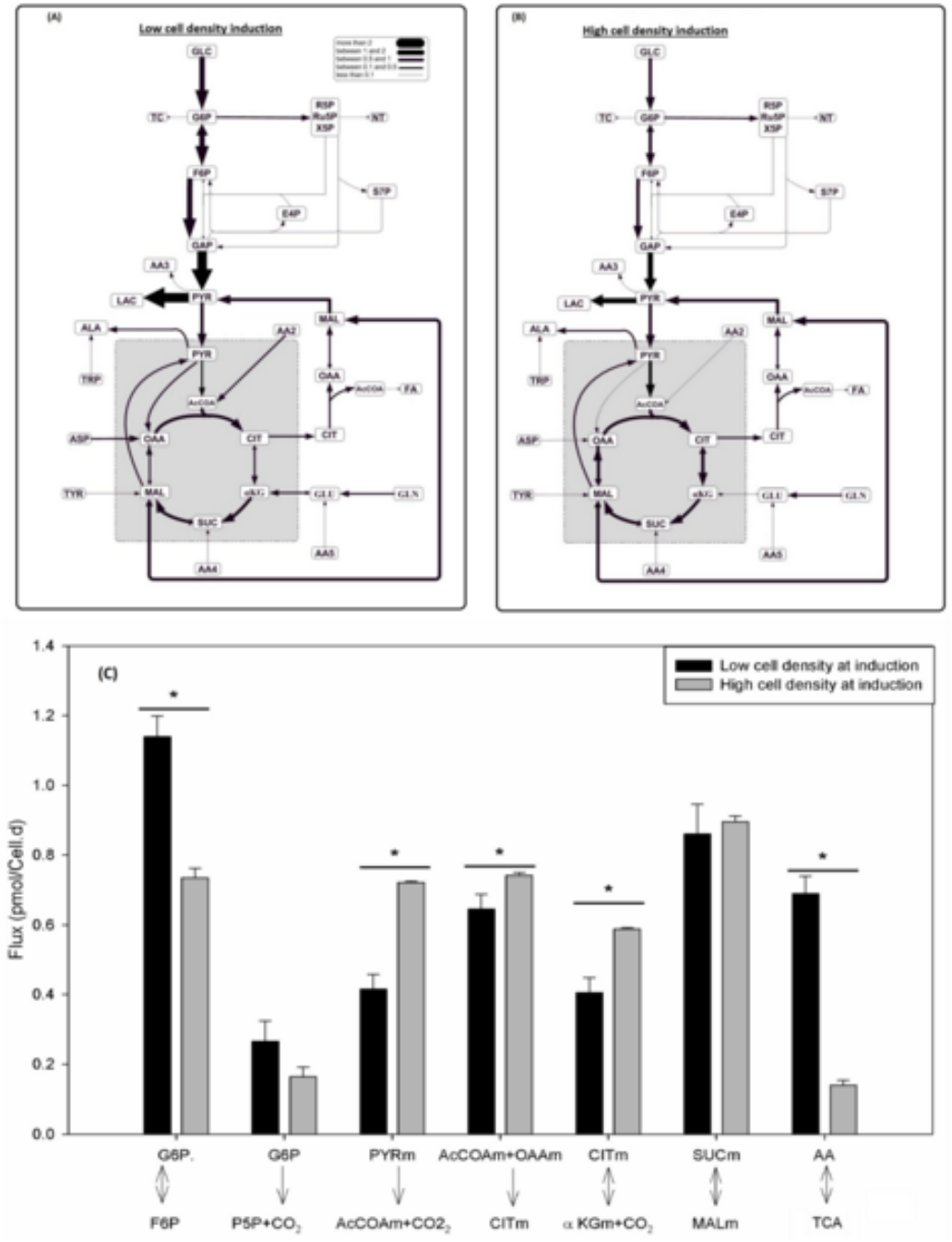

Figure 5-3: Metabolic flux maps 48h post-induction at low (A) and high (B) cell densities. (C) Comparison of key intracellular fluxes. Standard errors were calculated from the upper and lower bounds of the 95 % confidence intervals.

* indicates significance at $p<0.05$. Abbreviations: AA2 = Leu, Lys, Ile, Tyr, Trp, and Thr; AA4 = Val, Met, and Ile; AA5 = His, Arg, and Pro.

The measured mass isotopomer data and the specific uptake/production rates calculated at 48h post-induction were utilized to estimate the intracellular flux distributions. The model contained 19 free fluxes to optimize and since 24 independent mass isotopomer distributions were available for each induction conditions, the minimum and maximum allowable values for the variance-weighted sum of squared residuals (WSSR) were 1.1 and 11.1, respectively (chi-square test for 95% level of confidence with 5 degrees of freedom). The data and assumed metabolic network yielded statistically acceptable fits with WSSR values of 3.7 and 8.3 for low and high cell density conditions, respectively. The obtained flux maps are shown in Figure 5-3, along with the statistical significance of the observed differences. The complete flux distributions and the associated 95% confidence intervals are included as Supplementary Material (Table 5-4). For a number of key intracellular reactions, inductions performed at low and high cell densities yielded significantly different flux values (Figure 5-3C). These metabolic observations are further elaborated in the next section.

5.2.5 Discussion

For biphasic cultivation, the common approach consists in initially growing the cells to sufficiently high concentrations, while ensuring that they maintain high viability before the onset of the production phase. Hence, the induction is typically made when cells are still in their mid-exponential phase rather than at the maximum cell density (Bi, Shuttleworth, & Al-Rubeai, 2004; Kumar et al., 2008; Nam, Ermonval, & Sharfstein, 2009; Trummer et al., 2006b). Both the cumulative viable cell density and the cell specific productivity need to be balanced in order to maximize product titers and it is thus crucial to determine an optimal induction time. The goal of this study was to quantitatively assess the effects of the timing of induction on both MAb productivity and cell metabolism, so as to provide a sound basis for directing process improvement efforts. At the time of induction, the temperature was shifted to 30°C as mild-hypothermia conditions are commonly associated with increased cellular productivity and extended culture longevity due to cell arrest in G0/G1 phase (Sunley & Butler, 2010). The temperature shift caused a significant reduction in the cell specific growth rate for all the inductions, but this decrease was more pronounced with increasing cell densities, even though the cell viability was initially high in all the cultures. This behavior is not specific to biphasic

cultures with temperature shift, as a similar cellular growth reduction was reported for hybridoma cells inoculated at increasing inoculum age (Martial, Dardenne, Engasser, & Marc, 1991). In our experiments, the lowest growth rate observed during the production phase corresponded to cells harvested from late exponential/early stationary phase. It is thus likely that growth kinetics post-induction are determined by the levels of nutrients and waste metabolites present, but also by the physiological state of the cells prior to the harvest and the magnitude of the sudden change in environmental conditions resulting from the fresh medium exchange. In addition, high cell densities could not be maintained for more than 4 to 6 days post-induction, most likely due to a nutrient limitation as the decrease in cell viability coincided with glutamine depletion. Such early reduction in cell viability is obviously not desirable as proteolytic degradation may eventually hamper the stability and/or quality of the product (M. Yang & Butler, 2000). The cultures induced at high cell concentrations also had significantly reduced specific antibody productivity and, despite greater cell numbers, yielded lower final antibody titers. The presence of an optimal shift time with respect to culture productivity was also demonstrated in the case of CHO cells expressing a recombinant glycoprotein (Fox et al., 2004). Taken together, these results emphasized the need to balance both factors (biomass concentration and cell specific productivity) in order to maximize the volumetric yield. Given that cell growth was slowed but not fully arrested upon induction at low temperature, the growth phase should not simply aim at maximizing the biomass content, but should maintain the cells in a favorable productive metabolic state. Decreased cellular specific productivity with increasing cell densities have been previously reported, notably in perfusion cultures, and this apparent “cell density effect” was speculated to be related to the reduced availability of key nutrients in the culture environment (Craig Seamans & Hu, 1990; Zeng, 1996). In our cultures, glutamine was likely one of the key limiting factors considering that this substrate is both an important energy source for mammalian cells and one of the major building blocks for cellular and recombinant protein synthesis (Neermann & Wagner, 1996).

The kinetics of nutrient uptake and metabolite formation were also significantly affected by the cell density at induction. Increasing the cell concentration led to an overall decrease in the uptake rates of glucose and most amino acids. This may be related in part with the reduction in cellular growth observed, but was also due to the lower concentrations of these nutrients at 48h post-induction. Indeed, the metabolism of mammalian cells tends to become increasingly efficient as the residual substrate concentrations are small in the culture environment, and this is at the basis of common fed-batch strategies to minimize the formation of ammonia and lactate (T.A. Bibila & D.K. Robinson, 1995). A clear metabolic shift towards lactate consumption was observed in all the cultures, and appeared to coincide, or slightly precede, the time of glutamine depletion and the cessation of net cell growth. This is a common behavior reported for CHO cells in culture (Altamirano et al., 2006; Zagari et al., 2013), although it has not always been correlated directly with amino acid depletion (Mulukutla et al., 2012). This metabolic change occurred nonetheless more rapidly when the cells were induced at high cell density and thus, in this case, an early shift towards lactate consumption seems to be an indicator of poor process productivity. Even prior to the exhaustion of glutamine and the onset of lactate consumption, the measured kinetic rates 48h post-induction indicated that the cultures were already in distinct metabolic states as a result of being harvested and induced at different stages of cell growth.

The differences found in extracellular rate measurements for increasing cells densities at induction were further examined at the intracellular level by conducting a comparative ^{13}C-metabolic flux analysis. This approach is increasingly being used for the in-depth metabolic characterization of cultivated mammalian cells, as it allows the reliable quantification of central carbon metabolism (W. S. Ahn & Antoniewicz, 2012; Zamboni, 2011). In turn, this provides invaluable information to enable the targeted optimization of cell cultures, both at the cellular and process levels. When cells were induced at high density, the main glycolytic fluxes were significantly reduced (Figure 5-3), as could be inferred from the observed reduction in glucose uptake rate. However, extracellular rates alone do not allow determining the split between glycolysis and the pentose phosphate pathway (PPP), which is producing building blocks for nucleotides and is also the main source of cytosolic NADPH in mammalian cells. The latter is notably essential in the cell's anabolism, mainly in the synthesis of amino acids and fatty acids. In conventional metabolic balancing studies, it is usually assumed that PPP is only responsible

for nucleotides synthesis (Niklas & Heinzle, 2012), that is, the activity of transaldolase and transketolase is ignored and only the oxidative branch is considered (Martens, 2007). The use of labeled substrates alleviates the need of such questionable assumptions. Our analysis revealed that the oxidative branch of the pentose phosphate pathway was lower for the high cell density cultures (0.16 pmol/cell.d vs 0.26 pmol/cell.), although 95 % confidence intervals are overlapping. For both low and high cell density inductions, this flux corresponded approximately to 18 % of the total glucose uptake rate being channeled via PPP, which is in line with most previous isotopic investigations of mammalian cells in culture (H. P. Bonarius et al., 2001; C. Goudar et al., 2010), although it should be emphasized that these studies were all performed at 37°C. Recent studies have also reported that the PPP can be significantly enhanced when the cells are in the stationary phase, thereby generating more NADPH presumably to counteract oxidative stress (Woo Suk Ahn & Antoniewicz, 2011; Sengupta et al., 2011; Tuttle, Stamato, Perez, & Biaglow, 2000). However, in the present study, even the high cell density cultures displayed exponential growth for the first few days post-induction and such enhancement in PPP activity was not observed.

The main metabolic fluxes around the pyruvate branch point were markedly different for the two conditions under investigation. In cultures induced at low cell density, only about 17 % of the pyruvate intracellular pool entered the TCA, while 80 % was converted to lactate via lactate dehydrogenase, and the remaining fraction was converted into amino acids. This inefficient utilization of glucose, referred to as “overflow metabolism”, is commonly observed in animal cell systems under substrate excess conditions (Amribt, Niu, & Bogaerts, 2013; Doverskog, Ljunggren, Öhman, & Häggström, 1997; J. Ljunggren & Haggstrom, 1992), such as those prevailing at the beginning of batch cultures. In contrast, at high cell density, the fluxes were more evenly distributed between lactate and the TCA (59 % vs 41 %). Interestingly, this distribution of fluxes at the pyruvate branch point is very similar to the one previously reported for CHO cells grown in high cell density perfusion cultures (C. Goudar et al., 2010). For cultivated mammalian cells, the entry of pyruvate into the TCA cycle occurs mainly via pyruvate dehydrogenase (PDH), while the pyruvate carboxylase (PC) flux is often considered negligible (Quek et al., 2010). However, flux through this pathway can only be determined with the aid of labeled tracers. Previous recent isotopic studies on CHO cells have shown that this flux is indeed

active, albeit at a lower rate than PDH (Woo Suk Ahn & Antoniewicz, 2011; C. Goudar et al., 2010; Sengupta et al., 2011). Our analysis revealed that the anaplerotic conversion of pyruvate to oxaloacetate via PC accounted between 5 % and 27 % of the total pyruvate entering the TCA, with the greater contribution corresponding to low cell density conditions. Together with PC, the conversion of glutamate to α-ketoglutarate and the aspartate transaminase reaction were the other two significant anaplerotic pathways observed. Those pathways serve to replenish intermediates leaving the TCA cycle, mostly citrate for lipid synthesis, and were significantly more active in cultures induced at low cell density (Figure 5-3). This can be attributed, at least in part, to the varying anabolic needs, which were reduced at high cell density given that the cell specific growth rate was 30 % lower.

On the whole, amino acids accounted for approximately 60 % of the total carbon input into the TCA for cells induced at low cell concentration, whereas this fraction was reduced down to only 20 % at higher cell densities. In the latter case, this is compensated by a greater pyruvate influx into the TCA. While a high proportion of pyruvate originated directly from glycolysis, pyruvate recycling from the TCA was also significant, accounting for an estimated 17 to 22 % of the total pyruvate pool, through the conversion of malate via malic enzyme. Together with the oxidative branch of the PPP, this pathway is a major source of reducing agent for the cells. In fact, NADPH formation was distributed almost evenly between these two pathways. The estimated NAPDH production rates were 1.1 and 0.57 pmol/cell.d for the low and high cell density cultures, which is consistent with the reduction in growth rate and the resulting decrease in biosynthetic requirements of the latter.

Overall, the comparative ^{13}C-metabolic flux analysis performed in this worked allowed us to characterize the main physiological changes resulting from two distinct conditions at induction. While glucose utilization efficiency is increased in high cell density induction, thereby reducing the specific lactate production rate, it seems to be compensating for the decreased catabolic rates of amino acids. Moreover, this metabolic state is associated with a lower overall productivity and culture longevity. Further improvement in process productivity can thus only be expected if one

could maintain a desired flux distribution at higher cell concentrations by enriching the culture medium at induction or by feeding the cultures post-induction. The latter would most likely be preferable so as to avoid the build-up of toxic by-products and could be rationally defined based on the calculated fluxes (L. Xie & D.I.C. Wang, 1996). As mentioned previously, it is possible that in high cell density cultures, cells already reached distinct metabolic states even prior to their induction. Maximizing product yields may thus require to initiate fed-batch operation prior to the production phase so as to always maintain suitable nutrient and waste metabolite levels. Towards this goal, this study could aid in the development of dynamic models (Amribt et al., 2013; Ghorbaniaghdam et al., 2013; R. P. Nolan & Lee, 2012; Provost & Bastin, 2004), which are greatly needed tools for process optimization and control. In particular, such model could guide the establishment of an optimal feeding profile for a fed-batch process.

It should also be emphasized that the metabolic analysis in this work was confined to the exponential growth period immediately following the induction. It is evident that a significant flux rewiring occurred at a later stage of the production phase, most notably when lactate was consumed and/or as some nutrients reached limiting levels. However, in practice, process operation strategies should be devised so as to delay the attainment of such physiological state and consequently be determined based on the conditions prevailing at the beginning of the induction phase, i.e. prior to any limitation.

5.2.6 Conclusion

In this work, we have analyzed the impact of the timing of induction on the performance of a biphasic cell culture process. The greatest product yields were achieved when cultures were induced at low densities with exponentially growing cells. In contrast, and even with a complete medium exchange at the time of induction, high cell density cultures exhibited reduced culture longevity and cell specific productivity, most likely attributable to reduced nutrient availability.

The decreased production rates were correlated with differences in some intracellular fluxes of primary metabolism, which could help to identify reliable physiological indicators of cell productivity. It is likely that performing additional nutrient feeding prior to and during the production phase would allow to overcome, at least in part, the early limitations encountered at

elevated cell concentrations. To this end, the comprehensive metabolic characterization performed in this work could also help guide the development of an efficient feeding strategy pre- and post-induction.

AKNOWELDGMENTS

The authors wish to acknowledge Dr. Alexandra Furtos from Université de Montréal for ^{13}C QTOF-LCMS analysis, Jingkui Chen from Ecole Polytechnique for amino acids analysis, as well as Dr. Patrick Benoist and Dr. Patrick Daoust of Viropro Internal Inc. (Montreal, Canada) for providing the cell line employed in this study.

Table 5-3 : Biochemical reactions and their corresponding C atom transitions

Biochemical Reaction	***Carbon Transition***
Glycolysis	
GLC → G6P	abcdef = abcdef
G6P ↔ F6P	abcdef = abcdef
F6P → 2 GAP	abcdef = cba + def
GAP → PYR	abc = abc
PYR → LAC	abc = abc
PYR → PYRm	abc = abc
Pentose Phosphate Pathway	
G6P → P5P + CO_2	abcdef = bcdef + a
2P5P ↔ S7P + GAP	abcde + fghij = abfghij + cde
P5P + E4P ↔ F6P + GAP	abcde + fghi = abfghi + cde
S7P + GAP ↔ F6P + E4P	abcdefg + hij = abchij + defg
TCA Cycle	
PYRm → AcCOAm + CO_2	abc = bc + a
AcCOAm + OAAm → CITm	ab + cdef = fedbac
CITm ↔ aKGm + CO_2	abcdef = abcde + f
aKGm → SUCm + CO_2	abcde = bcde + a
SUCm ↔ 0.5 MALm + 0.5 MALm	abcd = 0.5 abcd + 0.5 dcba
MALm ↔ OAAm	abcd = abcd
CITm + MAL → CIT + MALm	abcdef + ghij = abcdef + ghij
CIT → AcCOAc + OAA	abcdef = ed + fcba
MALm ↔ MAL	abcd = abcd
OAA ↔ MAL	abcd = abcd
PYRm + CO2 → OAAm	abc + d = abcd

MALm → PYRm + CO_2	abcd = abc + d
MAL → PYR + CO_2	abcd = abc + d
Amino acid reactions	
GLN → GLU	abcde = abcde
GLU ↔ aKGm	abcde = abcde
PYRm + GLU → ALA + aKGm	abc = abc
ASP + aKGm ↔ OAAm + GLU	abcd + efghi = abcd + efghi
ASN → ASP	abcd = abcd
PYR → SER, GLY	abc = abc
CYS → PYR	abc = abc
VAL, MET, ILE → SUCm	abcd = abcd
LEU, LYS, ILE, TYR, TRP, THR → AcCOAm	ab = ab
HIS, ARG, PRO → GLU	abcde = abcde
Biomass and Product Biosynthesis	
0.912 PROTEIN + 0.0315 P5P + 0.0379 G6P + 0.317 AcCOAc + 0.0151 GAP → BIOMASS	–
0.0585 ALA + 0.0226 ARG + 0.0449 ASN + 0.0365 ASP + 0.0252 CYS + 0.0400 GLN + 0.0518 GLU + 0.0660 GLY + 0.0229 HIS + 0.0329 ILE + 0.0630 LEU + 0.0608 LYS + 0.0128 MET + 0.0415 PHE + 0.0717 PRO + 0.0106 SER + 0.1056 THR + 0.0224 TRP + 0.0288 TYR + 0.0857 VAL → ANTIBODY	–
0.0811 ALA + 0.0510 ARG + 0.0389 ASN + 0.0485 ASP + 0.0196 CYS + 0.0435 GLN + 0.0522 GLU + 0.0727 GLY + 0.0193 HIS + 0.0438 ILE + 0.0763 LEU + 0.0771 LYS + 0.0187 MET + 0.0296 PHE + 0.0423 PRO + 0.0581 SER + 0.0522 THR + 0.0059 TRP + 0.0246 TYR + 0.0562 VAL → PROTEIN	–

5.3 Supplementary Material

5.3.1 Metabolic flux analysis: description and assumptions

- Cells are at metabolic and isotopic steady states after 48h of exponential growth in presence of labeled substrates. This assumption is supported by additional mass distribution measurements for lactate and amino acids performed at 72h (see Supplementary Figures 5-5 and 5-6), showing no significant variation compared to 48h. Previous investigations with mammalian cells have demonstrated that constant labeling is attained after such time (Olivier Henry & Durocher, 2011; Maier et al., 2008; Munger et al., 2008; Niklas et al., 2011).
- Two distinct pools of pyruvate are assumed to be present; alanine is considered to be derived from mitochondrial pyruvate, while lactate is generated from cytosolic pyruvate. A similar assumption was employed by Walther et al. (Walther et al., 2012) and Gaglio et al. (Gaglio et al., 2011) for describing the distinct labeling patterns of lactate and alanine in their analysis.
- Carbon dioxide is not balanced in the model and treated as an unlabeled reactant in carboxylation reactions.
- For the transport of metabolites between compartments, it is assumed that citrate is co-transported with malate via the citrate/malate shuttle, pyruvate transport occurs via the pyruvate carrier, malate is transported via the dicarboxylate carrier and aspartate is transferred via the glutamate/aspartate shuttle.
- Cofactor balances (e.g. ATP, NADH) were not included in the model.
- Succinate and fumarate are symmetric species and the scrambling of ^{13}C-label was taken into account.
- The incorporation of unlabeled carbon into the TCA resulting from the oxidation of fatty acids was considered negligible.
- Although the mass isotopomer distributions of extracellular ketoglutarate and succinate were measured and used for the flux estimation, their secretion rates were below 0.1 %

that of the glucose uptake rate and were thus assumed to be negligible relative to all other uptake/production rates.

- Tracer dilution effects resulting from unmeasured sources (e.g. protein/lipid turnover, unlabeled pools in the culture medium, subcellular compartmentalization effects) were accounted for by introducing dilution fluxes in the model as additional free fluxes to be optimized (Gaglio et al., 2011; Noguchi et al., 2009).

5.3.2 Supplementary tables

Table 5-4 : Calculated fluxes (in pmol/cell.d) and associated confidence intervals for cells induced at low and high cell densities, respectively. Dilution fluxes represent the percentage of the total metabolite pool diluted by unlabeled sources.

			Low cell density induction		High cell density induction	
Biochemical Reaction			Flux	Conf. 95%	Flux	Conf. 95%
GLC	→	G6P	1.44	[1.17 , 1.7]	0.92	[0.72 , 1.12]
LAC	→	LACex	2.64	[2.1 , 3.19]	1.11	[0.9 , 1.32]
G6P	→	Biomass	0.03	[0.02 , 0.04]	0.02	[0.01 , 0.03]
P5P	→	Biomass	0.02	[0.01 , 0.03]	0.01	[0.01 , 0.02]
AcCOAc	→	Biomass	0.24	[0.17 , 0.31]	0.15	[0.08 , 0.23]
GAP	→	Biomass	0.01	[0.01 , 0.01]	0.01	[0.01 , 0.01]
GLNex	→	GLN	0.39	[0.26 , 0.51]	0.31	[0.16 , 0.45]
His/Arg /Pro	→	GLU	0.08	[0.06 , 0.1]	0.01	[0.01 , 0.01]
VAL/MET/ ILE	→	SUCm	0.08	[0.06 , 0.1]	0.03	[0.02 , 0.05]
Leu/Lys /Ile/Tyr/ Trp/Thr	→	AcCOAm	0.23	[0.16 , 0.3]	0.02	[0.01 , 0.03]
ALA	→	ALAex	0.21	[0.15 , 0.27]	0.22	[0.12 , 0.32]
ASP	→	ASPex	0.12	[0.08 , 0.15]	0.11	[0.05 , 0.17]
GLUin	→	GLUex	0.19	[0.14 , 0.25]	0.18	[0.09 , 0.27]
PYR	→	AA3	0.08	[0.06 , 0.1]	0	[0 , 0]

ASNex	→	ASP		0.26	[	0.19	, 0.32	]	0.12	[	0.07	, 0.17]
ASXex	→	ASPex		1.61	[	1.22	, 2	]	1.67	[	1.28	, 2.06]
G6P	↔	F6P	net	1.14	[	1.08	, 1.31	]	0.74	[	0.64	, 0.75]
			exch	0	[	0	, inf	]	>600	[	0	, inf]
F6P	→	GAP + GAP		1.3	[	1.29	, 1.34	]	0.84	[	0.81	, 0.84]
GAP	→	PYR		2.68	[	2.66	, 2.7	]	1.72	[	1.69	, 1.75]
PYR	→	LAC		2.64	[	2.1	, 3.19	]	1.11	[	0.9	, 1.33]
G6P	→	P5P+CO		0.27	[	0.1	, 0.33	]	0.16	[	0.15	, 0.26]
P5P +P5P	↔	S7P + GAP	net	0.08	[	0.05	, 0.1	]	0.05	[	0.05	, 0.08]
			exch	0	[	0	, inf	]	6.41	[	0	, inf]
P5P + E4P	↔	F6P + GAP	net	0.08	[	0.03	, 0.1	]	0.05	[	0.05	, 0.08]
			exch	0	[	0	, 0.08	]	0	[	0	, 0.04]
S7P + GAP	↔	F6P + E4P	net	0.08	[	0.03	, 0.1	]	0.05	[	0.05	, 0.08]
			exch	6.29	[	0	, 0.07	]	0.3	[	0	, 0.6]
PYR	→	PYRm		0.51	[	0.42	, 0.62	]	0.84	[	0.81	, 0.98]
PYRm	→	AcCOAm + CO		0.42	[	0.35	, 0.52	]	0.72	[	0.71	, 0.72]
AcCOAm + OAAm	→	CITm		0.65	[	0.58	, 0.75	]	0.74	[	0.73	, 0.76]
CITm	↔	aKGm + CO_2	net	0.41	[	0.34	, 0.51	]	0.59	[	0.57	, 0.59]
			exch	15	[	1.55	, 15	]	0	[	0	, 0.93]
aKGm	→	SUCm + CO_2		0.78	[	0.67	, 0.98	]	0.87	[	0.76	, 0.91]
SUCm	↔	0.5MALm +0.5MALm	net	0.86	[	0.74	, 1.07	]	0.9	[	0.88	, 0.94]
			exch	27	[	1.87	, inf	]	>600	[	0	, inf]
MALm	↔	OAAm	net	0.35	[	0.07	, 0.6	]	0.69	[	0.41	, 0.76]
			exch	8.5	[	0.1	, inf	]	0.69	[	0	, inf]
MALm	↔	MAL	net	0.56	[	0.44	, 0.61	]	0.24	[	0.15	, 0.32]
			exch	27	[	0.57	, inf	]	>600	[	0	, inf]
CITm	→	CIT		0.24	[	0.17	, 0.31	]	0.15	[	0.08	, 0.23]
CIT	→	AcCOAc + OAA		0.24	[	0.17	, 0.31	]	0.15	[	0.08	, 0.23]
OAA	↔	MAL	net	0.24	[	0.17	, 0.31	]	0.15	[	0.08	, 0.23]

				exch	2.23	[	0	, inf	]	6.27	[0 , inf]
GLN	→	GLU			0.39	[	0.39	, 0.39	]	0.31	[0.31 , 0.31]
GLU	↔	aKGm		net	0.38	[	0.32	, 0.49	]	0.09	[0.08 , 0.12]
				exch	5.44	[	0	, inf	]	69.4	[0 , inf]
PYRm + GLU	→	ALA + aKGm			0.13	[	0.12	, 0.14	]	0.2	[0.2 , 0.2]
OAAm + GLU	↔	ASP + aKGm		net	0.14	[	0.14	, 0.14	]	0.01	[0.01 , 0.01]
				exch	0.48	[	0.04	, inf	]	0.25	[0.04 , inf]
PYRm + COin	→	OAAm			0.16	[	0	, 0.35	]	0.04	[0 , 0.13]
MALm	→	PYRm + CO			0.19	[	0.1	, 0.33	]	0.12	[0.06 , 0.23]
MAL	→	PYR + CO			0.56	[	0.5	, 0.69	]	0.24	[0.15 , 0.34]
GLU	↔	GLUin		net	0.09	[	-0.02	, 0.14	]	0.04	[0.01 , 0.07]
				exch	0.24	[	0	, 1.64	]	9.31	[0.36 , inf]
Dilution fluxes					(%)					(%)	
SUCdil	→	SUCex			0.44	[	0.43	, 0.51	]	0.29	[0.19 , 0.32]
aKGdil	→	aKGex			0.29	[	0.26	, 0.36	]	0	[0 , 0.03]
ALAdil	→	ALAex			0.37	[	0.32	, 0.39	]	0.09	[0.07 , 0.09]
GLUdil	→	GLUin			0.35	[	0.27	, 0.54	]	0.44	[0.33 , 0.48]
ASPdil	→	ASPex			0.93	[	0.89	, 0.96	]	0.94	[0.87 , 0.97]

5.3.3 Supplementary Figures

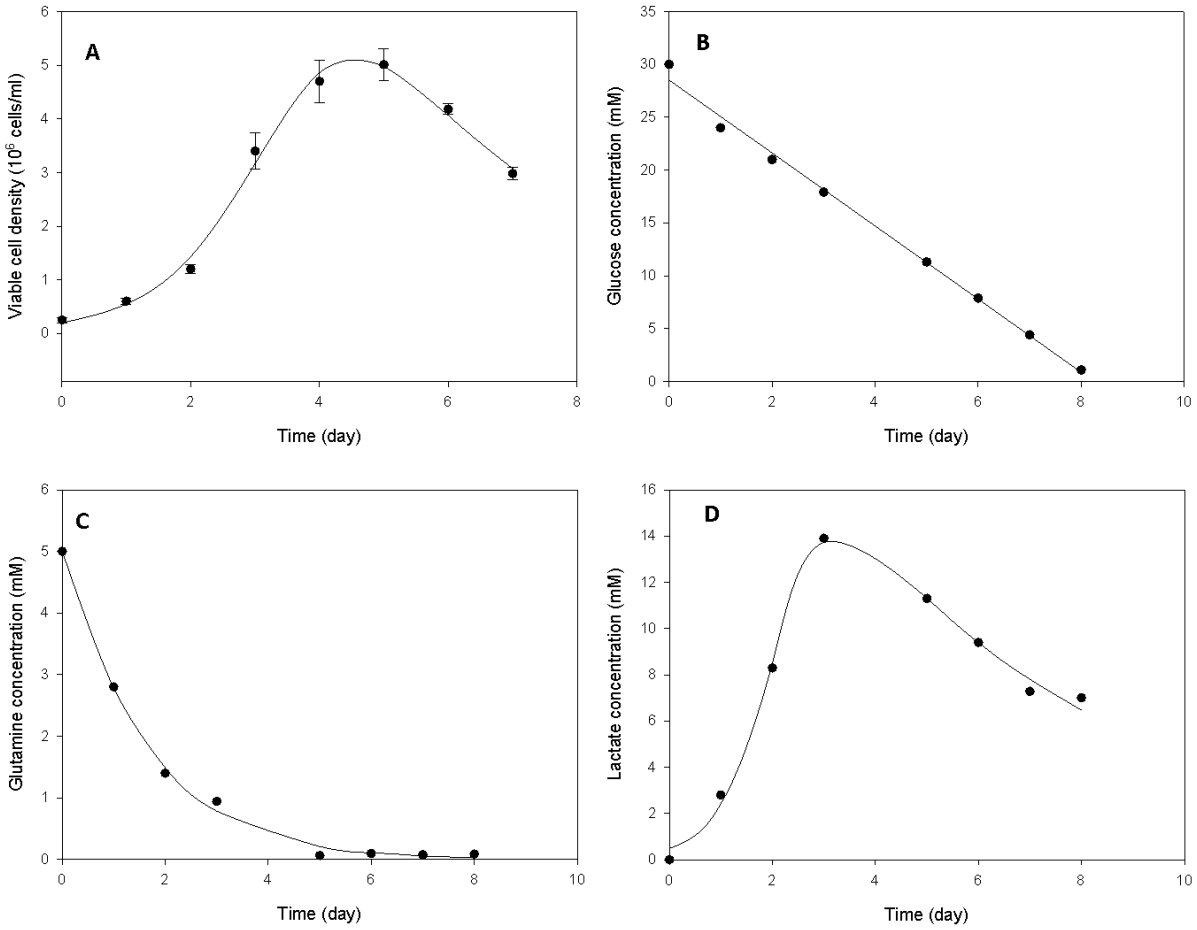

Figure 5-4 : Viable cell (A), glucose (B), glutamine (C) and lactate (D) concentration profiles during batch cultivation of CHO cells without induction

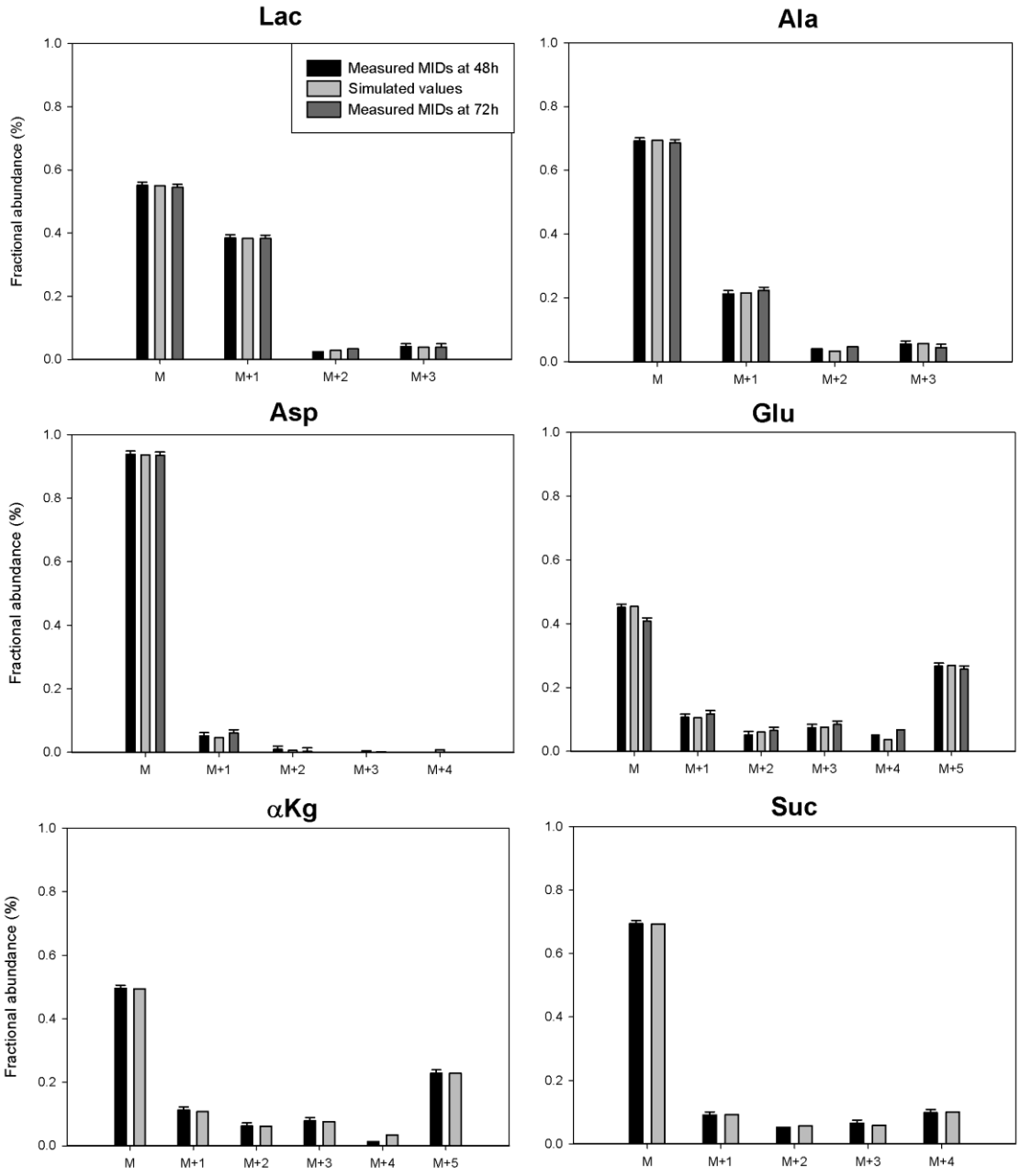

Figure 5-5 : Measured and fitted mass isotopomer distributions of lactate, alanine, aspartate, glutamate, succinate and ketoglutarate 48h post-induction at low cell density. Cells were induced in medium containing [1-^{13}C]- glucose and [U-$^{13}C_5$] Glutamine. Additional measurements for lactate and amino acids performed at 72h are also shown.

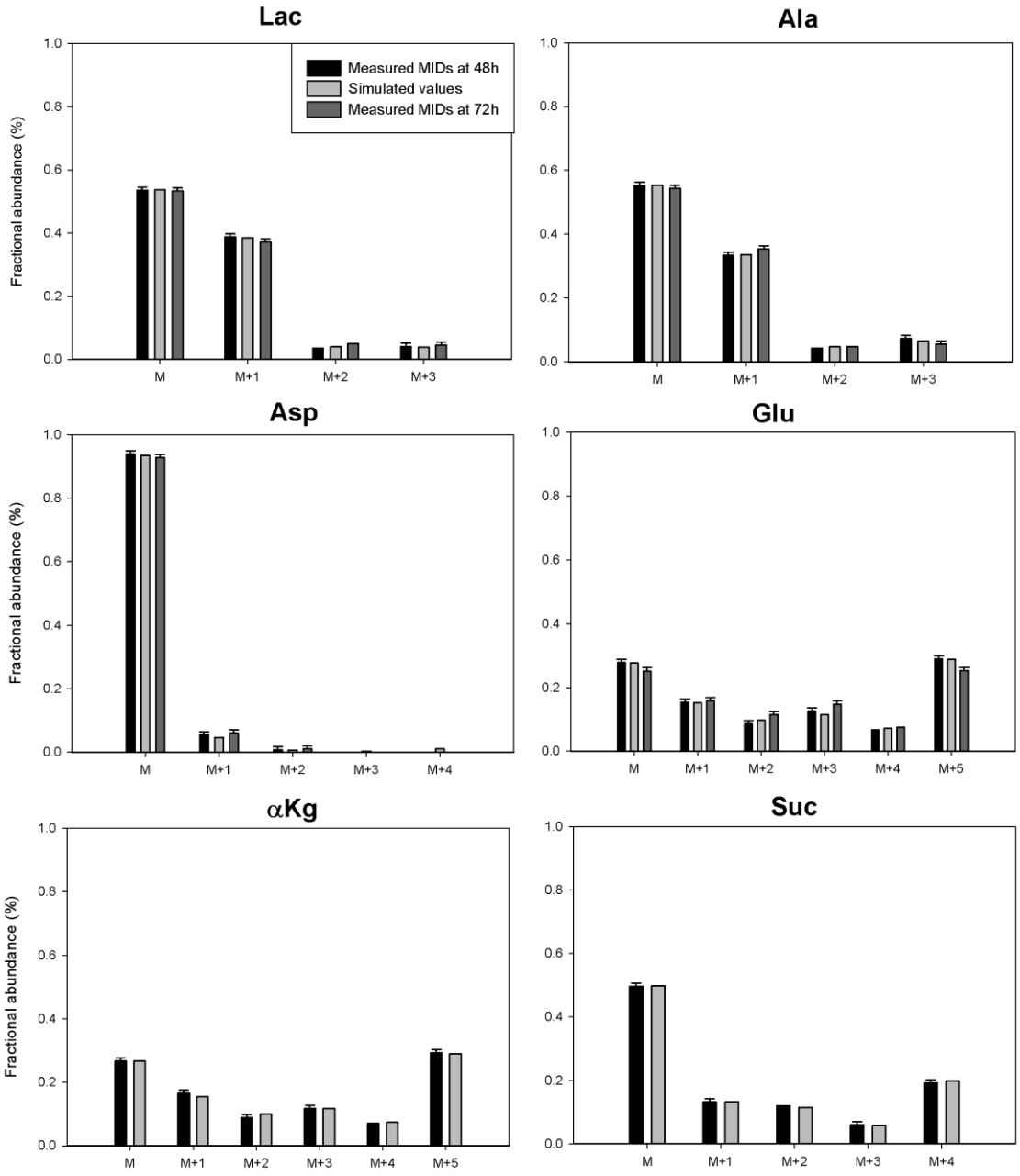

Figure 5-6: Measured and fitted mass isotopomer distributions of lactate, alanine, aspartate, glutamate, succinate and ketoglutarate 48h post induction at high cell density. Cells were induced in medium containing [1-^{13}C] glucose and [U-$^{13}C_5$] Glutamine. Additional measurements for lactate and amino acids performed at 72h are also shown.

CHAPTER 6 ELUCIDATING THE EFFECTS OF POST-INDUCTION GLUTAMINE FEEDING ON THE GROWTH AND PRODUCTIVITY OF CHO CELLS

6.1 Presentation of the article

This section contains the manuscript entitled "***Elucidating the effects of post-induction glutamine feeding on the growth and productivity of CHO cells***" which is being submitted for publication in "**Biotechnology Progress**". In this study, we first demonstrate that the application of a fed-batch strategy post-induction can successfully increase the product yield compared to simple batch mode. We also highlight a significant physiological impact of glutamine levels on cell metabolism and productivity. Depending on whether glutamine was present in excess or at limiting concentrations, despite achieving similar final product yields, the cultures reached two distinct metabolic states characterized by marked differences in terms of specific growth and productivity. While the cell specific productivity seems to be enhanced in glutamine-limited cultures, this benefit is offset by the lower cell concentrations attained. We thus conducted ^{13}C labeling experiments in semi-continuous cultures operated at respectively high and low glutamine concentrations. The resulting distinct intracellular flux maps can be associated with metabolic states favoring either cell proliferation or recombinant protein expression. As such, they can provide a sound basis for further fed-batch process development.

6.2 Elucidating the Effects of Post-induction Glutamine Feeding on the Growth and Productivity of CHO Cells

Zahra Sheikholeslami[1], Mario Jolicoeur[1], Olivier Henry[1*]

[1]Département de Génie Chimique, École Polytechnique de Montréal,

C.P. 6079, Succ. Centre-ville, Montréal, Québec, Canada, H3C 3A7

*Correspondence to:

Olivier Henry

Chemical Engineering Department

École Polytechnique de Montréal

C.P. 6079, Succ. Centre-ville,

Montréal, Québec, Canada, H3C 3A7

Tel: 1-514-340-4711 (2191)

Fax: 1-514-340-4159

Email: olivier.henry@polymtl.ca

6.3 Abstract

Inducible mammalian expression systems are increasingly being used for the production of valuable therapeutics. In such system, maximizing the product yield is achieved by carefully balancing the biomass concentration during the production phase and the specific productivity of the cells. These two factors are largely determined by the availability of nutrients and/or the presence of toxic waste metabolites in the culture environment. Glutamine is one of the most important components of cell culture medium, since this substrate is an important building block and source of energy for biomass and recombinant protein production. Its metabolism, however, ultimately leads to the formation of ammonia, a well-known inhibitor of cellular growth and productivity. In this work, we show that nutrient feeding post-induction can greatly enhance the product yield by alleviating early limitations encountered in batch. Moreover, varying the amount of glutamine in the feed yielded two distinct culture behaviors post-induction; whereas excess glutamine allowed to reach higher cell concentrations, glutamine-limited fed-batch led to increased cell specific productivity. These two conditions also showed distinctive lactate metabolism. To further assess the physiological impact of glutamine levels on the cells, a comparative ^{13}C-metabolic flux analysis was conducted and a number of key intracellular fluxes were found to be affected by the amount of glutamine present in the feed during the production phase. Such information may provide useful clues for the identification of physiological markers of cell growth and productivity that could further guide the optimization of inducible expression systems.

Keywords: inducible mammalian expression system, fed-batch, ^{13}C metabolic flux analysis, glutamine metabolism

6.3.1 Introduction

In recent years, mammalian cell culture has become the most important platform for the production of secreted products such as recombinant proteins and monoclonal antibodies (Langdom, 2008). To reduce the process development costs and time, as well as to cope with the demand of the ever expanding biopharmaceuticals market, continuous efforts are made to improve the productivity of cell culture processes. Significant increases in product titers have been achieved mainly through the ooptimization of culture conditions, the development of suitable cell culture media and the implantation of efficient feeding strategies to support high cell density in either fed-batch or perfusion cultures (Zhu, 2012). Considerable work has also been done at the genetic engineering level to improve the robustness of host cell system, for example by decreasing programmed cell death (Elmore, 2007; Mohan et al., 2008) or reducing toxic by-product accumulation (Irani, Wirth, van den Heuvel, & Wagner, 1999; Lim et al., 2010).

The use of inducible mammalian expression systems offers another interesting avenue for the production of recombinant proteins. Many efficient regulated gene expression systems have been developed such as the tetracycline- or ecdysone-based systems (Kaufmann et al., 2001; No et al., 1996), or the recent cumate gene-switch (Mullick et al., 2006). In such system, the growth and production phases can be effectively decoupled, thereby allowing optimizing each phase independently. Although significant product yield enhancement relative to batch were reported with the use of fed-batch (Huang, Marquis, & Gray, 2004) and perfusion (Lipscomb et al., 2004) modes, to date, optimization studies specific to inducible mammalian expression systems remain relatively sparse.

In batch or fed-batch cell culture processes, the final product titers is determined by both the cell specific productivity and the integral of viable cells (P. W. Sauer et al., 2000). The challenge lies in the definition of suitable process conditions that can either simultaneously enhance these factors, or provide an optimal trade-off between the two. For instance, a number of investigations have shown that temperature reduction during the production phase leads to cell growth reduction or cessation, but a concomitant increase in cell specific productivity and a prolongation of culture duration is typically observed (Becerra, Berrios, Osses, & Altamirano, 2012; Sunley & Butler,

2010). Given the complex, sometimes inverse, relation between cellular growth and productivity, it is instrumental to decipher how process variables affect these kinetic rates.

Several feeding strategies have been developed in industrial fed-batch processes to provide the optimal necessary nutrients for cells to grow and to produce protein. In fact, growth and protein production are two complex metabolic functions, but it is not well understood how these two functions and nutritional requirements are related. Providing excessive amounts of glucose and glutamine in the extracellular environment can indeed inhibit the growth or protein production due to the formation and accumulation of toxic metabolic by-products (lactate and ammonia). Minimizing the accumulation of these by-products by limiting the levels of glucose and glutamine is at the basis of several fed-batch control strategies (Dowd, Kwok, & Piret, 2001; Maranga & Goochee, 2006; Takuma, Hirashima, & Piret, 2007). With CHO cells, lactate accumulation has been found to have a lesser negative impact on cell growth and productivity, as a metabolic shift from lactate production to net consumption is frequently observed (Mulukutla et al., 2012; Tsao et al., 2005; Zagari et al., 2013). Glutamine is a major source of energy, nitrogen and, to some extent, carbon for mammalian cells. High rates of glutamine utilization are typically observed in CHO cells and many other cultivated mammalian cells (Neermann & Wagner, 1996) and its partial oxidation will lead to the formation of ammonia. Due to the detrimental effects of ammonia on growth and productivity (H. J. Cruz et al., 2000; S.S. Ozturk et al., 1992; Schneider, Marison, & von Stockar, 1996), as well as on product quality (M Yang & Butler, 2002), there is a greater concern about controlling the level of glutamine in fed-batch cultures (J. Kim, Kim, & Lee, 2012).

Although the effect of extracellular glutamine levels on cell growth and antibody production have been investigated for CHO cell lines in both batch (Rajendra, Kiseljak, Baldi, Hacker, & Wurm, 2012; Taschwer et al., 2012) and fed-batch (Jardon et al., 2012) cultures, comprehensive physiological studies of the regulation of glutaminolysis are still missing and greater understanding of the cell metabolism is needed to allow further significant cell culture process improvements.

The goal of this work was thus to examine the effects of glutamine feeding on the metabolism and recombinant protein productivity of induced CHO cells. To this end, two fed-batch strategies

employing respectively low and high amounts of glutamine were performed and compared to a control batch culture. The two conditions leading to marked differences in terms of cell growth and productivity, a ^{13}C-metabolic flux analysis was then conducted to further assess the impact of glutamine feeding at the intracellular level. So as to perform the analysis under pseudo-steady state conditions, this characterization was performed in semi-continuous cultures with varying concentrations of glutamine in the feed. The resulting intracellular flux distributions were compared in relation with the observed growth and production kinetics.

6.3.2 Materials and methods

6.3.2.1 Cell line and culture conditions

The CHO cell line employed in this study harbors the *cumate gene-switch* transcription system that allows the regulated-expression of a recombinant antibody (Sheikholeslami, Jolicoeur, & Henry, 2013). The basal medium used in our investigation was SFM4CHO (Hyclone), a chemically defined and serum-free formulation initially free of glucose and glutamine as this was a requirement for the isotopic tracer studies described below. Cell maintenance and inoculum preparation were performed in shake flasks maintained at 37^0C in humidified air with 5% CO_2 and the culture medium was supplemented with 30mM glucose and 5mM glutamine. For fed-batch cultures, exponentially growing cells were inoculated in 125mL shake flasks with a working volume of 25mL and at a viable cell density of approximately 2×10^5 cells/mL. All cultures were induced by the addition of 1 µg/mL of cumate on day 2 to trigger recombinant antibody expression. The feeding protocol was initiated at the same time and consisted in adding every two days a fixed volume (10% of the initial culture volume) of a commercial chemically defined concentrated feed, CHO CD EfficientFeed B (Invitrogen). The feed was supplemented with either 4mM or 20mM of glutamine, referred to as low and high glutamine feeding, respectively. All culture conditions were performed in duplicate flasks, including controlled batch cultures. Supernatants were collected by centrifugation at 300 g for 5 min and samples were stored at -20^0C for subsequent analysis.

6.3.2.2 Isotope labeling experiments

For conducting the isotopic tracer studies, cells were inoculated at 2×10^5 cells/mL in basal medium supplemented with unlabeled glucose and glutamine at 37°C in a 5% CO_2 and 95% humid atmosphere. Following induction with 1 µg/mL of cumate at 48h, the cultures were operated in semi-continuous mode, whereby a fixed culture volume was replaced by fresh medium on a daily basis so as to maintain pseudo-constant cell and nutrient concentrations (Olivier Henry et al., 2008). Two sets of semi-continuous cultures were performed, one in which the medium was supplemented with 1mM of glutamine, while the second set was supplemented with 5mM. Due to its unknown exact composition that would have hindered the ^{13}C -flux analysis, the concentrated commercial feed employed in the fed-batch cultures was not used for the semi-continuous cultures. Upon reaching pseudo-steady conditions, cells were fed using the specific label-containing media and feeding was resumed for a minimum of five days to ensure the achievement of an isotopic pseudo-steady state. This period of time has been previously shown to be sufficient in the case of CHO cell cultures (Deshpande et al., 2009; Sheikholeslami et al., 2013). Multiple parallel isotope labeling experiments were performed, containing respectively unlabeled, [1-^{13}C], [6-^{13}C], [U- $^{13}C_6$]- glucose (Cambridge isotopes, all at 99% purity) and [U– $^{13}C_5$] glutamine (Cambridge isotopes, 97–99% purity). The culture samples were centrifuged at 300 g for 5 min to separate cells and the supernatant. The supernatant samples were stored at -20^{0}C for subsequent analysis and cell samples were extracted for determination of mass isotopomers of intracellular metabolites.

6.3.2.3 Analytical methods

Cell density was determined using hemacytometer and cell viability as assessed using trypan blue by the dye exclusion method. The recombinant antibody titers were quantified using an enzyme-linked immunosorbent assay (ELISA) as described previously (Sheikholeslami et al., 2013). The concentrations of glucose, lactate and glutamine in the culture supernatant were determined with a biochemistry analyser (YSI 2700). Ammonia concentration in the supernatants was quantified by an enzymatic assay kit (AA0100, Sigma-Aldrich). Amino acid concentration was determined by an Agilent 1290 UPLC system (Agilent technologies, Montreal, Canada) coupled to an

Agilent 6460 triple quadruple mass spectrometer (Agilent technologies, Montreal, Canada) using the same conditions described in (Sheikholeslami et al., 2013).

6.3.2.4 Metabolite extraction and LC-MS analysis

For intracellular metabolite analysis, cells harvested daily from semi-continuous cultures were washed with cold PBS and extracted with 400 µL of 80% cold methanol. After 10 min on dry ice, the mixture was vortexed and then sonicated in ice and water. Suspensions were then centrifuged at 4°C for 7 min at 21,000 *g*. The supernatants were then transferred to a clean tube as extracts. Pellets were re-extracted as mentioned above with 200 µL of 50% cold methanol and 200 µl of cold water. At each extraction, supernatants were combined with the first extract and stored in −80 °C prior to analysis. The ^{13}C fractional enrichment of intracellular metabolites in the samples was measured on an Agilent 1100 series LC-MSTOF (Agilent technologies, Quebec, Canada). First, 200µL of cell extract samples were deproteinized by adding 1mL cold acetone (-20^{0}C) and then were vortexed strongly. After centrifugation at 20,000g for 5 min, the solutions were filtered and evaporated *in vacuo*. Finally, 400 µL of water was added to the samples. The analysis was done in negative electrospray mode without derivatization using a Kinetex HILIC Phenomenex column, 100 x 4.6mm and 2.6um particle size. The eluents used were 5mM ammonium formate (in water) and acetonitrile containing 0.1% formic acid. The gradient was in HILIC mode and went from 90% to 50% ACN with a total run time of 20 minutes.

6.3.2.5 Determination of specific rates

For fed-batch cultures, the specific rate of nutrient consumption, metabolite formation and production formation were estimated as outlined in (P. W. Sauer et al., 2000). First, the integral of viable cells for each discrete time interval was calculated according to:

$$\int_{t_1}^{t_2} X_v V dt = \left(\frac{(X_v V)_1 + (X_v V)_2}{2}\right)(t_2 - t_1) \qquad (1)$$

where $(X_v V)_1$ and $(X_v V)_2$ are the total number of viable cells at times t_1 and t_2, respectively. The specific antibody production rate was calculated by:

$$q_{Ab} = \frac{(Ab_2.V_2 - Ab_1.V_1)}{\int_{t_1}^{t_2} X_v V dt} \qquad (2)$$

Where Ab_1 and Ab_2 denote the antibody concentrations at times t_1 and t_2. The specific formation rates of lactate and ammonia were calculated in a similar manner. The specific consumption rates of nutrients were obtained by dividing the cumulative amount of substrate consumed by the integral of viable cells:

$$q_s = \frac{(S_2.V_2 - S_1.V_1) + V_{feed}.S_{feed}}{\int_{t_1}^{t_2} X_v V dt} \quad (3)$$

The uptake rate of glutamine was corrected for the spontaneous decomposition rate of this nutrient in the culture media, which was experimentally determined in the absence of cells under the same incubation conditions. The first order degradation constant k was found to be 0.03 day^{-1}. For semi-continuous cultures, the cell specific rates were determined from pseudo-steady state measurements and the daily medium exchange rate, as described in (Olivier Henry et al., 2008):

$$q_s = \frac{F}{V}\frac{(S_{feed} - S)}{X_v} \quad (4)$$

where F correspond to the number of volume exchanges per time unit.

6.3.2.6 Metabolic network model and intracellular flux evaluation

The metabolic network considered in this work contains the major reactions of central metabolism and is based on previously established models for cultivated CHO cells (C. Goudar et al., 2010; Sheikholeslami et al., 2013; Zamorano et al., 2009). These include reactions for glycolysis, TCA cycle and the main amino acid degradation pathways. To account for biosynthetic requirements, the model includes simplified reactions for the synthesis of biomass and antibody, which were established from published average biomass/production composition data (Quek et al., 2010) and by assuming a dry cell weight of 0.350 $mg/10^6$ for CHO cells (Woo Suk Ahn & Antoniewicz, 2011; Altamirano et al., 2001). The metabolic network is compartmentalized into mitochondria and cytosol and reversible reactions were separated into forward and backward fluxes constrained to be non-negative. The list of all reactions considered in the reaction network is presented in the Supplementary Table 1. The ^{13}C-metabolic flux analysis was performed in Matlab R2009a using the elementary metabolite unit network decomposition method (M.R. Antoniewicz et al., 2007). The nonlinear least-squares regression

was performed using the built-in Matlab “fmincon” function to minimize the sum of weighted squared residuals (WSR) between measured and simulated variables. The labeling data from all parallel experiments of each set were simultaneously fitted to the same isotopomer model, thereby providing 60 independent measurements. The minimization was repeated ten times with random feasible initial estimates of free fluxes to ensure the attainment of a global optimal solution. Validation of the fit was performed based on a standard chi-square goodness-of-fit test and 95 % confidence intervals for the intracellular fluxes were evaluated as outlined in (Antoniewicz et al., 2006; Sheikholeslami et al., 2013). For statistical comparison between corresponding fluxes of two conditions under investigation, unpaired two-tailed Student's t-test was performed in Excel.

6.3.3 Results

6.3.3.1 Batch and Fed-batch Cultures

CHO cells cultures that had been started from the same inoculum were grown for two days and then induced at a cell density of about $1.5x10^6$ cells/mL. Following induction, cultures were fed every two days with a fixed volume of a concentrated feed containing either low or high glutamine concentrations. Induced but unfed cultures were also performed to serve as control. The resulting growth curves, glucose, glutamine and lactate concentration profiles are shown in Figure 6-1. Although exponential cell growth was observed in all the cultures post-induction, the fed-batch strategies, which only differed by the amount of glutamine present in the concentrated feed, yielded significantly different cell density profiles. High glutamine fed-batch reached a maximum viable cell density of around 11×10^6 cells/ml, which was 1.8 times more than the low glutamine fed-batch cultures (6.2×10^6 cells/ml) and 2.5 times more than the control batch cultures (4.4×10^6 cells/ml). Similar to the control batch, the low glutamine fed-batch was most likely limited by glutamine between day 3 and day 4 (Figure 6-1C), as the onset of the stationary phase in these cultures coincided with the times when this substrate reached concentrations that were below the detection limit. The low glutamine feed nonetheless allowed to prolong the culture compared to the batch, which translated into a 30 % increase in the integral of viable cells

(IVC) (Table 6-1). In contrast, the high-glutamine feed led to a nearly 3-fold improvement in terms of IVC.

Table 6-1: Effect of glutamine levels on maximum viable cell density, final antibody titer and specific productivity (average of two runs in each condition)

	Batch culture (control)	**Low glutamine fed-batch culture**	**High glutamine fed-batch culture**
Maximum cell density ($\times 10^6$ cells/mL)	4.8 ± 0.7	6.2 ± 0.4	11.2 ± 0.9
Integral of viable cells ($\times 10^6$ cells-d)	673.9 ± 31	880.8 ± 42	1971.9 ± 51
Maximum antibody titer (mg/L)	110 ± 14	292 ± 31	327 ± 22
Cell specific productivity (pg/cell/d)	3.6 ± 0.2	10.2 ± 0.3	4.7 ± 0.7

Another striking difference between the two fed-batch regimes is noted on their respective lactate concentration profiles. A significant metabolic shift to lactate consumption was observed in high-glutamine fed-batch cultures at around day 4. This shift occurred while the cells were still exponentially growing and with residual glucose concentrations still well above 30 mM. In contrast, the low glutamine cultures exhibited much less lactate consumption and the metabolic shift was observed later during the culture (between day 6 and day 7).

Glucose uptake rates tended to decrease over the course of all the cultures, even though glucose concentrations were always maintained above 15 mM in our experiments (Figure 6-1B). The reduction in glucose consumption rate coincided with the onset of lactate consumption, suggesting some correlation between the uptake rates of these two carbon sources and a salient change in nutrient utilization efficiency by the cells. Compared to the control batch, fed-batch cultures achieved higher final levels of ammonia. However, these concentrations remained below 5mM in all culture conditions (Table 6-1), that is, much less than commonly reported toxic levels of 10mM for CHO cells (P. Chen & Harcum, 2005).

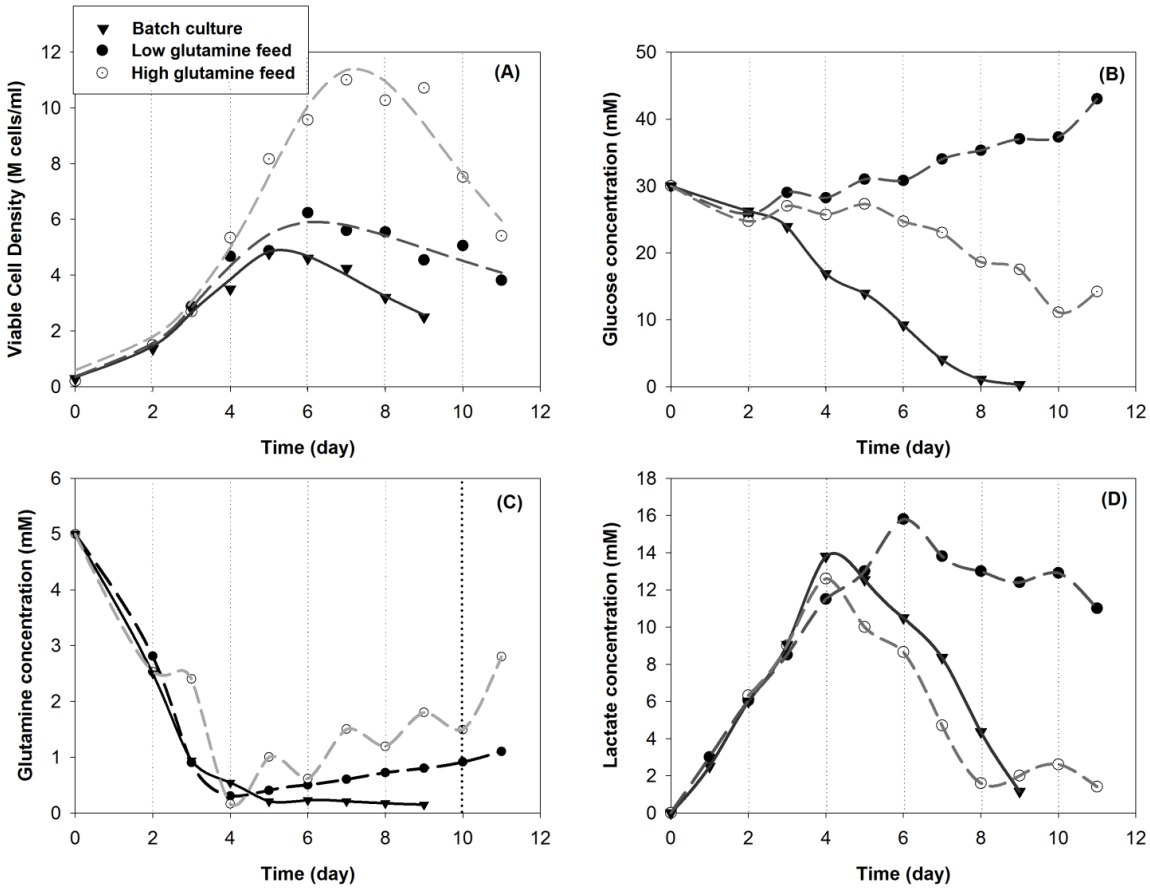

Figure 6-1: Viable cell (A), glucose (B), glutamine (C) and lactate (D) concentration profiles in induced fed-batch cultures supplemented with respectively low and high levels of glutamine. The corresponding profiles obtained in a control batch culture are also shown. Error bars represent the standard error of duplicate experiments.

The maximal antibody concentration achieved in high glutamine fed-batch was 327 mg/L, which was slightly higher than the low glutamine fed batch (292 mg/L), whereas batch cultures reached a maximum of 110 mg/L (Table 6-1). However, the feeding regimes led to significant differences in terms of cell specific productivity, as determined by dividing the final antibody titer by the integral of viable cells. While the cell specific productivity of the high glutamine fed-batch was similar to the one obtained in batch, the low glutamine fed-batch exhibited a two-fold greater specific recombinant protein expression rate (Table 6-1).

Overall, this set of experiments demonstrated the potential to significantly enhance either the growth or the productivity of an inducible expression system through fed-batch operation.

However, an increase in growth was at the expense of productivity (and vice versa). Moreover, these results suggested the apparent sensitivity of CHO cell metabolism to glutamine levels.

6.3.3.2 Semi-Continuous Cultures and Isotopomer Analysis

To further investigate the metabolic response to varying levels of glutamine in the culture medium, a comprehensive ^{13}C-metabolic flux analysis was conducted. Given the ever-changing conditions observed in batch and fed-batch cultures, the analysis was performed by growing cells under a semi-continuous mode of operation so as to obtain reliable kinetic rates corresponding to a defined metabolic pseudo-steady state. The effects of glutamine were investigated by using basal medium supplemented with either low and high concentration of this amino acid in the feed. For each condition, five parallel cultures containing different labeled substrates were maintained in a similar physiological state to allow reliable intracellular flux estimation (Crown & Antoniewicz, 2013; Olivier Henry & Durocher, 2011). The resulting cell density profiles are shown in Figure 6-2, by considering the average and standard deviation from all parallel cultures of the same experimental set. Performing a medium exchange on a daily basis was thus able to maintain the cells in pseudo-steady state conditions for several days. From the medium exchange rates required to maintain a stable cell density, the apparent growth rates were determined to be 0.7 and $0.5 d^{-1}$ for the high and low glutamine cultures, respectively. Similar to what was observed in the fed-batch cultures, the high glutamine condition reached higher cell concentrations ($4.7 \pm 0.2 \times 10^6$ cells/ml) compared to the low glutamine culture ($2.9 \pm 0.2 \times 10^6$ cells/ml) (Fig 2). The effects of glutamine concentration on antibody production was also determined and, consistent with the trend noted in fed-batch cultures, the highest protein productivity was observed in the culture with low glutamine (Table 6-2).

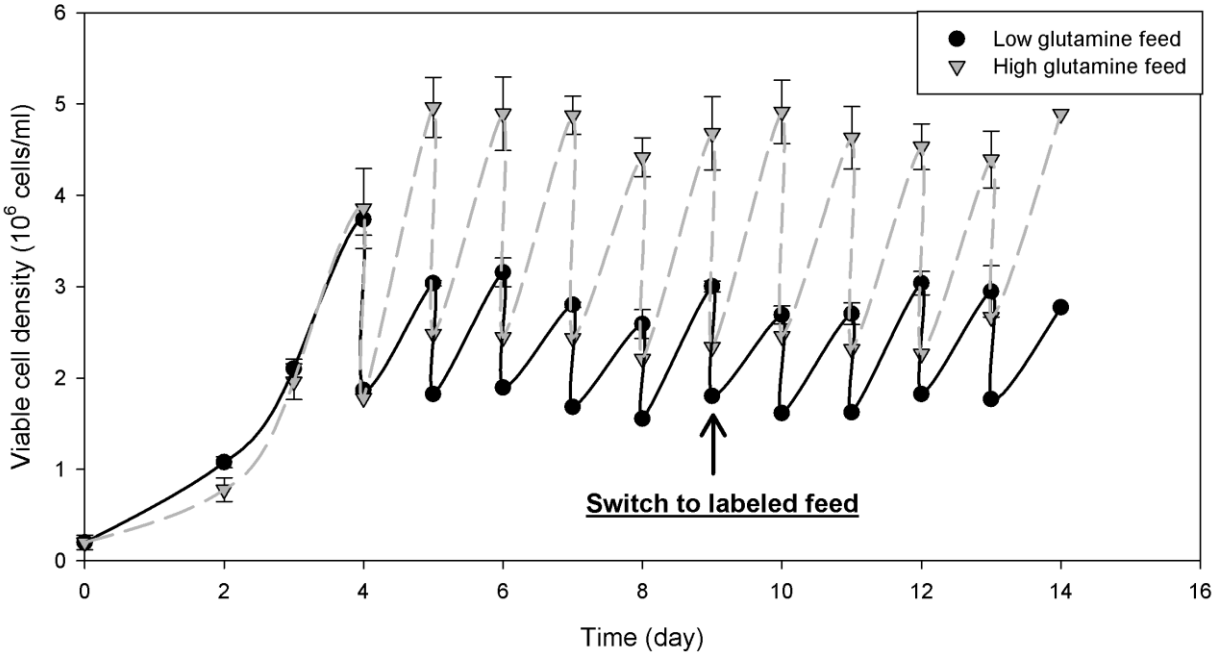

Figure 6-2: Time profile of the average viable cell density for induced cells in semi-continuous cultures performed with respectively low and high levels of glutamine. Labeled substrates were introduced at day 9 and the cultures were maintained for five subsequent days. Standard deviations were computed from five parallel cultures in each set

Cultures were also compared in terms of the main extracellular rates. The consumption/production of glucose, lactate, glutamine and other amino acids are shown in Figure 6-3. While glucose consumption rates were only marginally different between the two culture conditions, the lactate production rate was reduced in the low glutamine cultures. Consequently, increase in glutamine supply was directly accompanied by an increase in lactate production/glucose consumption ratio (1.1 vs. 0.7). Both cultures showed relatively low values compared with the typical values reported for mammalian cells in cultures under non-limiting glucose concentrations ($Y_{Lac/Glc}$ ~= 1–2) indicating that this cell line exhibits a relatively efficient glucose metabolism. As shown in Figure 6-3, most of amino acids were consumed by the cells in both cultures except glutamate, alanine, glycine and aspartate which all had a net production rate.

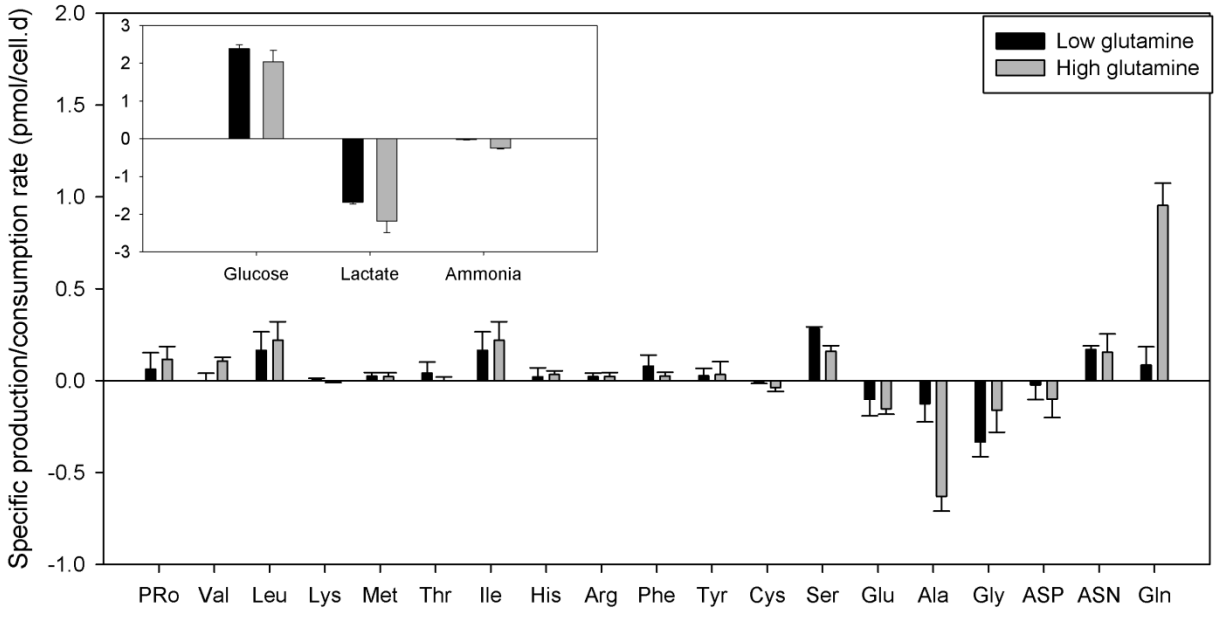

Figure 6-3: Average cell specific consumption/production rates of amino acids in induced semi-continuous cultures performed with respectively low and high levels of glutamine

Except for glutamine and alanine, there were no clear trend in the consumption patterns of most essential and non-essential amino acids when considering measurement errors. Alanine production was significantly augmented as a result of a higher glutamine concentration in the feed. This suggests a higher transamination reaction from glutamate to pyruvate (yielding alanine), an effective route in preventing ammonia intoxication (Niklas, Priesnitz, Rose, Sandig, & Heinzle, 2012).

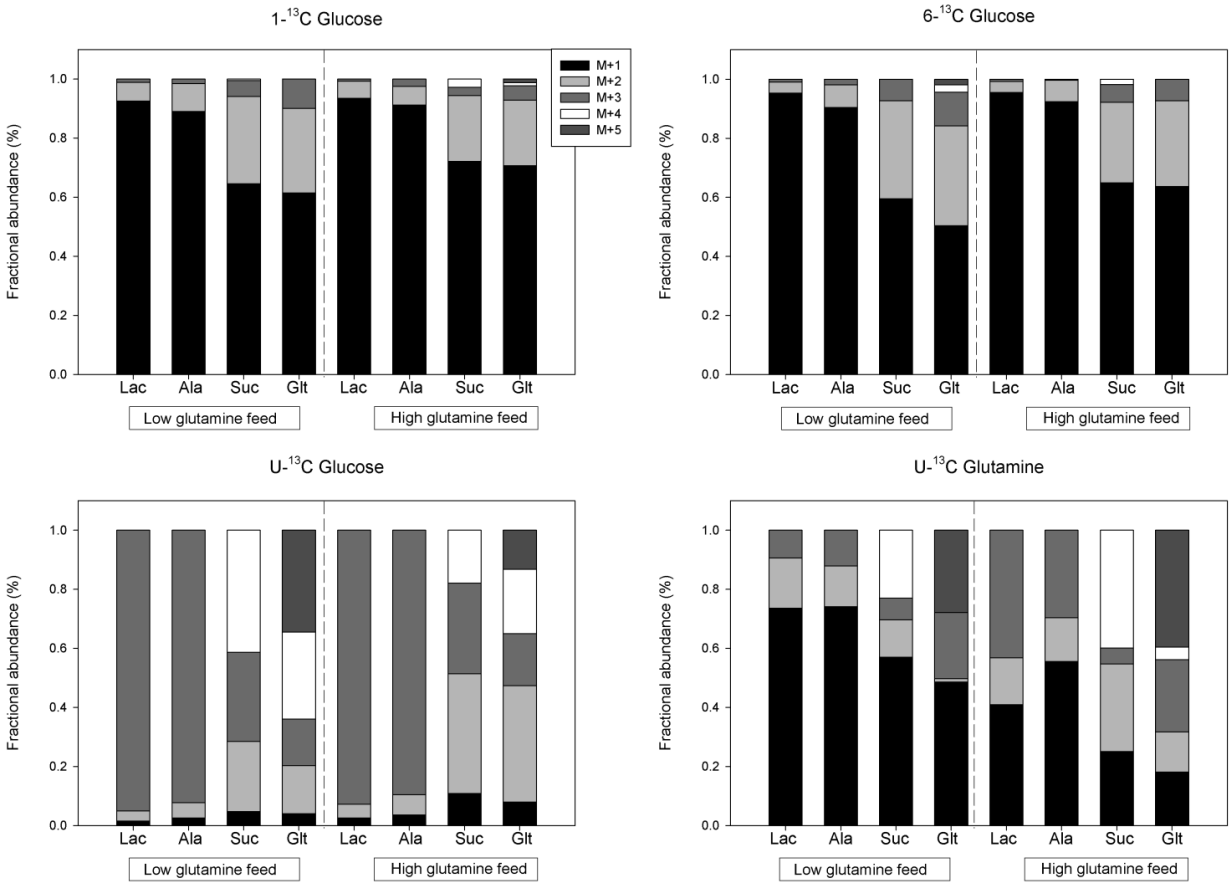

Figure 6-4: Fractional abundances of labeled mass isotopomers after inductions performed respectively at low and high cell densities, for the following metabolites: lactate, alanine, succinate and glutamate. Cultures were performed with fresh medium containing 1-^{13}C, 6-^{13}C and U-^{13}C glucose, as well as U-^{13}C glutamine

On day 9, after the cultures reached and maintained pseudo-steady state conditions, semi-continuous operation was continued, but the cultures were fed with specific labeled containing media. The feeding was continued for 5 consecutive days, so as to maximize the wash out of unlabeled nutrients and metabolites. Cells were then harvested and extraction was performed to

measure the labeling pattern of key intracellular metabolites: lactate, alanine, succinate and glutamate. As shown in Figure 6-4, cultures at low and high glutamine levels exhibited distinct labeling patterns for all measured metabolites and the differences were more pronounced in the case of experiments performed with [U-$^{13}C_6$] glucose and [U-$^{13}C_5$] glutamine. These measured fractional abundances reflect the activity of the main intracellular pathways and data inspection can provide qualitative information about cell metabolism. For example, in cultures fed with [U-$^{13}C_6$] glucose, the higher fractional abundance of M+4 succinate observed for low glutamine conditions is indicative of a greater influx of glucose-derived carbons into TCA cycle. When cells were fed with [U-$^{13}C_5$] glutamine, the fractional abundance of M+3 lactate significantly dropped in high glutamine cultures compared to low glutamine conditions, which is clear indication of a lower contribution of this substrate towards lactate formation. However useful such information may be, a more detailed and quantitative description of cellular metabolism can be obtained using ^{13}C-metabolic flux analysis. For both low/high glutamine conditions, the measured mass distribution data from the four parallel labeling experiments ([1-^{13}C]- glucose, [6-^{13}C] glucose, [U-$^{13}C_6$] glucose and [U-$^{13}C_5$] glutamine) were fitted simultaneously together to the same metabolic flux model (reaction and carbon transitions shown in Table A1).

Table 6-2: Comparison between semi-continuous cultures operated with a low and a high glutamine feeding regime, respectively. Values are average from n=5 measurements.

Pseudo-Steady State Measurements	**Low glutamine culture**	**High glutamine culture**
Cell Concentration ($\times 10^6$ cells/mL)	2.9 ± 0.2	4.7 ± 0.2
Apparent growth rate (d^{-1})	0.49 ± 0.04	0.69 ± 0.05
Cell specific productivity (pg/cell/d)	9.6 ± 0.3	5.5 ± 0.2

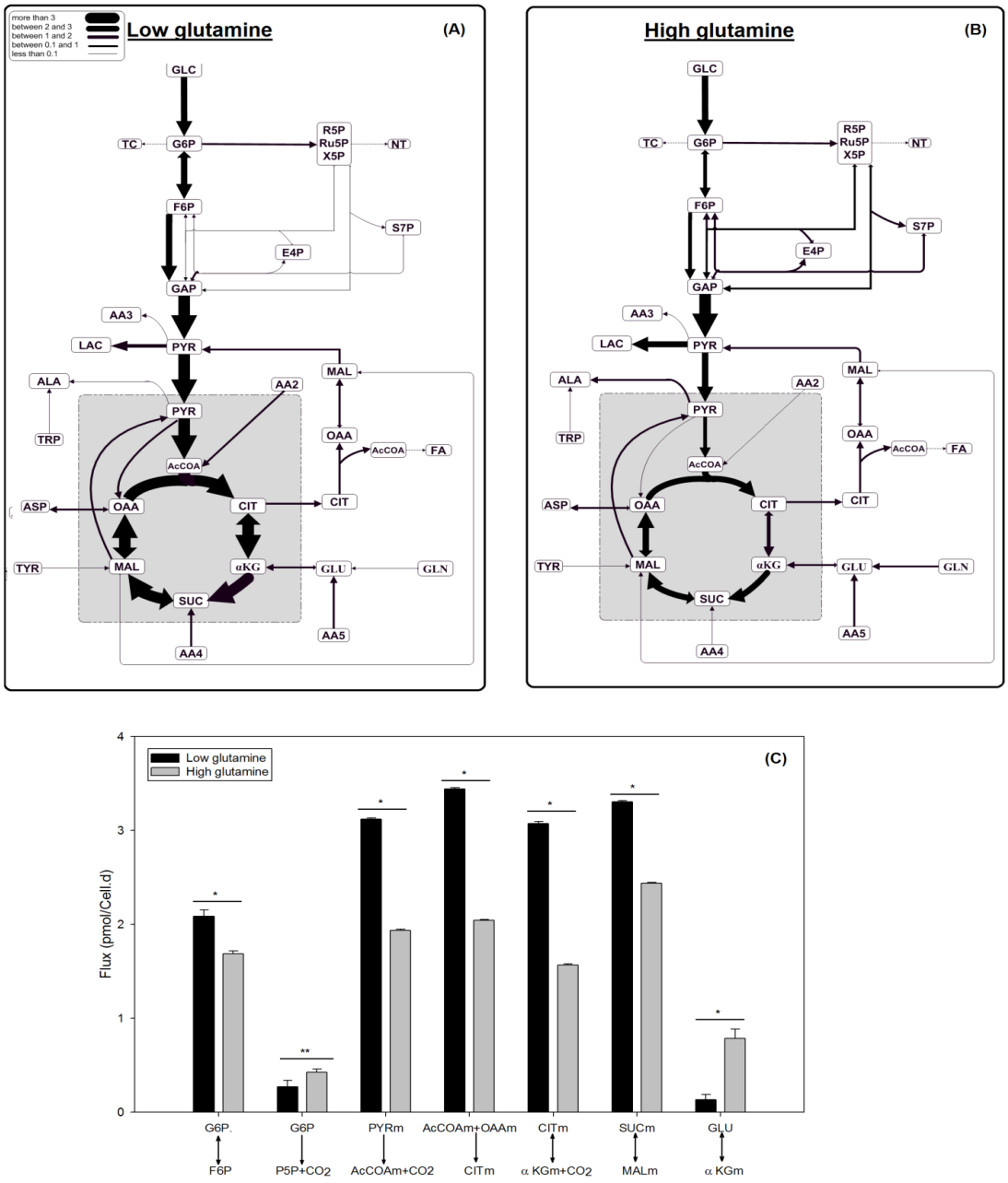

Figure 6-5 : Metabolic flux maps corresponding to low (A) and high (B) glutamine levels. (C) Comparison of key intracellular fluxes. Standard errors were calculated from the upper and lower bounds of the 95 % confidence intervals.

* indicates significance at $p<0.05$. Abbreviations: AA2 = Leu, Lys, Ile, Tyr, Trp, and Thr; AA4 = Val, Met, and Ile; AA5 = His, Arg, and Pro.

The metabolic model contained 16 free fluxes to optimize and, by combining the labeling data from all parallel cultures, 60 independent mass isotopomer distributions were available for both low/high glutamine conditions. The minimum and maximum allowable values for the variance-weighted sum of squared residuals (WSSR) were 29.8 and 60.5, respectively (chi square test for 95% level of confidence with 44 degrees of freedom). With the assumed metabolic network, statistically acceptable fits were obtained with WSSR values of 45.8 and 47.1 for low and high glutamine cultures, respectively. The resulting flux maps corresponding to the two studied conditions are shown in Figure 6-5, along with the statistical comparison of key selected intracellular fluxes. The complete list of flux values along with the associated 95% confidence intervals are reported in Supplementary Material. The main metabolic differences and their implication are discussed in the following section.

6.3.4 Discussion

Glucose and glutamine are typically the major sources of energy and carbon for cultivated mammalian cells. Setting their concentrations in the basal medium and in the feeding solution is instrumental in any fed-batch process. Typically, it is desired to maintain low but non-limiting nutrient concentrations so as to minimize the accumulation of waste metabolites (ammonia and lactate), which are known to affect both cellular growth and productivity (Takeshi Omasa, Higashiyama, Shioya, & Suga, 1992; S.S. Ozturk et al., 1992), as well as product quality (Borys, Linzer, & Papoutsakis, 1994; Gawlitzek, Valley, & Wagner, 1998). While glucose uptake rate is typically varying through the course of a batch culture (decreasing with the concentration), these variations are often not associated with changes in cell growth (Pörtner & Schäfer, 1996) until limiting concentrations are reached, the excess glucose being essentially diverted towards lactate formation (the so called overflow metabolism). The observation in induced batch cultures that glutamine is rapidly depleted, quickly followed by a metabolic shift towards lactate consumption (Figure 6-1A) strongly suggests that this nutrient is a key determinant of the overall cell metabolic activity. In order to determine its impact on cellular growth and productivity, we have compared the kinetics of fed-batch cultivations performed with high and low levels of glutamine. Our results revealed that varying the availability of glutamine had a profound impact on the kinetics of growth, productivity, nutrient consumption and waste metabolite formation.

In order to shed more light on the underlying physiological changes associated with glutamine concentration and cell metabolism, two sets of CHO cell cultures were studied at different glutamine concentrations by performing carbon labeling experiments. This investigation was performed by running the cultures in a semi-continuous mode, as the later can provide pseudo-steady state conditions approaching those of a chemostat system while maintaining the relative simplicity of batch culture operation (Olivier Henry et al., 2008). It was previously shown to be suitable for conducting reliable tracer studies (Olivier Henry & Durocher, 2011), provided that constant cell growth is maintained sufficiently long to meet the requirements for metabolic and isotopic pseudo-steady states (Sheikholeslami et al., 2013). Similar to the trends observed in fed-batch, the semi-continuous cultures were also shown to be affected by the level of glutamine in the feed. High glutamine cultures exhibited higher pseudo-steady-state cell concentrations, but reduced cell specific productivity. The two culture conditions were also characterized by some significant changes in the uptake/production rates of several key nutrients. It is thus not surprising that the intracellular flux maps derived from isotopic tracers also revealed significant metabolic flux rewiring, which are described in the following sections.

Glycolytic fluxes

The main glycolytic fluxes were significantly increased in cultures corresponding to a low glutamine concentration in the feed. Hexokinase (HK), fructose-1,6-bisphophate aldolase (FBPA), and pyruvate kinase (PK) fluxes were all increased by 15 to 25% compared to high glutamine cultures. In most metabolic flux studies of cultivated mammalian cells, high glycolytic fluxes are typically associated with high production rates of lactate. However, in our induced cultures, this increase was in fact associated with a concomitant 20 % decrease of the lactate dehydrogenase (LDH) flux. It could be thought that this reduction is solely due to the lesser contribution of glutamine towards lactate formation when the uptake of this substrate is small. However, from the mass distribution of lactate in experiments fed with [U-$^{13}C_6$] glucose, it is found that the percentage of lactate directly metabolized from glucose was relatively similar in both cases (86% and 91% for high and low glutamine supplemented cultures, respectively).

Pentose Phosphate Pathway

The increased glycolytic activity of low glutamine cultures was accompanied by a decreased oxidative pentose phosphate pathway (0.27±0.07 vs. 0.43±0.04). The split ratio of glucose toward PPP was estimated to be 20% for high glutamine cultures, while the value reduced to 11% for low glutamine conditions. Oxidative PPP is regarded as a major source of both building blocks for nucleotides and reductant (NADPH) for biosynthetic processes, such as fatty acids. The observed difference maybe attributable to the reduction in biomass formation, and thus related to reduced biosynthetic needs. The obtained splits ratios are within the range of values typically reported for cultivated mammalian cells (H. P. Bonarius et al., 2001; C. Goudar et al., 2010). Despite the varying biosynthetic rates, the demand in terms of ribose-5-phosphate is quite small and the flux through the non-oxidative branch of this pathway (transketolase activity) was consequently also observed to be decreased for the low glutamine feed compared to the high glutamine feed (0.08 ± 0.02 vs. 0.12 ± 0.01).

TCA cycle and anaplerotic reactions

The main metabolic fluxes around the pyruvate branch point were markedly different for the two conditions under investigation. In low glutamine cultures, a higher portion of the intracellular pyruvate pool entered TCA (66%), while only 33% was converted to lactate and the remaining fraction was converted into amino acids. In contrast, the fluxes were more evenly distributed between lactate and the TCA (52 % vs 48%) for cultures with a high uptake rate of glutamine. Such even distribution was also reported for CHO cells under high cell density perfusion cultures (C. Goudar et al., 2010). Pyruvate carboxylase (PC) activity can be one of possible ways to decrease the ratio of lactate produced per glucose consumed. While an increase in the PC flux was noted for low glutamine cultures, it does not have a great impact on the flux distribution; for both culture conditions, the vast majority of pyruvate was channeled into the TCA via the pyruvate dehydrogenase flux and the contribution of the pyruvate carboxylase flux remained marginal (below 5 %). Owing to the increased oxidative decarboxylation of mitochondrial pyruvate to form acetyl-CoA, the main TCA cycle reactions were also significantly increased in low glutamine cultures. This increase TCA cycle activity might be related in part to some compensatory mechanism for the decreased production of ATP by glycolysis.

In low glutamine cultures, 82 % of the total carbon entering the TCA originated from pyruvate, while the contribution of glutamine, via ketoglutarate, represented a mere 5 %. In contrast, for high glutamine cultures, this amino acid accounted for nearly 40 % of the total carbon intake. Conversion of glutamate to ketoglutarate may occur either via glutamate dehydrogenase or transaminase reactions. A lower extracellular level of alanine was observed in the low glutamine cultures, which is indicative of a decrease in the activity of alanine transaminase. Transaminase was reported to be the main pathway for the utilisation of glutamine in mammalian cells based on previous studies using enzyme activity measurements or flux analysis (DeBerardinis et al., 2007; Neermann & Wagner, 1996).

While pyruvate is mostly derived from glucose metabolized through glycolysis, 11 and 16 % of the intracellular pool originated from the conversion of malate via malic enzyme for low and high glutamine cultures, respectively. Such pyruvate recycling is the reason for the presence of ^{13}C label in lactate produced in the cultures fed with [U-$^{13}C_5$] glutamine as the sole source of labeled carbon (Figure 6-4). This pathway, together with the oxidative branch of PPP, constitutes a major source of reducing agent for the cells. In total, approximately 0.9 and 1.3 pmol/cell.d of NADPH are produced from these pathway for low and high glutamine cultures, respectively, which is consistent with the reduction in growth rate and the resulting decrease in biosynthetic requirements.

Overall, the comparative ^{13}C -metabolic flux analysis performed in this worked allowed to characterize the main physiological changes resulting from supplying cells with either excess or limiting amounts of glutamine post-induction. The resulting distinct intracellular flux maps can be associated with metabolic states favoring either cell proliferation or recombinant protein expression. While this analysis was performed in semi-continuous mode, the effects of glutamine on the growth and productivity were consistent with the ones observed in the fed-batch cultures. In both cases, higher cell specific productivities were attained when the specific growth rate was reduced, perhaps due to the fact that cells are diverting more resources (precursors and energy) towards recombinant protein expression.

6.3.5 Conclusion

In this work, we have demonstrated that fed-batch additions performed post-induction can significantly enhance the growth and productivity compared to batch cultures. Moreover, reducing the amount of glutamine present in the feed was shown to limit cell growth, but increased the cell specific productivity. Further improvement can be anticipated by reducing the temperature during the production phase to further prolong the culture time, through the addition of productivity enhancer (e.g. sodium butyrate) or by employing a dynamic feeding strategy. For the latter, the development of a dynamic model to predict the intracellular flux response to changing extracellular concentrations will undoubtedly help in that endeavor (Ghorbaniaghdam et al., 2013; Ryan P Nolan & Lee, 2011). The results of this study can provide valuable information and constraints for guiding the development of such model.

AKNOWELDGMENTS

The authors wish to acknowledge Dr. Alexandra Furtos from Université de Montréal for ^{13}C QTOF-LCMS analysis, Jingkui Chen from Ecole Polytechnique for amino acids analysis, as well as Dr. Patrick Benoist and Dr. Patrick Daoust of Viropro International Inc. (Montreal, Canada) for providing the cell line employed in this study.

Table 6-3 : Biochemical reactions and their corresponding C atom transitions

Biochemical Reaction	***Carbon Transition***
Glycolysis	
GLC → G6P	abcdef = abcdef
G6P ↔ F6P	abcdef = abcdef
F6P → 2 GAP	abcdef = cba + def
GAP → PYR	abc = abc
PYR → LAC	abc = abc
PYR → PYRm	abc = abc
Pentose Phosphate Pathway	
G6P → P5P + CO_2	abcdef = bcdef + a
2P5P ↔ S7P + GAP	abcde + fghij = abfghij + cde
P5P + E4P ↔ F6P + GAP	abcde + fghi = abfghi + cde
S7P + GAP ↔ F6P + E4P	abcdefg + hij = abchij + defg
TCA Cycle	
PYRm → AcCOAm + CO_2	abc = bc + a
AcCOAm + OAAm → CITm	ab + cdef = fedbac
CITm ↔ aKGm + CO_2	abcdef = abcde + f
aKGm → SUCm + CO_2	abcde = bcde + a
SUCm ↔ 0.5 MALm + 0.5 MALm	abcd = 0.5 abcd + 0.5 dcba
MALm ↔ OAAm	abcd = abcd
CITm + MAL → CIT + MALm	abcdef + ghij = abcdef + ghij
CIT → AcCOAc + OAA	abcdef = ed + fcba
MALm ↔ MAL	abcd = abcd
OAA ↔ MAL	abcd = abcd
PYRm + CO2 → OAAm	abc + d = abcd
MALm → PYRm + CO_2	abcd = abc + d

MAL → PYR + CO_2	`abcd = abc + d`
Amino acid reactions	
GLN → GLU	`abcde = abcde`
GLU ↔ aKGm	`abcde = abcde`
PYRm + GLU → ALA + aKGm	`abc = abc`
ASP + aKGm ↔ OAAm + GLU	`abcd + efghi = abcd + efghi`
ASN → ASP	`abcd = abcd`
PYR → SER, GLY	`abc = abc`
CYS → PYR	`abc = abc`
VAL, MET, ILE → SUCm	`abcd = abcd`
LEU, LYS, ILE, TYR, TRP, THR → AcCOAm	`ab = ab`
HIS, ARG, PRO → GLU	`abcde = abcde`
Biomass and Product Biosynthesis	
0.912 PROTEIN + 0.0315 P5P + 0.0379 G6P + 0.317 AcCOAc + 0.0151 GAP → BIOMASS	–
0.0585 ALA + 0.0226 ARG + 0.0449 ASN + 0.0365 ASP + 0.0252 CYS + 0.0400 GLN + 0.0518 GLU + 0.0660 GLY + 0.0229 HIS + 0.0329 ILE + 0.0630 LEU + 0.0608 LYS + 0.0128 MET + 0.0415 PHE + 0.0717 PRO + 0.0106 SER + 0.1056 THR + 0.0224 TRP + 0.0288 TYR + 0.0857 VAL → ANTIBODY	–
0.0811 ALA + 0.0510 ARG + 0.0389 ASN + 0.0485 ASP + 0.0196 CYS + 0.0435 GLN + 0.0522 GLU + 0.0727 GLY + 0.0193 HIS + 0.0438 ILE + 0.0763 LEU + 0.0771 LYS + 0.0187 MET + 0.0296 PHE + 0.0423 PRO + 0.0581 SER + 0.0522 THR + 0.0059 TRP + 0.0246 TYR + 0.0562 VAL → PROTEIN	–

6.4 Supplementary data

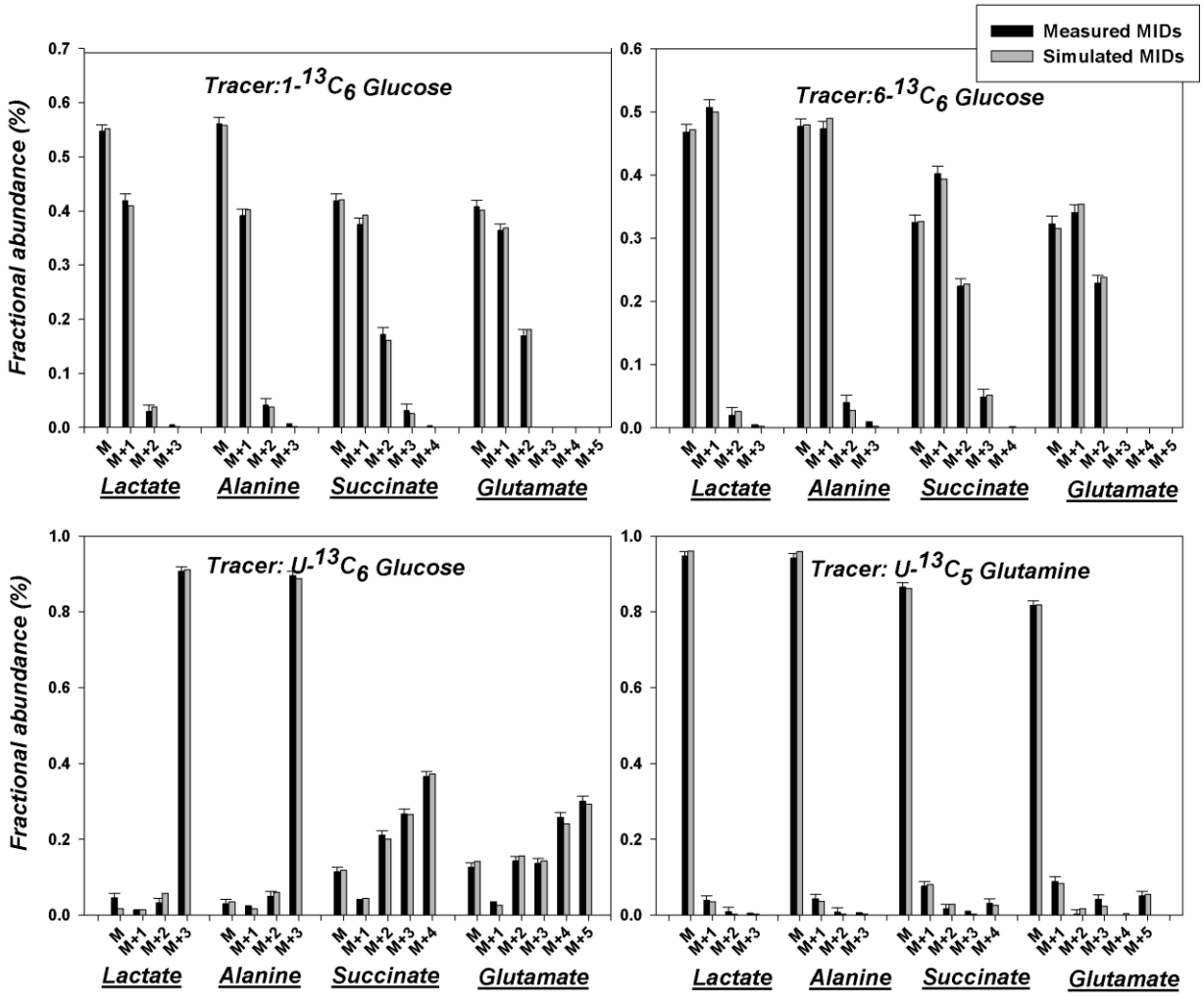

Figure 6-6: Measured and fitted mass distributions of lactate, alanine, succinate, and glutamate in low glutamine feeded cells grown in [1-^{13}C]- glucose, [6-^{13}C] glucose, [U–$^{13}C_6$] -glucose and [U–$^{13}C_5$]- glutamine;

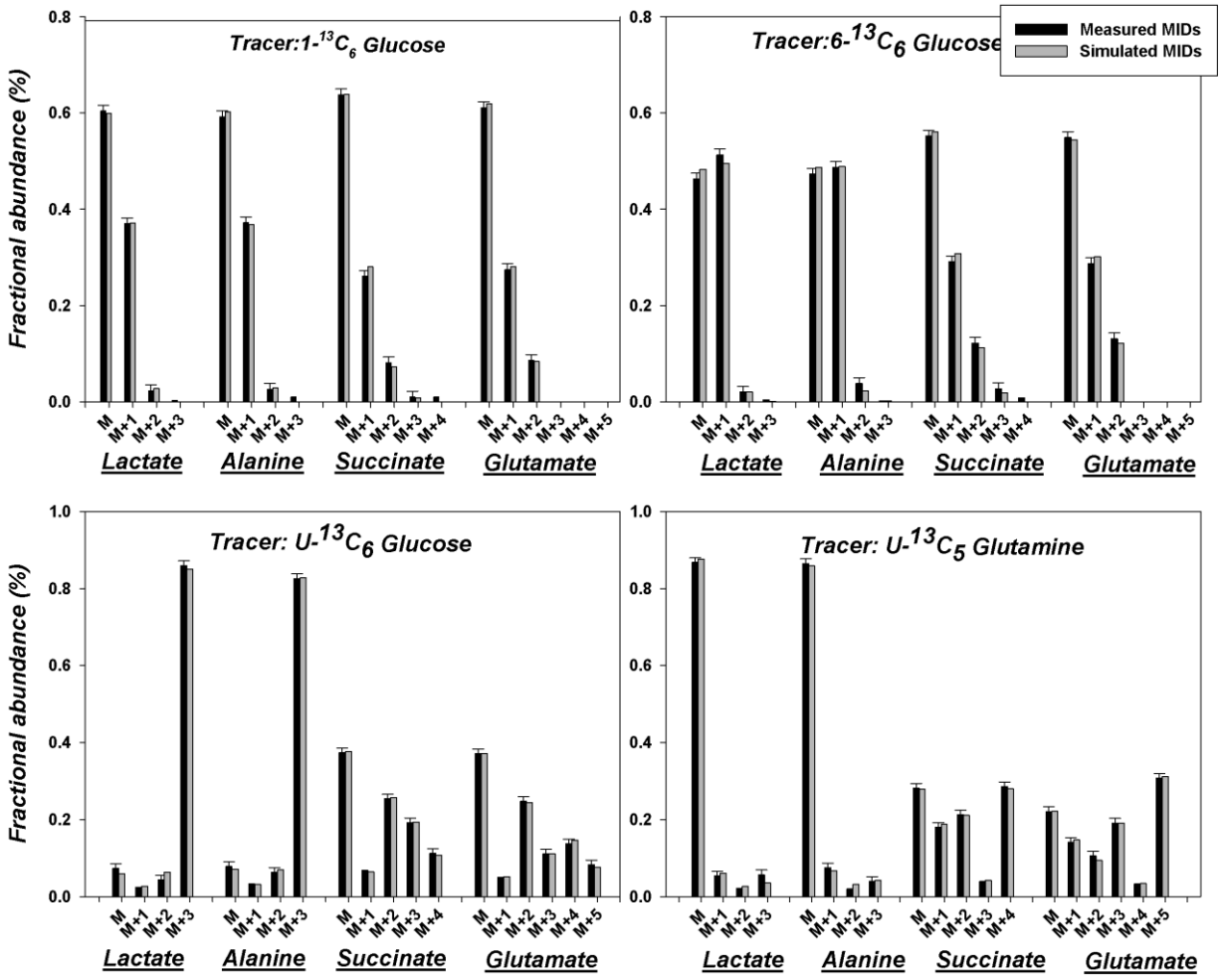

Figure 6-7: Measured and fitted mass distributions of lactate, alanine, succinate, and glutamate in high glutamine fed cells grown in [1-^{13}C]- glucose, [6-^{13}C] glucose, [U–$^{13}C_6$] -glucose and [U–$^{13}C_5$]- glutamine;

Table 6-4: Calculated fluxes (in pmol/cell.d) and associated confidence intervals for induced semi-continuous cultures operated with low and high glutamine concentrations in the feed, respectively.

				Low glutamine		High glutamine	
Biochemical Reaction				**Flux**	**Conf. 95%**	**Flux**	**Conf. 95%**
GLC	→	G6P		2.40	[2.20 , 2.59]	2.18	[1.99 , 2.38]
LAC	→	LACex		1.68	[1.48 , 1.88]	2.13	[1.93 , 2.32]
G6P	→	Biomass		0.04	[0.02 , 0.06]	0.07	[0.05 , 0.09]
P5P	→	Biomass		0.04	[0.02 , 0.06]	0.06	[0.04 , 0.08]
AcCOAc	→	Biomass		0.37	[0.17 , 0.56]	0.47	[0.28 , 0.67]
GAP	→	Biomass		0.02	[0.00 , 0.21]	0.03	[0.00 , 0.05]
GLNex	→	GLN		0.11	[0.00 , 0.31]	0.88	[0.68 , 1.08]
His/Arg/Pro	→	GLU		0.14	[0.00 , 0.54]	0.11	[0.00 , 0.27]
VAL/MET/ ILE	→	SUCm		0.10	[0.00 , 0.35]	0.09	[0.00 , 0.28]
Leu/Lys/Ile/Tyr/ Trp/Thr	→	AcCOAm		0.32	[0.00 , 0.71]	0.10	[0.00 , 0.30]
ALA	→	ALAex		0.09	[0.00 , 0.48]	0.59	[0.39 , 0.78]
ASP	→	ASPex		0.04	[0.00 , 0.19]	0.17	[0.00 , 0.37]
GLUin	→	GLUex		0.12	[0.00 , 0.30]	0.21	[0.00 , 0.41]
PYR	→	AA3		0.05	[0.00 , 0.40]	0.00	[0.00 , 0.20]
ASNex	→	ASP		0.17	[0.00 , 0.36]	0.00	[0.00 , 0.20]
G6P	↔	F6P	net	2.09	[1.95 , 2.22]	1.69	[1.63 , 1.76]
			exch	0.00	[0.00 , inf]	40.8	[1.87 , inf]
F6P	→	GAP + GAP		2.24	[2.19 , 2.28]	1.93	[1.91 , 1.96]
GAP	→	PYR		4.54	[4.49 , 4.58]	3.96	[3.94 , 3.98]
PYR	→	LAC		1.68	[1.48 , 1.88]	2.13	[1.93 , 2.32]
G6P	→	P5P+CO		0.27	[0.14 , 0.41]	0.43	[0.35 , 0.49]
P5P +P5P	↔	S7P + GAP	net	0.08	[0.04 , 0.10]	0.12	[0.10 , 0.14]
			exch	0.85	[0.06 , 1.42]	0.00	[0.00 , 0.10]
P5P + E4P	↔	F6P + GAP	net	0.08	[0.04 , 0.10]	0.12	[0.10 , 0.14]
			exch	0.00	[0.00 , 2.07]	29.9	[0.00 , inf]
S7P + GAP	↔	F6P + E4P	net	0.08	[0.04 , 0.10]	0.12	[0.10 , 0.14]

				exch	11.8	[	0.07	, inf	]	35.2	[	0.00 , inf]
PYR	→	PYRm	net		3.22	[	2.80	, 3.48	]	2.27	[	1.81 , 2.55]
			exch		6.78	[	0.00	, inf	]	6.68	[	0.00 , inf]
PYRm	→	AcCOAm + CO			3.12	[	3.10	, 3.16	]	1.94	[	1.92 , 1.96]
AcCOAm + OAAm	→	CITm			3.44	[	3.42	, 3.49	]	2.04	[	2.02 , 2.07]
CITm	↔	aKGm + CO_2	net		3.07	[	3.03	, 3.12	]	1.57	[	1.55 , 1.60]
			exch		29..1	[	0.00	, inf	]	12.9	[	2.60 , inf]
aKGm	→	SUCm + CO_2			3.21	[	3.18	, 3.25	]	2.35	[	2.33 , 2.38]
SUCm	↔	0.5MALm +0.5MALm	net		3.31	[	3.28	, 3.34	]	2.44	[	2.42 , 2.47]
			exch		0.77	[	0.00	, inf	]	0.25	[	0.00 , 3.24]
MALm	↔	OAAm	net		3.14	[	3.00	, 3.26	]	2.17	[	2.10 , 2.24]
			exch		31.9	[	0.00	, inf	]	33.2	[	0.00 , inf]
MALm	↔	MAL	net		0.04	[	0.00	, 0.30	]	-0.03	[	-0.47 , 0.25]
			exch		27.5	[	0.23	, inf	]	38.9	[	0.26 , inf]
CITm	→	CIT			0.37	[	0.17	, 0.56	]	0.47	[	0.28 , 0.67]
CIT	→	AcCOAc + OAA			0.37	[	0.17	, 0.56	]	0.47	[	0.28 , 0.67]
OAA	↔	MAL	net		0.37	[	0.17	, 0.56	]	0.47	[	0.28 , 0.67]
			exch		38.3	[	0.00	, inf	]	6.30	[	0.00 , inf]
GLN	→	GLU			0.11	[	0.00	, 0.31	]	0.88	[	0.68 , 1.08]
GLU	↔	aKGm	net		0.18	[	0.17	, 0.18	]	0.03	[	0.03 , 0.04]
			exch		1.46	[	0.00	, 4.10	]	12.4	[	0.00 , inf]
PYRm + GLU	→	ALA + aKGm			0.09	[	0.08	, 0.09	]	0.59	[	0.58 , 0.59]
OAAm + GLU	↔	ASP+aKGm	net		-0.13	[	0.13	, 0.10	]	0.17	[	0.00 , 0.17]
			exch		1.97	[	0.13	, 4.60	]	12.2	[	0.00 , inf]
PYRm + COin	→	OAAm			0.17	[	0.06	, 0.29	]	0.04	[	0.00 , 0.11]
MALm	→	PYRm + CO			0.16	[	0.00	, 0.70	]	0.30	[	0.01 , 0.80]
MAL	→	PYR + CO			0.41	[	0.00	, 0.67	]	0.44	[	0.00 , 0.72]

CHAPTER 7 GENERAL DISCUSSION

The present thesis deals with the detailed investigation of an inducible mammalian expression system using ^{13}C-metabolic flux analysis to examine the implicit relationship between cell metabolism and cellular productivity. In line with this general goal, investigations were designed and performed aiming at (i) determining the metabolic pathways that are correlated to an increased production, (ii) assessing the impact of the timing of induction on the productivity and (iii) developing a rational fed-batch strategy pre- and post-induction and analyzing its impact on cellular growth and productivity.

For the first investigation, the aim was to characterize the metabolism of induced/non-induced cells in order to quantitatively assess if recombinant protein expression exert a significant "burden" (or "metabolic load") on the cells, as was demonstrated in the cases of yeasts and bacteria. More specifically, we sought to identify the main metabolic pathways whose activity is associated with increased production, using comparative ^{13}C -MFA (Chapter 4). This approach is increasingly being applied for the investigation of cultivated mammalian cells, as it allows a more accurate quantification of intracellular fluxes. To this end, a recombinant CHO cell line producing an antibody and harboring an efficient cumate-inducible expression system was employed. The cells were grown in semi-continuous cultures to permit a reliable determination of the main cell kinetic rates. Upon addition of a non-toxic concentration of cumate and under mid-hypothermic conditions (30°C), induced cells exhibited a slight reduction in the apparent specific growth rate (~9%) and a concomitant decrease in glucose uptake rate (~8%) compared with uninduced cells. It should be stressed that, albeit at a much lower rate, antibody production was also measured in the case of uninduced cultures due to minor leaky expression. Our study revealed that recombinant protein production correlated with an increase load on the cells. Although small in amplitude, significant changes were detected in a number of key intracellular pathways related to ATP and NADPH formation, including the pentose phosphate pathway, the malic enzyme reaction and the TCA cycle. Since the increase of total cellular protein resulting from MAb production is estimated to be at most 15 % of the total cellular protein mass, these changes occur presumably to support the additional energy required for protein synthesis and other related cellular events (e.g. post-translational modifications and secretion).

Irrespective of the level of recombinant protein expression, the percentage of the pyruvate pool entering the TCA was relatively high in both cultures (induced and non-induced cells) as compared to most published flux distributions of cultivated animal cells. Such highly efficient nutrient utilization is most likely related to the mild-hypothermic conditions prevailing in our experiments. However, induced cells notably exhibited a more efficient utilization of glucose, characterized by a higher fraction of pyruvate entering the TCA cycle (58% vs. 49%) mainly through pyruvate dehydrogenase. Conversely, the catabolic rates of most amino acids, including glutamine, were small and remained relatively unaffected by the onset of protein expression. The results of this study provided a quantitative indication that recombinant protein expression is associated with detectable changes in the primary metabolism of CHO cells. A number of important points should be emphasized regarding this study. First of all, we did not look at the effects of cell density at induction nor at the impact of cumate concentrations, two parameters that can potentially greatly affect cell productivity. The former is discussed in the second paper but the latter would indeed require more investigation. Preliminary experiments were performed with increasing cumate concentrations at induction only to assess any potential cytotoxic effect of this compound on the cells. Concentrations up to 5 µg/mL (5 times the concentration used in our study) had no detectable impact on the cell specific growth rate (data not shown), but the effects on productivity were not evaluated. Besides, as the focus was to evaluate the impact of recombinant protein expression, we have not characterized and compared the metabolism of the parental cell line (i.e. not harboring the inducible expression system) or clones exhibiting different expression levels. A number of studies have reported that clonal variations can lead to significant metabolic changes (Dietmair et al., 2012) that are potentially more important than the ones directly attributable to protein expression. Also, at this stage of the work, no efforts were done to optimize the production, for example by using better medium formulations. The chemically defined medium employed in the study was chosen primarily because it allowed conducting more precise labeling experiments.

Having revealed differences in the primary metabolism of induced and uninduced cells, the goal of the subsequent study was to determine the impact of process conditions on productivity and to assess if these changes could also be reflected in the primary metabolism, and thereby provide some indications to guide further process optimization. More specifically, we studied the impact

of the timing of induction, as the latter determines the amount of biomass during the production phase, as well as the availability of nutrients. Although it is a commonly studied factor in the case of inducible microbial systems, to our knowledge no comprehensive metabolic study has been performed to date in the case of induced mammalian cells. Our investigation was performed by taking cells at different stages of growth and comparing the main kinetics upon transfer and induction in fresh medium (while maintaining the various cell densities prevailing at the time of induction). Our study demonstrated that it is not beneficial, in terms of product yield, to induced cells at high concentrations, due to an apparent "cell density effect" (whereby the specific productivity is negatively correlated with cell density) most likely due to a combination of cell age effects, reduced availability of nutrients and/or the presence of waste metabolites. To gain more physiological insights, cultures induced respectively at low and high cell densities were further characterized by ^{13}C -MFA and a number of key intracellular fluxes were found to be affected by the cell density at induction and the corresponding availability of nutrients. While glucose utilization was more efficient in high cell density cultures, with notably a greater fraction of pyruvate entering the TCA cycle (41% vs. 17%), the catabolic rates of most amino acids were found to be reduced. The entry of pyruvate into the TCA cycle mostly occurs via pyruvate dehydrogenase (PDH), while the anaplerotic conversion of pyruvate to oxaloacetate via pyruvate carboxylase (PC) accounted approximately 5 % and 27 % of the total pyruvate entering the TCA for cells induced at respectively high and low cell concentrations. On the whole, amino acids accounted for approximately 60 % of the total carbon input into the TCA for cells induced at low cell concentration, whereas this fraction was reduced down to only 20 % at higher cell densities. In the latter case, this is compensated by a greater pyruvate influx into the TCA. It should be underlined that, in this study, the metabolic comparison was restricted to the exponential growth period immediately following induction of the cultures with cumate. As evident from extracellular rate measurements, a significant flux rewiring also occurred at later stage of the production phase when cells were still secreting the recombinant product. Obtaining the intracellular flux distributions corresponding to these states would however require the application of unstationary ^{13}C -MFA and hence required additional measurements.

While valuable information was obtained with the use of isotopic tracers, from a process optimization point of view, a key limitation of the aforementioned studies rests on the fact that a

complete medium exchange was performed at the time of induction, which is not practical to implement at large scale (i.e. in the context of industrial manufacturing). Fed-batch operation remains the most prominent mode in industry to avoid the early nutrient limitations encountered in batch cultures. For this reason and given the fact that nutrient availability was shown to have a significant impact, the next study was focused on investigating the use of feeding strategies for maximising the productivity of the inducible expression platform, while retaining a relative ease of operation (i.e. without the need for complete medium exchange).

Compared to induced batch cultures, the use of fed-batch operation allowed to significantly enhance both the cell and product concentrations during the production phase. More interestingly, varying the amount of glutamine present in the feed led to two distinct metabolic states characterized by different cell specific rates of growth and production. Glutamine has long been identified as a major source of energy, nitrogen and carbon for cultivated mammalian cells and its metabolism can lead to the detrimental accumulation of ammonia in the culture environment. Carbon labeling experiments at different glutamine concentrations were thus performed in semi-continuous cultures to further decipher the impact of this nutrient on the cell metabolism. The main glycolytic fluxes were found to increase by 15 to 25% in cultures fed with low glutamine levels compared to high glutamine cultures and it was accompanied by a decreased oxidative pentose phosphate pathway. Also, fluxes around the pyruvate branch point were markedly different for the two conditions under investigation. In low glutamine cultures, a higher portion of the intracellular pyruvate pool entered TCA (66%), while the fraction was 48% for cultures with a high uptake rate of glutamine. Although pyruvate is mostly derived from glucose metabolized through glycolysis, pyruvate recycling from the TCA was also significant, accounting for an estimated 11 and 16 % of the intracellular pool originated through the conversion of malate via malic enzyme for low and high glutamine cultures, respectively. Overall, our findings of physiological impact of glutamine levels on the cells suggest that reducing the amount of glutamine present in the feed could increase the specific productivity of cells although it might limit the cell growth.

It should be emphasized that, unlike the previous two studies, these fed-batch experiments were all performed at 37°C. Combined with a fed-strategy, performing a temperature shift at the time of induction would in all likelihood further extend the production phase, but the impact on the product yield would have to be assessed.

To perform the various metabolic investigations described above, ^{13}C labeling experimental procedures had to be adapted or developed throughout this thesis. At the early stage of our work, labeling studies were performed in parallel semi-continuous (or repeated batch) cultures, which provided a relative ease of operation with good approximation of (pseudo) steady-state conditions. However, only the mass isotopomer distributions of extracellular metabolites (three excreted amino acids and lactate) could be readily measured and used for the analysis. Since the number of measurements was limited, parallel labeling experiments containing various labeled glucose and glutamine tracers were conducted to improve the resolution of the calculated intracellular fluxes. For each condition under investigation, we conducted 5 parallel experiments containing unlabeled, [1-^{13}C], [6-^{13}C], [U-$^{13}C_6$] glucose and [U–$^{13}C_5$] glutamine. This selection of tracers was motivated by their impact on the identifiability of intracellular flux estimates. The main experimental constraint was to maintain all the parallel cultures in a similar physiological state, but proved to be achievable with careful culture inoculation/maintenance procedures. Although the approach involved repeated feeding of expensive tracers, this was partly compensated by the fact that the cultures were operated at relatively small volumes.

While we were able to quantify the main intracellular fluxes with relatively narrow confidence intervals, efforts were subsequently done to optimize the labeling conditions using the prior knowledge gained from the first comprehensive labeling study. With the aid of simulations, we evaluated ^{13}C -tracers that may allow fluxes to be reliably determined by performing a single labeling experiment involving a mixture of labeled substrates. The challenge here was to create an appropriate precision scoring metric that allows comparing different labeling scenarios more efficiently. The simulation results revealed that for a single labeling experiment, using a mixture of [1-^{13}C] glucose and [U-$^{13}C_5$] glutamine will generally be more effective and provide the best resolution score. For the second study, analytical methods to measure labeled metabolites had also significantly improved and the labeling patterns of three secreted extracellular amino acids (aspartate, alanine and glutamate) and three extracellular organic acids (lactate, succinate and α-

ketoglutarate) could be successfully measured. The first two labeling investigations were carried out by assuming that the mass distribution of extracellular metabolites is reflective of their corresponding intracellular counterparts. The use of “dilution fluxes” permits to correct any potential dilution effects resulting from the presence of unlabeled sources, but will the present the drawback of increasing the confidence intervals as more fluxes need to be estimated. For the last labeling study, the optimization of cell extraction protocols allowed us to analyse the labeling pattern of intracellular metabolites (lactate, alanine, succinate and glutamate) thereby providing further confidence in the experimental data used for flux quantification.

CHAPTER 8 CONCLUSION AND RECOMMENDATIONS

The main objective of this thesis was to quantitatively characterize the primary metabolism of an inducible mammalian expression system. The experimental and mathematical methods developed in this thesis allowed to obtain reliable estimation of important intracellular fluxes. ^{13}C - metabolic flux analysis has been recently used by others for the characterization of CHO cells in culture, mainly to describe the metabolic flux distributions during the exponential growth or stationary phases, on in high cell density perfusion cultures. The main novelty of this work resides in its application to investigate and compare different process conditions in an effort to further understand the links between the cell metabolism and specific productivity, so as to provide a rational basis for process development. We have established that the onset of recombinant protein expression is associated with small but detectable changes in the primary metabolism of the cells. We have then demonstrated that cultures yielding different levels of productivity (due to different process conditions) were also characterized by distinct intracellular flux distributions. Finally, we have shown that through different feeding regimes, induced cultures can be driven towards metabolic states favoring either cell growth or cellular productivity.

The main original contributions of this work can thus be summarized as follows:

- The comprehensive metabolic characterization of the “ON” and “OFF” states of an inducible mammalian expression system, thereby allowing an assessment of the metabolic load exerted by heterologous protein expression on the primary metabolism of cells
- The ^{13}C-based metabolic characterization of CHO cells under mild hypothermia conditions
- A quantitative assessment of how the timing of induction impacts the metabolism and productivity of the cells in a biphasic process
- The development and application of fed-batch protocols to enhance the yield for an inducible expression system

- The ^{13}C -MFA based analysis of different feeding regimes having distinct impact on cellular growth and productivity

The following outlines some recommendations for future work:

Characterization of clones with varying expression levels: Given that the work described in this thesis was performed on a particular cell line expressing a specific product, the extent to which the main findings can be generalized to other mammalian cell expression systems remains an open question. To complement our work, it could be interesting to perform a detailed ^{13}C -based metabolic comparison of distinct cell clones exhibiting different productivity levels. Such work could confirm (or refute) the presumed links between specific productivity and the cell primary metabolism. Analyzing clones with similar productivity levels would also be important to assess the relative importance of metabolic changes solely due to clonal variations. Provided that general trends could be inferred and generalized from such analysis, it would bring a valuable tool for the selection of clones and speed-up an important step in cell culture process development.

Non-stationary ^{13}C-MFA: Due to the intrinsic transient nature of many cell culture processes (including inducible expression systems), it would be appealing to apply non-stationary ^{13}C metabolic flux analysis so as to enable the characterization at any point during a culture. Non-stationary ^{13}C-flux analysis has been applied in many microbial systems (Noh et al., 2007; Schaub et al., 2007), but several aspects have to be taken into account before it can practically be applied to mammalian cell systems. Non-stationary labeling experiments require both exact quantification of intracellular metabolite concentrations and determination of relative isotopomer fractions of the respective intermediates. Nonetheless, recent emerging studies have demonstrated the potential of this approach for mammalian cells (Woo Suk Ahn & Antoniewicz, 2011). The main challenge lies in the establishment of proper procedures for sample preparation, including inactivation of metabolism and efficient extraction of the required metabolites, as well as analytical methods for quantification of these metabolites and determination of the isotopic distributions must also be established.

Substitution of glutamine in fed-batch cultures: Glutamine level in the feed was shown to have a determinant impact on the growth/productivity of the cells. Several studies have demonstrated that glutamine can be substituted by pyruvate (Genzel, Ritter, König, Alt, & Reichl, 2005) or glutamate (Altamirano et al., 2000). These strategies could be explored in the context of induction. One strategy could involve the complete replacement of glutamine (both in the basal medium and in the concentrated feed) and another one would study partial replacement of glutamine (replacement in the feed only). The effects of those substitutions would be comprehensively characterized using ^{13}C-labeling experiment. Furthermore, fed-batch cultures could potentially be enhanced with a dynamic feeding protocol, with the feed adjusted based on the specific uptake rate of a reference nutrient.

Integrative "omics" analysis: There are several potential bottlenecks limiting recombinant protein production in mammalian cells. The most important limitations can potentially be at the transcription, translation and/or post-translation processing levels. Our studies were strictly based on metabolic flux analysis, but the application of other 'omics' approaches (transcriptomics, proteomics, metabolomics) could potentially provide useful and complementary information to the present work.

REFERENCES

Ahn, W. S., & Antoniewicz, M. R. (2011). Metabolic flux analysis of CHO cells at growth and non-growth phases using isotopic tracers and mass spectrometry. *Metabolic Engineering, 13*(5), 598-609.

Ahn, W. S., & Antoniewicz, M. R. (2012). Towards dynamic metabolic flux analysis in CHO cell cultures. *Biotechnology Journal, 7*(1), 61-74.

Ahn, W. S., & Antoniewicz, M. R. (2013). Parallel labeling experiments with [1,2-13C]glucose and [U-13C]glutamine provide new insights into CHO cell metabolism. *Metabolic Engineering, 15*(0), 34-47.

Al-Rubeai, M., Emery, A., Chalder, S., & Jan, D. (1992). Specific monoclonal antibody productivity and the cell cycle-comparisons of batch, continuous and perfusion cultures. *Cytotechnology, 9*(1-3), 85-97.

Al Zaid Siddiquee, K., Arauzo-Bravo, M. J., & Shimizu, K. (2004). Metabolic flux analysis of pykF gene knockout Escherichia coli based on 13C-labeling experiments together with measurements of enzyme activities and intracellular metabolite concentrations. *Applied Microbiology and Biotechnology, 63*(4), 407-417.

Altamirano, C., Illanes, A., Becerra, S., Cairo, J. J., & Godia, F. (2006). Considerations on the lactate consumption by CHO cells in the presence of galactose. *Journal of Biotechnololgy, 125*(4), 547-556.

Altamirano, C., Illanes, A., Casablancas, A., Gamez, X., Cairo, J. J., & Godia, C. (2001). Analysis of CHO cells metabolic redistribution in a glutamate-based defined medium in continuous culture. *Biotechnology Progress, 17*(6), 1032-1041.

Altamirano, C., Paredes, C., Cairo, J. J., & Godia, F. (2000). Improvement of CHO cell culture medium formulation: simultaneous substitution of glucose and glutamine. *Biotechnology Progress, 16*(1), 69-75.

Altamirano, C., Paredes, C., Illanes, A., Cairo, J. J., & Godia, F. (2004). Strategies for fed-batch cultivation of t-PA producing CHO cells: substitution of glucose and glutamine and rational design of culture medium. *Journal of Biotechnology, 110*(2), 171-179.

Amribt, Z., Niu, H., & Bogaerts, P. (2013). Macroscopic modelling of overflow metabolism and model based optimization of hybridoma cell fed-batch cultures. *Biochemical Engineering Journal, 70*(0), 196-209.

Antoniewicz, M. R., Kelleher, J. K., & Stephanopoulos, G. (2006). Determination of confidence intervals of metabolic fluxes estimated from stable isotope measurements. *Metabolic Engineering, 8*(4), 324-337.

Antoniewicz, M. R., Kelleher, J. K., & Stephanopoulos, G. (2007). Accurate assessment of amino acid mass isotopomer distributions for metabolic flux analysis. *Analytical Chemistry, 79*(19), 7554-7559.

Antoniewicz, M. R., Kelleher, J. K., & Stephanopoulos, G. (2007). Elementary metabolite unites (EMU): a novel framwork for modeling isotopic distributions. *Metabolic Engineering, 9*(1), 68-86.

Aoyama, T., & Chua, N. H. (1997). A glucocorticoid-mediated transcriptional induction system in transgenic plants. *The Plant Journal, 11*(3), 605-612.

Baughman, A. C., Huang, X., Sharfstein, S. T., & Martin, L. L. (2010). On the dynamic modeling of mammalian cell metabolism and mAb production. *Computers & Chemical Engineering, 34*(2), 210-222.

Becerra, S., Berrios, J., Osses, N., & Altamirano, C. (2012). Exploring the effect of mild hypothermia on CHO cell productivity. *Biochemical Engineering Journal, 60*, 1-8.

Bi, J.-X., Shuttleworth, J., & Al-Rubeai, M. (2004). Uncoupling of cell growth and proliferation results in enhancement of productivity in p21CIP1-arrested CHO cells. *Biotechnology and Bioengineering, 85*(7), 741-749.

Bibila, T. A., & Robinson, D. K. (1995). In pursuit of the optimal fed-batch process for monoclonal antibody production. *Biotechnology Progress, 11*, 1-13.

Blum, J. J., & Stein, R. B. (1982). On the analysis of metabolic networks. Goldberger RF (Eds). In *Biological Regulation and Development*. New York: Plenum Press; 1982:99-124.

Boghigian, B. A., Seth, G., Kiss, R., & Pfeifer, B. A. (2010). Metabolic flux analysis and pharmaceutical production. *Metabolic Engineering, 12*(2), 81-95.

Bonarius, H. P., Hatzimanikatis, V., Meesters, K. P., de Gooijer, C. D., Schmid, G., & Tramper, J. (1996). Metabolic flux analysis of hybridoma cells in different culture media using mass balances. *Biotechnology and Bioengineering, 50*(3), 299-318.

Bonarius, H. P., Ozemre, A., Timmerarends, B., Skrabal, P., Tramper, J., Schmid, G., & Heinzle, E. (2001). Metabolic-flux analysis of continuously cultured hybridoma cells using (13)CO(2) mass spectrometry in combination with (13)C-lactate nuclear magnetic resonance spectroscopy and metabolite balancing. *Biotechnology and Bioengineering, 74*(6), 528-538.

Bonarius, H. P., Schmid, G., & Tramper, J. (1997). Flux analysis of underdetermined metabolic networks: the quest for the missing constraints. *Trends in Biotechnology, 15*, 308-314.

Bonarius, H. P., Timmerarends, B., de Gooijer, C. D., & Tramper, J. (1998). Metabolite-balancing techniques vs. 13C tracer experiments to determine metabolic fluxes in hybridoma cells. *Biotechnology and Bioengineering, 58*(2-3), 258-262.

Borys, M. C., Linzer, D. I., & Papoutsakis, E. T. (1994). Ammonia affects the glycosylation patterns of recombinant mouse placental lactogen-I by chinese hamster ovary cells in a pH-dependent manner. *Biotechnology and Bioengineering, 43*(6), 505-514.

Brown, I. R., & Rush, S. J. (1990). Expression of heat shock genes (hsp70) in the mammalian brain: Distinguishing constitutively expressed and hyperthermia-inducible mRNA species. *Journal of Neuroscience Research, 25*(1), 14-19.

Burdon, R. H. (1986). Heat shock and the heat shock proteins. *Biochemical Journal, 240*(2), 313.

Burleigh, S., van de Laar, T., Stroop, C., van Grunsven, W., O'Donoghue, N., Rudd, P., & Davey, G. (2011). Synergizing metabolic flux analysis and nucleotide sugar metabolism to understand the control of glycosylation of recombinant protein in CHO cells. *BMC Biotechnology, 11*(1), 95.

Butler, M., & Meneses-Acosta, A. (2012). Recent advances in technology supporting biopharmaceutical production from mammalian cells. *Applied Microbiology and Biotechnology, 96*(4), 885-894.

Chen, F., Kou, T., Fan, L., Zhou, Y., Ye, Z., Zhao, L., & Tan, W.-S. (2011). The combined effect of sodium butyrate and low culture temperature on the production, sialylation, and biological activity of an antibody produced in CHO cells. *Biotechnology and Bioprocess Engineering, 16*(6), 1157-1165.

Chen, P., & Harcum, S. W. (2005). Effects of amino acid additions on ammonium stressed CHO cells. *Journal of Biotechnology, 117*(3), 277-286.

Choi, J. H., Keum, K. C., & Lee, S. Y. (2006). Production of recombinant proteins by high cell density culture of Escherichia coli. *Chemical Engineering Science, 61*(3), 876-885.

Chon, J. H., & Zarbis-Papastoitsis, G. (2011). Advances in the production and downstream processing of antibodies. *New Biotechnology, 28*(5), 458-463.

Christensen, B., & Nielsen, J. (2000a). Metabolic network analysis of Penicillium chrysogenum using (13)C-labeled glucose. *Biotechnology and Bioengineering, 68*(6), 652-659.

Christensen, B., & Nielsen, J. (2000b). Metabolic network analysis. A powerful tool in metabolic engineering. *Advances in Biochemical Engineering/Biotechnology, 66*, 209-231.

Chun, B.-H., Park, S.-Y., Chung, N., & Bang, W.-G. (2003). Enhanced production of recombinant B-domain deleted factor VIII from Chinese hamster ovary cells by propionic and butyric acids. *Biotechnology Letters, 25*(4), 315-319.

Costenoble, R., Muller, D., Barl, T., van Gulik, W. M., van Winden, W. A., Reuss, M., & Heijnen, J. J. (2007). 13C-Labeled metabolic flux analysis of a fed-batch culture of elutriated Saccharomyces cerevisiae. *FEMS Yeast Res, 7*(4), 511-526.

Craig Seamans, T., & Hu, W.-S. (1990). Kinetics of growth and antibody production by a hybridoma cell line in a perfusion culture. *Journal of fermentation and bioengineering, 70*(4), 241-245.

Crown, S. B., Ahn, W. S., & Antoniewicz, M. R. (2012). Rational design of 13C-labeling experiments for metabolic flux analysis in mammalian cells. *BMC Systems Biology, 6*(43).

Crown, S. B., & Antoniewicz, M. R. (2013). Parallel labeling experiments and metabolic flux analysis: Past, present and future methodologies. *Metabolic Engineering, 16*(0), 21-32.

Cruz, H. J., Freitas, C. M., Alves, P. M., Moreira, J. L., & Carrondo, M. J. T. (2000). Effects of ammonia and lactate on growth, metabolism, and productivity of BHK cells. *Enzyme and Microbial Technology, 27*(1-2), 43-52.

Cruz, H. J., Moreira, J. L., & Carrondo, M. J. T. (2000). Metabolically optimised BHK cell fed-batch cultures. *Journal of Biotechnology, 80*(2), 109-118.

Dalm, M. C. F., Lamers, P. P., Cuijten, S. M. R., Tjeerdsma, A. M., Grunsven, W. M. J., Tramper, J., & Martens, D. E. (2007). Effect of Feed and Bleed Rate on Hybridoma Cells in an Acoustic Perfusion Bioreactor: Metabolic Analysis. *Biotechnology Progress, 23*, 560-569.

Datta, P., Linhardt, R. J., & Sharfstein, S. T. (2013). An 'omics approach towards CHO cell engineering. *Biotechnology and Bioengineering*, 110(5):1255-71

DeBerardinis, R. J., Mancuso, A., Daikhin, E., Nissim, I., Yudkoff, M., Wehrli, S., & Thompson, C. B. (2007). Beyond aerobic glycolysis: Transformed cells can engage in glutamine metabolism that exceeds the requirement for protein and nucleotide synthesis. *Proceedings of the National Academy of Sciences, 104*(49), 19345-19350.

Deshpande, R., Yang, T. H., & Heinzle, E. (2009). Towards a metabolic and isotopic steady state in CHO batch cultures for reliable isotope-based metabolic profiling. *Biotechnology Journal, 4*(2), 247-263.

Dietmair, S., Hodson, M. P., Quek, L.-E., Timmins, N. E., Gray, P., & Nielsen, L. K. (2012). A multi-omics analysis of recombinant protein production in hek293 cells. *PloS one, 7*(8), e43394.

Dietmair, S., Nielsen, L. K., & Timmins, N. E. (2011). Engineering a mammalian super producer. *Journal of Chemical Technology & Biotechnology, 86*(7), 905-914.

Dinnis, D. M., & James, D. C. (2005). Engineering mammalian cell factories for improved recombinant monoclonal antibody production: lessons from nature? *Biotechnology and Bioengineering, 91*(2), 180-189.

Dinnis, D. M., Stansfield, S. H., Schlatter, S., Smales, C. M., Alete, D., Birch, J. R., . . . James, D. C. (2006). Functional proteomic analysis of GS-NS0 murine myeloma cell lines with varying recombinant monoclonal antibody production rate. *Biotechnology and Bioengineering, 94*(5), 830-841.

Doverskog, M., Ljunggren, J., Öhman, L., & Häggström, L. (1997). Physiology of cultured animal cells. *Journal of Biotechnology, 59*(1–2), 103-115.

Dowd, J. E., Kwok, K. E., & Piret, J. M. (2001). Glucose-based optimization of CHO-cell perfusion cultures. *Biotechnology and Bioengineering, 75*(2), 252-256.

Elmore, S. (2007). Apoptosis: A Review of Programmed Cell Death. *Toxicologic Pathology, 35*(4), 495-516.

Fischer, E., & Sauer, U. (2005). Large-scale in vivo flux analysis shows rigidity and suboptimal performance of Bacillus subtilis metabolism. [10.1038/ng1555]. *Nature genetics, 37*(6), 636-640.

Fogolin, M. B., Wagner, R., Etcheverrigaray, M., & Kratje, R. (2004). Impact of temperature reduction and expression of yeast pyruvate carboxylase on hGM-CSF-producing CHO cells. *Journal of Biotechnology, 109*(1-2), 179-191.

Follstad, B. D., & Stephanopoulos, G. (1998). Effect of reversible reactions on isotope label redistribution Analysis of the pentose phosphate pathway. *European Journal of Biochemistry, 252*, 360-371.

Forster, K., Helbl, V., Lederer, T., Urlinger, S., Wittenburg, N., & Hillen, W. (1999). Tetracycline-inducible expression systems with reduced basal activity in mammalian cells. *Nucleic Acids Research, 27*(2), 708-710.

Fox, S. R., Patel, U. A., Yap, M. G. S., & Wang, D. I. C. (2004). Maximizing interferon-γ production by chinese hamster ovary cells through temperature shift optimization: Experimental and modeling. *Biotechnology and Bioengineering, 85*(2), 177-184.

Fussenegger, M., Morris, R. P., Fux, C., Rimann, M., von Stockar, B., Thompson, C. J., & Bailey, J. E. (2000). Streptogramin-based gene regulation systems for mammalian cells. [10.1038/81208]. *Nature Biotechnology, 18*(11), 1203-1208.

Gaglio, D., Metallo, C. M., Gameiro, P. A., Hiller, K., Danna, L. S., Balestrieri, C., Chiaradonna, F. (2011). Oncogenic K-Ras decouples glucose and glutamine metabolism to support cancer cell growth. *Molecular Systems Biology, 7*(1).

Gaillet, B., Gilbert, R., Amziani, R., Guilbault, C., Gadoury, C., Caron, A. W., Massie, B. (2007). High-Level Recombinant Protein Production in CHO Cells Using an Adenoviral Vector and the Cumate Gene-Switch. *Biotechnology Progress, 23*(1), 200-209.

Gaillet, B., Gilbert, R., Broussau, S., Pilotte, A., Malenfant, F., Mullick, A., Massie, B. (2010). High-level recombinant protein production in CHO cells using lentiviral vectors and the cumate gene-switch. *Biotechnology and Bioengineering, 106*(2), 203-215.

Gawlitzek, M., Valley, U., & Wagner, R. (1998). Ammonium ion and glucosamine dependent increases of oligosaccharide complexity in recombinant glycoproteins secreted from cultivated BHK-21 cells. *Biotechnology and Bioengineering, 57*(5), 518-528.

Geisse, S., & Voedisch, B. (2012). Transient Expression Technologies: Past, Present, and Future. In V. Voynov & J. A. Caravella (Eds.), *Therapeutic Proteins* (Vol. 899, pp. 203-219): Humana Press.

Genzel, Y., Ritter, J. B., König, S., Alt, R., & Reichl, U. (2005). Substitution of Glutamine by Pyruvate To Reduce Ammonia Formation and Growth Inhibition of Mammalian Cells. *Biotechnology Progress, 21*(1), 58-69.

Ghorbaniaghdam, A., Henry, O., & Jolicoeur, M. (2013). A kinetic-metabolic model based on cell energetic state: study of CHO cell behavior under Na-butyrate stimulation. *Bioprocess and Biosystems Engineering, 36*(4), 469-487.

Glacken, M. W. (1986). Reduction of Waste Product Excretion via Nutrient Control: Possible Strategies for Maximizing Product and Cell yields on Serum in Cultures of Hybridoma Cells. *Biotechnology and Bioengineering, 28*, 1376-1389.

Glick, B. R. (1995). Metabolic load and heterologous gene expression. *Biotechnology Advances, 13*(2), 247-261.

Go, E. P., Liao, H.-X., Alam, S. M., Hua, D., Haynes, B. F., & Desaire, H. (2013). Characterization of Host-Cell Line Specific Glycosylation Profiles of Early Transmitted/Founder HIV-1 gp120 Envelope Proteins. *Journal of Proteome Research, 12*(3), 1223-1234.

Gombert, A. K., & Nielsen, J. (2000). Mathematical modelling of metabolism. *Current Opinion in Biotechnology, 11*(2), 180-186.

Gossen, M., & Bujard, H. (1992). Tight control of gene expression in mammalian cells by tetracycline-responsive promoters. *Proceedings of the National Academy of Sciences, 89*(12), 5547-5551.

Goudar, C., Biener, R., Boisart, C., Heidemann, R., Piret, J., de Graaf, A., & Konstantinov, K. (2010). Metabolic flux analysis of CHO cells inperfusion culture by metabolite balancing and 2D [13C,1H] Cosy NMR spectroscopy. *Metabolic Engineering, 12*(2), 138-149.

Goudar, C., Biener, R., Zhang, C., Michaels, J., Piret, J., & Konstantinov, K. (2006). Towards Industrial Application of Quasi Real-Time Metabolic Flux Analysis for Mammalian Cell Culture. In W.-S. Hu (Ed.), *Cell Culture Engineering* (Vol. 101, pp. 99-118): Springer Berlin Heidelberg.

Goudar, C. T., Biener, R., Konstantinov, K. B., & Piret, J. M. (2009). Error propagation from prime variables into specific rates and metabolic fluxes for mammalian cells in perfusion culture. *Biotechnology Progress, 25*(4), 986-998.

Goudar, C. T., Joeris, K., Konstantinov, K. B., & Piret, J. M. (2005). Logistic Equations Effectively Model Mammalian Cell Batch and Fed-Batch Kinetics by Logically Constraining the Fit. *Biotechnology Progress, 21*(4), 1109-1118.

Han, Y. K., Koo, T. Y., & Lee, G. M. (2009). Enhanced interferon-β production by CHO cells through elevated osmolality and reduced culture temperature. *Biotechnology Progress, 25*(5), 1440-1447.

Hendrick, V., Winnepenninckx, P., Abdelkafi, C., Vandeputte, O., Cherlet, M., Marique, T., . . . Werenne, J. (2001). Increased productivity of recombinant tissular plasminogen activator (t-PA) by butyrate and shift of temperature: a cell cycle phases analysis. *Cytotechnology, 36*(1), 71-83.

Henry, O., & Durocher, Y. (2011). Enhanced glycoprotein production in HEK-293 cells expressing pyruvate carboxylase. *Metabolic Engineering, 13*, 499-507.

Henry, O., Jolicoeur, M., & Kamen, A. (2010). Unraveling the metabolism of HEK-293 cells using lactate isotopomer analysis. *Bioprocess and Biosystems Engineering, 34*(3), 263-273.

Henry, O., Kamen, A., & Perrier, M. (2007). Monitoring the physiological state of mammalian cell perfusion processes by on-line estimation of intracellular fluxes *Journal of Process Control, 17*, 241-251.

Henry, O., Kwok, E., & Piret, J. M. (2008). Simpler noninstrumented batch and semicontinuous cultures provide mammalian cell kinetic data comparable to continuous and perfusion cultures. *Biotechnology Progress, 24*(4), 921-931.

Henry, P. G., Adriany, G., Deelchand, D., Gruetter, R., Marjanska, M., Oz, G., . . . Ugurbil, K. (2006). In vivo 13C NMR spectroscopy and metabolic modeling in the brain: a practical perspective. *Magnetic Resonance Imaging, 24*, 527-539.

Heuchel, R., Radtke, F., Georgiev, O., Stark, G., Aguet, M., & Schaffner, W. (1994). The transcription factor MTF-1 is essential for basal and heavy metal-induced metallothionein gene expression. *The EMBO journal, 13*(12), 2870.

Heyland, J., Blank, L. M., & Schmid, A. (2011). Quantification of metabolic limitations during recombinant protein production in Escherichia coli. *Journal of Biotechnology, 155*(2), 178-184.

Heyland, J., Fu, J., Blank, L. M., & Schmid, A. (2010). Quantitative physiology of Pichia pastoris during glucose-limited high-cell density fed-batch cultivation for recombinant protein production. *Biotechnology and Bioengineering, 107*(2), 357-368.

Heyland, J., Fu, J., Blank, L. M., & Schmid, A. (2011). Carbon metabolism limits recombinant protein production in Pichia pastoris. *Biotechnology and Bioengineering, 108*(8), 1942-1953.

Hofmann, U., Maier, K., Niebel, A., Vacun, G., Reuss, M., & Mauch, K. (2008). Identification of metabolic fluxes in hepatic cells from transient 13C-labeling experiments: Part I. Experimental observations. *Biotechnology and Bioengineering, 100*(2), 344-354.

Holmes, W., Darby, R., Wilks, M., Smith, R., & Bill, R. (2009). Developing a scalable model of recombinant protein yield from Pichia pastoris: the influence of culture conditions, biomass and induction regime. *Microbial Cell Factories, 8*(1), 35.

Hoppe, U. C., Marban, E., & Johns, D. C. (2000). Adenovirus-Mediated Inducible Gene Expression in Vivo by a Hybrid Ecdysone Receptor. *Molecular Therapy, 1*(2), 159-164.

Huang, E. P., Marquis, C. P., & Gray, P. P. (2004). Process development for a recombinant Chinese hamster ovary (CHO) cell line utilizing a metal induced and amplified metallothionein expression system. *Biotechnology and Bioengineering, 88*(4), 437-450.

Huber, R., & Buchs, J. (2011). Utilizing high-throughput experimentation to enhance specific productivity of an E.coli T7 expression system by phosphate limitation. *BMC Biotechnology, 11*(22).

Irani, N., Wirth, M., van den Heuvel, J., & Wagner, R. (1999). Improvement of the primary metabolism of cell cultures by introducing a new cytoplasmic pyruvate carboxylase reaction. *Biotechnology and Bioengineering, 66*(4), 238-246.

Jain, E., & Kumar, A. (2008). Upstream processes in antibody production: Evaluation of critical parameters. *Biotechnology Advances, 26*(1), 46-72.

Jardon, M. A., Sattha, B., Braasch, K., Leung, A. O., Côté, H. C. F., Butler, M., . . . Piret, J. M. (2012). Inhibition of glutamine-dependent autophagy increases t-PA production in CHO Cell fed-batch processes. *Biotechnology and Bioengineering, 109*(5), 1228-1238.

Jayapal, K., Wlaschin, K., Hu, W.-S., & Yap, M. (2007). Recombinant Protein Therapeutics from Cho Cells - 20 Years and Counting. *CHO Consortium: SBE Special Edition*, 40-47.

Jeong, D., Kim, T. S., Lee, J. W., Kim, K. T., Kim, H. J., Kim, I. H., & Kim, I. Y. (2001). Blocking of acidosis-mediated apoptosis by a reduction of lactate dehydrogenase activity through antisense mRNA expression. *Biochem Biophys Res Commun, 289*(5), 1141-1149.

Kaufmann, H., Mazur, X., Fussenegger, M., & Bailey, J. E. (1999). Influence of low temperature on productivity, proteome and protein phosphorylation of CHO cells. *Biotechnology and Bioengineering, 63*(5), 573-582.

Kaufmann, H., Mazur, X., Marone, R., Bailey, J. E., & Fussenegger, M. (2001). Comparative analysis of two controlled proliferation strategies regarding product quality, influence on tetracycline-regulated gene expression, and productivity. *Biotechnology and Bioengineering, 72*(6), 592-602.

Kelleher, J. K. (2001). Flux Estimation Using Isotopic Tracers: Common Ground for Metabolic Physiology and Metabolic Engineering. *Metabolic Engineering, 3*, 100-110.

Kim, J., Kim, Y.-G., & Lee, G. (2012). CHO cells in biotechnology for production of recombinant proteins: current state and further potential. *Applied Microbiology and Biotechnology, 93*(3), 917-930.

Kim, N. S., & Lee, G. M. (2002). Response of recombinant Chinese hamster ovary cells to hyperosmotic pressure: effect of Bcl-2 overexpression. *J Biotechnol, 95*(3), 237-248.

Kim, S. H., & Lee, G. M. (2007). Down-regulation of lactate dehydrogenase-A by siRNAs for reduced lactic acid formation of Chinese hamster ovary cells producing thrombopoietin. *Appl Microbiol Biotechnol, 74*(1), 152-159.

Klamt, S., & Schuster, S. (2002). Calculating as Many Fluxes as Possible in Underdetermined Metabolic Networks. *Molecular Biology Reports, 29*(1-2), 243-248.

Klapa, M. I., Park, S. M., Sinskey, A. J., & Stephanopoulos, G. (1999). Metabolite and isotopomer balancing in the analysis of metabolic cycles: I. Theory. *Biotechnology and Bioengineering, 62*(4), 375-391.

Kleijn, R. J., Geertman, J. M., Nfor, B. K., Ras, C., Schipper, D., Pronk, J. T., van Winden, W. A. (2007). Metabolic flux analysis of a glycerol-overproducing Saccharomyces cerevisiae strain based on GC-MS, LC-MS and NMR-derived C-labelling data. *FEMS Yeast Research, 7*(2), 216-231.

Kochanowski, N., Blanchard, F., Cacan, R., Chirat, F., Guedon, E., Marc, A., & Goergen, J. L. (2008). Influence of intracellular nucleotide and nucleotide sugar contents on recombinant interferon-γ glycosylation during batch and fed-batch cultures of CHO cells. *Biotechnology and Bioengineering, 100*(4), 721-733.

Kou, T.-C., Fan, L., Zhou, Y., Ye, Z.-Y., Liu, X.-P., Zhao, L., & Tan, W.-S. (2011). Detailed understanding of enhanced specific productivity in Chinese hamster ovary cells at low culture temperature. *Journal of Bioscience and Bioengineering, 111*(3), 365-369.

Kumar, N., Gammell, P., Meleady, P., Henry, M., & Clynes, M. (2008). Differential protein expression following low temperature culture of suspension CHO-K1 cells. *BMC Biotechnology, 8*(1), 42.

Kurokawa, H., Park, Y. S., Iijima, S., & Kobayashi, T. (1994). Growth characteristics in fed-batch culture of hybridoma cells with control of glucose and glutamine concentrations. *Biotechnology and Bioengineering, 44*(1), 95-103.

Kuystermans, D., Krampe, B., Swiderek, H., & Al-Rubeai, M. (2007). Using cell engineering and omic tools for the improvement of cell culture processes. *Cytotechnology, 53*(1-3), 3-22.

Langdom, S. P. (2008). Mammalian cell culture. In: Walker, JM, Rapley, R (Eds). *Molecular Biomethods Handbook*, pp. 861–873.

Lee, F. W., Elias, C. B., Todd, P., & Kompala, D. S. (1998). Engineering Chinese hamster ovary (CHO) cells to achieve an inverse growth-associated production of a foreign protein, β-galactosidase *Cell Culture Engineering VI* (pp. 73-80): Springer.

Lee, K., Berthiaume, F., Stephanopoulos, G., & Yamush, M. L. (1999). Metabolic Flux Analysis: A Powerful Tool for Monitoring Tissue Function. *Tissue Engineering, 5*(4), 347-368.

Lee, M. S., Kim, K. W., Kim, Y. H., & Lee, G. M. (2003). Proteome analysis of antibody-expressing CHO cells in response to hyperosmotic pressure. *Biotechnol Prog, 19*(6), 1734-1741.

Li, F., Vijayasankaran, N., Shen, A., Kiss, R., & Amanullah, A. (2010). Cell culture processes for monoclonal antibody production. *MAbs, 2*(5), 466-477.

Libourel, I. G. L., Gehan, J. P., & Shachar-Hill, Y. (2007). Design of substrate label for steady state flux measurements in plant system using the metabolic network of Brassica napus embryos. *Phytochemistry, 68*(16-18), 2211-2221.

Lim, Y., Wong, N. S. C., Lee, Y. Y., Ku, S. C. Y., Wong, D. C. F., & Yap, M. G. S. (2010). Engineering mammalian cells in bioprocessing – current achievements and future perspectives. *Biotechnology and Applied Biochemistry, 55*(4), 175-189.

Lipscomb, M. L., Mowry, M. C., & Kompala, D. S. (2004). Production of a secreted glycoprotein from an inducible promoter system in a perfusion bioreactor. *Biotechnology Progress, 20*(5), 1402-1407.

Ljunggren, J., & Haggstrom, L. (1992). Glutamine Limited Fed-Batch Culture Reduces the Overflow Metabolism of Amino Acids in Myeloma Cells. *Cytotechnology, 8*, 45-56.

Ljunggren, J., & Häggström, L. (1994). Catabolic control of hybridoma cells by glucose and glutamine limited fed batch cultures. *Biotechnology and Bioengineering, 44*(7), 808-818.

Llaneras, F., Pic, amp, & Jes. (2007). A procedure for the estimation over time of metabolic fluxes in scenarios where measurements are uncertain and/or insufficient. *BMC Bioinformatics, 8*(1), 421.

Llaneras, F., & Pico, J. (2008). Stoichiometric modelling of cell metabolism. *Journal of Bioscience and Bioengineering, 105*(1), 1-11.

Luo, J., Vijayasankaran, N., Autsen, J., Santuray, R., Hudson, T., Amanullah, A., & Li, F. (2012). Comparative metabolite analysis to understand lactate metabolism shift in Chinese hamster ovary cell culture process. *Biotechnology and Bioengineering, 109*(1), 146-156.

Maier, K., Hofmann, U., Reuss, M., & Mauch, K. (2008). Identification of metabolic fluxes in hepatic cells from transient 13C-labeling experiments: Part II. Flux estimation. *Biotechnology and Bioengineering, 100*(2), 355-370.

Mancuso, A., Sharfstein, S. T., Fernandez, E. J., Clark, D. S., & Blanch, H. W. (1998). Effect of extracellular glutamine concentration on primary and secondary metabolism of a murine hybridoma: an in vivo 13C nuclear magnetic resonance study. *Biotechnology and Bioengineering, 57*(2), 172-186.

Mancuso, A., Sharfstein, S. T., Tucker, S. N., Clark, D. S., & Blanch, H. W. (1994). Examination of primary metabolic pathways in a murine hybridoma with carbon-13 nuclear magnetic resonance spectroscopy. *Biotechnology and Bioengineering, 44*(5), 563-585.

Maranga, L., & Goochee, C. F. (2006). Metabolism of PER.C6TM cells cultivated under fed-batch conditions at low glucose and glutamine levels. *Biotechnology and Bioengineering, 94*(1), 139-150.

Martens, D. E. (2007). Metabolic Flux Analysis of Mammalian Cells. In M. Al-Rubeai & M. Fussenegger (Eds.), *Systems Biology* (Vol. 5, pp. 275-299): Springer Netherlands.

Martens, D. E., de Gooijer, C. D., van der Velden-de Groot, C. A. M., Beuvery, E. C., & Tramper, J. (1993). Effect of dilution rate on growth, productivity, cell cycle and size, and shear sensitivity of a hybridoma cell in a continuous culture. *Biotechnology and Bioengineering, 41*(4), 429-439.

Martial, A., Dardenne, M., Engasser, J. M., & Marc, A. (1991). Influence of Inoculum Age on Hybridoma Culture Kinetics. *Cytotechnology, 5*, 165-171.

Martinez, V. S., Dietmair, S., Quek, L. E., Hodson, M. P., Gray, P., & Nielsen, L. K. (2013). Flux balance analysis of CHO cells before and after a metabolic switch from lactate production to consumption. *Biotechnol Bioeng, 110*(2), 660-666.

Marx, A., de Graaf, A. A., Wiechert, W., Eggeling, L., & Sahm, H. (1996). Determination of the fluxes in the central metabolism of Corynebacterium glutamicum by nuclear magnetic resonance spectroscopy combined with metabolite balancing. *Biotechnology and Bioengineering, 49*(2), 111-129.

Matasci, M., Hacker, D. L., Baldi, L., & Wurm, F. M. (2008). Recombinant therapeutic protein production in cultivated mammalian cells: current status and future prospects. *Drug Discovery Today: Technologies, 5*(2–3), e37-e42.

McMurray-Beaulieu, V., Hisiger, S., Durand, C., Perrier, M., & Jolicoeur, M. (2009). Na-butyrate sustains energetic states of metabolism and t-PA productivity of CHO cells. *Journal of Bioscience and Bioengineering, 108*(2), 160-167.

Meleady, P., Doolan, P., Henry, M., Barron, N., Keenan, J., O'Sullivan, F., . . . Leonard, M. (2011). Sustained productivity in recombinant Chinese Hamster Ovary (CHO) cell lines: proteome analysis of the molecular basis for a process-related phenotype. *BMC Biotechnology, 11*(1), 78.

Mercille, S., Johnson, M., Lanthier, S., Kamen, A. A., & Massie, B. (2000). Understanding factors that limit the productivity of suspension-based perfusion cultures operated at high medium renewal rates. *Biotechnology and Bioengineering, 67*(4), 435-450.

Metallo, C. M., Walther, J. L., & Stephanopoulos, G. (2009). Evaluation of 13C isotopic tracers for metabolic flux analysis in mammalian cells. *Journal of Biotechnology, 144*(3), 167-174.

Miller, W. M., Blanch, H. W., & Wilke, C. R. (1988). A kinetic analysis of hybridoma growth and metabolism in batch and continuous suspension culture: Effect of nutrient concentration, dilution rate, and pH. *Biotechnology and Bioengineering, 32*(8), 947-965.

Mohan, C., Kim, Y.-G., Koo, J., & Lee, G. M. (2008). Assessment of cell engineering strategies for improved therapeutic protein production in CHO cells. *Biotechnology Journal, 3*(5), 624-630.

Mollney, M., Wiechert, W., Kownatzki, D., & de Graaf, A. A. (1999). Bidirectional reaction steps in metabolic networks: IV. Optimal design of isotopomer labeling experiments. *Biotechnology and Bioengineering, 66*(2), 86-103.

Morgan, J. A., & Rhodes, D. (2002). Mathematical Modeling of Plant Metabolic Pathways *Metabolic Engineering, 4*, 80-89.

Mullick, A., Xu, Y., Warren, R., Koutroumanis, M., Guilbault, C., Broussau, S., . . . Lo, R. (2006). The cumate gene-switch: a system for regulated expression in mammalian cells. *BMC Biotechnology, 6*(1), 43.

Mulukutla, B. C., Gramer, M., & Hu, W.-S. (2012). On metabolic shift to lactate consumption in fed-batch culture of mammalian cells. *Metabolic Engineering, 14*(2), 138-149.

Munger, J., Bennett, B. D., Parikh, A., Feng, X. J., McArdle, J., Rabitz, H. A., . . . Rabinowitz, J. D. (2008). Systems-level metabolic flux profiling identifies fatty acid synthesis as a target for antiviral therapy. *Nature Biotechnology, 26*(10), 1179-1186.

Nam, J. H., Ermonval, M., & Sharfstein, S. T. (2009). The effects of microcarrier culture on recombinant CHO cells under biphasic hypothermic culture conditions. *Cytotechnology, 59*(2), 81-91.

Neermann, J., & Wagner, R. (1996). Comparative analysis of glucose and glutamine metabolism in transformed mammalian cell lines, insect and primary liver cells. *Journal of Cellular Physiology, 166*(1), 152-169.

Niklas, J., & Heinzle, E. (2012). Metabolic Flux Analysis in Systems Biology of Mammalian Cells. In W. S. Hu & A.-P. Zeng (Eds.), *Genomics and Systems Biology of Mammalian Cell Culture* (Vol. 127, pp. 109-132): Springer Berlin / Heidelberg.

Niklas, J., Priesnitz, C., Rose, T., Sandig, V., & Heinzle, E. (2012). Primary metabolism in the new human cell line AGE1.HN at various substrate levels: increased metabolic efficiency and α1-antitrypsin production at reduced pyruvate load. *Applied Microbiology and Biotechnology, 93*(4), 1637-1650.

Niklas, J., Sandig, V., & Heinzle, E. (2011). Metabolite channeling and compartmentation in the human cell line AGE1.HN determined by 13C labeling experiments and 13C metabolic flux analysis. *Journal of Bioscience and Bioengineering, 112*(6), 616-623.

No, D., Yao, T. P., & Evans, R. (1996). Ecdysone-inducible gene expression in mammalian cells and transgenic mice. *Proceedings of the National Academy of Sciences, 93*(8), 3346-3351.

Noguchi, Y., Young, J. D., Aleman, J. O., Hansen, M. E., Kelleher, J. K., & Stephanopoulos, G. (2009). Effect of anaplerotic fluxes and amino acid availability on hepatic lipoapoptosis. *Journal of Biological Chemistry, 284*(48), 33425-33436.

Noh, K., Gronke, K., Luo, B., Takors, R., Oldiges, M., & Wiechert, W. (2007). Metabolic flux analysis at ultra short time scale: isotopically non-stationary 13C labeling experiments. *Journal of Biotechnology, 129*(2), 249-267.

Noh, K., Wahl, A., & Wiechert, W. (2006). Computational tools for isotopically instationary 13C labeling experiments under metabolic steady state conditions. *Metabolic Engineering, 8*(6), 554-577.

Noh, K., & Wiechert, W. (2006). Experimental design principles for isotopically instationary 13C labeling experiments. *Biotechnology and Bioengineering, 94*(2), 234-251.

Nolan, R. P., & Lee, K. (2011). Dynamic model of CHO cell metabolism. *Metabolic Engineering, 13*(1), 108-124.

Nolan, R. P., & Lee, K. (2012). Dynamic model for CHO cell engineering. *Journal of Biotechnology, 158*(1-2), 24-33.

Nyberg, G. B., Balcarcel, R. R., Follstad, B. D., Stephanopoulos, G., & Wang, D. I. C. (1999). Metabolism of peptide amino acids by Chinese hamster ovary cells grown in a complex medium. *Biotechnology and Bioengineering, 62*(3), 324-335.

Nyberg, G. B., Balcarcel, R. R., Follstad, B. D., Stephanopoulos, G., & Wang, D. I. C. (2000). Metabolic Effects on Recombinant Interferon; Glycosylation in Continuous Culture of Chinese Hamster Ovary Cells. *IBM Journal of Research and Development, 44*(5), 770-783.

O'Callaghan, P. M., & James, D. C. (2008). Systems biotechnology of mammalian cell factories. *Briefings in Functional Genomics & Proteomics, 7*(2), 95-110.

Omasa, T., Furuichi, K., Iemura, T., Katakura, Y., Kishimoto, M., & Suga, K. (2010). Enhanced antibody production following intermediate addition based on flux analysis in mammalian cell continuous culture. *Bioprocess and Biosystems Engineering, 33*(1), 117-125.

Omasa, T., Higashiyama, K. I., Shioya, S., & Suga, K. i. (1992). Effects of lactate concentration on hybridoma culture in lactate-controlled fed-batch operation. *Biotechnology and Bioengineering, 39*(5), 556-564.

Ozturk, S. S., & Hu, W. S. (2005). *Cell culture technology for pharmaceutical and cell-based therapies*: Taylor & Francis.

Ozturk, S. S., & Palsson, B. O. (1991). Growth, metabolic, and antibody production kinetics of hybridoma cell culture: 2. Effects of serum concentration, dissolved oxygen concentration, and medium pH in a batch reactor. *Biotechnology Progress, 7*(6), 481-494.

Ozturk, S. S., Riley, M. R., & Palsson, B. O. (1992). Effects of ammonia and lactate on hybridoma growth, metabolism, and antibody production. *Biotechnology and Bioengineering, 39*(4), 418-431.

Panda, A. (2003). Bioprocessing of Therapeutic Proteins from the Inclusion Bodies of Escherichia coli. In T. Ghose, P. Ghosh, S. Chand, S. K. Gupta, B. B. Lohray, K. Mazumdar-Shaw, P. Mishra, S. Nath, A. K. Panda & S. Suryanarayan (Eds.), *Biotechnology in India II* (Vol. 85, pp. 43-93): Springer Berlin Heidelberg.

Paredes, C., Sanfeliu, A., Cardenas, F., Cairó, J. J., & Gòdia, F. (1998). Estimation of the intracellular fluxes for a hybridoma cell line by material balances. *Enzyme and Microbial Technology, 23*(3–4), 187-198.

Park, J. H., Lee, S. Y., Kim, T. Y., & Kim, H. U. (2008). Application of systems biology for bioprocess development. *Trends in Biotechnology, 26*(8), 404-412.

Park, S. M., Klapa, M. I., Sinskey, A. J., & Stephanopoulos, G. (1999). Metabolite and isotopomer balancing in the analysis of metabolic cycles: II. Applications. *Biotechnology and Bioengineering, 62*(4), 392-401.

Petersen, S., de Graaf, A. A., Eggeling, L., Mollney, M., Wiechert, W., & Sahm, H. (2000). In vivo quantification of parallel and bidirectional fluxes in the anaplerosis of Corynebacterium glutamicum. *Journal of Biological Chemistry, 275*(46), 35932-35941.

Peuhkurinen, K. J., Hiltunen, J. K., & Hassinen, I. E. (1983). Metabolic compartmentation of pyruvate in the isolated perfused rat heart. *Biochemical Journal, 210*(1), 193-198.

Pörtner, R., & Schäfer, T. (1996). Modelling hybridoma cell growth and metabolism—a comparison of selected models and data. *Journal of Biotechnology, 49*(1), 119-135.

Provost, A., & Bastin, G. (2004). Dynamic metabolic modelling under the balanced growth condition. *Journal of Process Control, 14*(7), 717-728.

Quek, L.-E., Dietmair, S., Krömer, J. O., & Nielsen, L. K. (2010). Metabolic flux analysis in mammalian cell culture. *Metabolic Engineering, 12*(2), 161-171.

Quek, L.-E., Wittmann, C., Nielsen, L., & Kromer, J. (2009). OpenFLUX: efficient modelling software for 13C-based metabolic flux analysis. *Microbial Cell Factories, 8*.

Rajendra, Y., Kiseljak, D., Baldi, L., Hacker, D., & Wurm, F. (2012). Reduced glutamine concentration improves protein production in growth-arrested CHO-DG44 and HEK-293E cells. *Biotechnology Letters, 34*(4), 619-626.

Rita Costa, A., Elisa Rodrigues, M., Henriques, M., Azeredo, J., & Oliveira, R. (2010). Guidelines to cell engineering for monoclonal antibody production. *European Journal of Pharmaceutics and Biopharmaceutics, 74*(2), 127-138.

Rühl, M., Rupp, B., Nöh, K., Wiechert, W., Sauer, U., & Zamboni, N. (2012). Collisional fragmentation of central carbon metabolites in LC-MS/MS increases precision of 13C metabolic flux analysis. *Biotechnology and Bioengineering, 109*(3), 763-771.

Sanderson, C. S., Phillips, P. J., & Barford, J. P. (1996). Structured modelling of animal cells. *Cytotechnology, 21*(2), 149-153.

Sauer, P. W., Burky, J. E., Wesson, M. C., Sternard, H. D., & Qu, L. (2000). A high-yielding, generic fed-batch cell culture process for production of recombinant antibodies. *Biotechnology and Bioengineering, 67*(5), 585-597.

Sauer, U. (2006). Metabolic networks in motion: 13C-based flux analysis. *Molecular Systems Biology, 2*, 1-10.

Schaub, J., Mauch, K., & Reuss, M. (2007). Metabolic flux analysis in Enscherichia coli by integrating isotopic dynamic and isotopic stationary 13C labeling data. *Biotechnology and Bioengineering, 99*(5), 1170-1185.

Schmidt, K., Carlsen, M., Nielsen, J., & Villadsen, J. (1997). Modeling isotopomer distributions in biochemical networks using isotopomer mapping matrices. *Biotechnology and Bioengineering, 55*(6), 831-840.

Schmidt, K., Nielsen, J., & Villadsen, J. (1999). Quantitative analysis of metabolic fluxes in Encherichia coli, using two-dimentional NMR spectrometry and complete isotopomer models. *Journal of Biotechnology, 71*, 175-190.

Schneider, M., Marison, I. W., & von Stockar, U. (1996). The importance of ammonia in mammalian cell culture. *Journal of Biotechnology, 46*(3), 161-185.

Schützendübel, A., & Polle, A. (2002). Plant responses to abiotic stresses: heavy metal-induced oxidative stress and protection by mycorrhization. *Journal of Experimental Botany, 53*(372), 1351-1365.

Selvarasu, S., Ho, Y. S., Chong, W. P. K., Wong, N. S. C., Yusufi, F. N. K., Lee, Y. Y., . . . Lee, D.-Y. (2012). Combined in silico modeling and metabolomics analysis to characterize fed-batch CHO cell culture. *Biotechnology and Bioengineering, 109*(6), 1415-1429.

Sengupta, N., Rose, S. T., & Morgan, J. A. (2011). Metabolic Flux Analysis of CHO Cell Metabolism in the Late Non-Growth Phase. *Biotechnology and Bioengineering, 108*(1), 82-92.

Seth, G., Hossler, P., Yee, J. C., & Hu, W. S. (2006). Engineering cells for cell culture bioprocessing--physiological fundamentals *Cell Culture Engineering* (Vol. 101): Springer Berlin.

Sheikh, K., Förster, J., & Nielsen, L. K. (2005). Modeling Hybridoma Cell Metabolism Using a Generic Genome-Scale Metabolic Model of Mus musculus. *Biotechnology Progress, 21*(1), 112-121.

Sheikholeslami, Z., Jolicoeur, M., & Henry, O. (2013). Probing the metabolism of an inducible mammalian expression system using extracellular isotopomer analysis. *Journal of Biotechnology, 164*(4), 469-478.

Shen, J., Petersen, K. F., Behar, K. L., Brown, P., Nixon, T. W., Mason, G. F., . . . Rothman, D. L. (1999). Determination of the rate of the glutamate/glutamine cycle in the human brain by in vivo 13C NMR. *Proceedings of the National Academy of Sciences, 96*(14), 8235-8240.

Sidoli, F. R., Mantlaris, A., & Asprey, S. P. (2004). Modelling of mammalian cells and cell culture processes. *Cytotechnology, 44*, 27-46.

Sidorenko, Y., Wahl, A., Dauner, M., Genzel, Y., & Reichl, U. (2008). Comparison of Metabolic Flux Distributions for MDCK Cell Growth in Glutamine- and Pyruvate-Containing Media. *Biotechnology Progress, 24*(2), 311-320.

Simpson, N. E., & Constantinidis, I. (2007). 13C NMR isotopomeric analysis and its application in the study of endocrine cell metabolism and function. *Acta Bio-medica, 78*, 99-112.

Stephanopoulos, G. (1999). Metabolic Fluxes and Metabolic Engineering. *Metabolic Engineering, 1*, 1-11.

Stephanopoulos, G., Aristidou, A. A., & Nielsen, J. (1998). *Metabolic engineering: principles and methodologies*: Academic Press.

Sun, Z., Zhou, R., Liang, S., McNeeley, K. M., & Sharfstein, S. T. (2004). Hyperosmotic stress in murine hybridoma cells: effects on antibody transcription, translation, posttranslational processing, and the cell cycle. *Biotechnol Prog, 20*(2), 576-589.

Sunley, K., & Butler, M. (2010). Strategies for the enhancement of recombinant protein production from mammalian cells by growth arrest. *Biotechnology Advances, 28*(3), 385-394.

Suthers, P. F., Burgard, A. P., Dasika, M. S., Nowroozi, F., Van Dien, S., Keasling, J. D., & Maranas, C. D. (2007). Metabolic flux elucidation for large-scale models using 13C labeled isotopes. *Metabolic Engineering, 9*, 387-405.

Suthers, P. F., Chang, Y. J., & Maranas, C. D. (2010). Improved computational performance of MFA using elementary metabolite units and flux coupling. *Metabolic Engineering, 12*(2), 123-128.

Takuma, S., Hirashima, C., & Piret, J. M. (2007). Dependence on glucose limitation of the pCO2 influences on CHO cell growth, metabolism and IgG production. *Biotechnology and Bioengineering, 97*(6), 1479-1488.

Taschwer, M., Hackl, M., Hernández Bort, J. A., Leitner, C., Kumar, N., Puc, U., . . . Borth, N. (2012). Growth, productivity and protein glycosylation in a CHO EpoFc producer cell line adapted to glutamine-free growth. *Journal of Biotechnology, 157*(2), 295-303.

Templeton, N., Dean, J., Reddy, P., & Young, J. D. (2013). Peak antibody production is associated with increased oxidative metabolism in an industrially relevant fed-batch CHO cell culture. *Biotechnol Bioeng, 110*(7), 2013-2024.

Trummer, E., Fauland, K., Seidinger, S., Schriebl, K., Lattenmayer, C., Kunert, R., . . . Katinger, H. (2006a). Process parameter shifting: Part I. Effect of DOT, pH, and temperature on the

performance of Epo-Fc expressing CHO cells cultivated in controlled batch bioreactors. *Biotechnology and Bioengineering, 94*(6), 1033-1044.

Trummer, E., Fauland, K., Seidinger, S., Schriebl, K., Lattenmayer, C., Kunert, R., . . . Katinger, H. (2006b). Process parameter shifting: Part II. Biphasic cultivation—A tool for enhancing the volumetric productivity of batch processes using Epo-Fc expressing CHO cells. *Biotechnology and Bioengineering, 94*(6), 1045-1052.

Tsao, Y. S., Cardoso, A. G., Condon, R. G. G., Voloch, M., Lio, P., Lagos, J. C., . . . Liu, Z. (2005). Monitoring Chinese hamster ovary cell culture by the analysis of glucose and lactate metabolism. *Journal of Biotechnology, 118*, 316- 327.

Tuttle, S., Stamato, T., Perez, M. L., & Biaglow, J. (2000). Glucose-6-phosphate dehydrogenase and the oxidative pentose phosphate cycle protect cells against apoptosis induced by low doses of ionizing radiation. *Radiat Res, 153*(6), 781-787.

van Winden, W., Schipper, D., Verheijen, P., & Heijnen, J. (2001). Innovations in generation and analysis of 2D [(13)C,(1)H] COSY NMR spectra for metabolic flux analysis purposes. *Metabolic Engineering, 3*(4), 322-343.

van Winden, W. A., van Dam, J. C., Ras, C., Kleijn, R. J., Vinke, J. L., van Gulik, W. M., & Heijnen, J. J. (2005). Metabolic-flux analysis of Saccharomyces cerevisiae CEN.PK113-7D based on mass isotopomer measurements of (13)C-labeled primary metabolites. *FEMS Yeast Research, 5*(6-7), 559-568.

Walsh, G. (2010). Biopharmaceutical benchmarks 2010. *Nature Biotechnology, 28*, 917-924.

Walther, J. L., Metallo, C. M., Zhang, J., & Stephanopoulos, G. (2012). Optimization of 13C isotopic tracers for metabolic flux analysis in mammalian cells. *Metabolic Engineering, 14*(2), 162-171.

Wang, X.-h., Xu, J., Zhang, Y., Li, L., Feng, Q., Mi, L., & Chen, Z.-n. (2004). Inducible expression of Bcl-XLinhibits sodium butyrate-induced apoptosis in hybridoma, resulting in enhanced antibody production. *Cell Biology International, 28*(3), 185-191.

Weuster-Botz, D., Altenbach-Rehm, J., & Arnold, M. (2001). Parallel substrate feeding and pH-control in shaking-flasks. *Biochemical Engineering Journal, 7*(2), 163-170.

Wiechert, W. (2001). 13C metabolic flux analysis. *Metabolic Engineering, 3*(3), 195-206.

Wiechert, W., & de Graaf, A. A. (1997). Bidirectional reaction steps in metabolic networks: I. Modeling and simulation of carbon isotope labeling experiments. *Biotechnology and Bioengineering, 55*(1), 101-117.

Wiechert, W., Mollney, M., Isermann, N., Wurzel, M., & de Graaf, A. A. (1999). Bidirectional reaction steps in metabolic networks: III. Explicit solution and analysis of isotopomer labeling systems. *Biotechnology and Bioengineering, 66*(2), 69-85.

Wiechert, W., & Noh, K. (2005). From stationary to instationary metabolic flux analysis. *Advances in Biochemical Engineering/Biotechnology, 92*, 145-172.

Wiechert, W., Siefke, C., de Graaf, A. A., & Marx, A. (1997). Bidirectional reaction steps in metabolic networks: II. Flux estimation and statistical analysis. *Biotechnology and Bioengineering, 55*(1), 118-135.

Wilkens, C., Altamirano, C., & Gerdtzen, Z. (2011). Comparative metabolic analysis of lactate for CHO cells in glucose and galactose. *Biotechnology and Bioprocess Engineering, 16*(4), 714-724.

Wittmann, C. (2002). Metabolic flux analysis using mass spectrometry. *Advances in Biochemical Engineering/Biotechnology, 74*, 39-64.

Wittmann, C. (2007). Fluxome analysis using GC-MS. *Microbial Cell Factories, 6*, 6.

Wong, D. C. F., Wong, N. S. C., Goh, J. S. Y., May, L. M., & Yap, M. G. S. (2010). Profiling of N-glycosylation gene expression in CHO cell fed-batch cultures. *Biotechnology and Bioengineering, 107*(3), 516-528.

Woodside, S., Bowen, B., & Piret, J. (1998). Mammalian cell retention devices for stirred perfusion bioreactors. *Cytotechnology, 28*(1-3), 163-175.

Xie, L., & Wang, D. I. (1996). Material balance studies on animal cell metabolism using a stoichiometrically based reaction network. *Biotechnology and Bioengineering, 52*(5), 579-590.

Xie, L., & Wang, D. I. C. (1996). Energy metabolism and ATP balance in animal cell cultivation using a stoichiometrically based reaction network. *Biotechnology and Bioengineering, 52*(5), 591-601.

Xie, L., & Wang, D. I. C. (1996). High Cell Density and High Monoclonal Antibody Production Through Medium Design and Rational Control in a Bioreactor. *Biotechnology and Bioengineering, 51*, 725-729.

Xie, L., & Wang, D. I. C. (2006). Fed-batch cultivation of animal cells using different medium design concepts and feeding strategies. *Biotechnology and Bioengineering, 95*(2), 270-284.

Xing, Z., Kenty, B., Koyrakh, I., Borys, M., Pan, S.-H., & Li, Z. J. (2011). Optimizing amino acid composition of CHO cell culture media for a fusion protein production. *Process Biochemistry, 46*(7), 1423-1429.

Yallop, C. A., Nørby, P. L., Jensen, R., Reinbach, H., & Svendsen, I. (2003). Characterisation of G418-induced metabolic load in recombinant CHO and BHK cells: effect on the activity and expression of central metabolic enzymes. *Cytotechnology, 42*(2), 87-99.

Yang, M., & Butler, M. (2000). Enhanced erythropoietin heterogeneity in a CHO culture is caused by proteolytic degradation and can be eliminated by a high glutamine level. *Cytotechnology, 34*(1), 83-99.

Yang, M., & Butler, M. (2002). Effects of ammonia and glucosamine on the heterogeneity of erythropoietin glycoforms. *Biotechnology Progress, 18*(1), 129-138.

Yoon, S. K., Hwang, S. O., & Lee, G. M. (2004). Enhancing Effect of Low Culture Temperature on Specific Antibody Productivity of Recombinant Chinese Hamster Ovary Cells: Clonal Variation. *Biotechnology Progress, 20*(6), 1683-1688.

Young, J. D., Shastri, A. A., Stephanopoulos, G., & Morgan, J. A. (2011). Mapping photoautotrophic metabolism with isotopically nonstationary 13C flux analysis. *Metabolic Engineering, 13*(6), 656-665.

Young, J. D., Walther, J. L., Antoniewicz, M. R., Yoo, H., & Stephanopoulos, G. (2007). An Elementary Metabolite Unit (EMU) Based Method of Isotopically Nonstationary Flux Analysis. *Biotechnology and Bioengineering, 99*(3), 686-699.

Zagari, F., Jordan, M., Stettler, M., Broly, H., & Wurm, F. M. (2013). Lactate metabolism shift in CHO cell culture: the role of mitochondrial oxidative activity. *New Biotechnology, 30*(2), 238-245.

Zamboni, N. (2011). (13)C metabolic flux analysis in complex systems. *Current Opinion in Biotechnology, 22*(1), 103-108.

Zamorano, F., Vande Wouwer, A., & Bastin, G. (2009). *Metabolic Flux Interval Analysis of CHO cells*. Proceedings of the 6th mathmod conference, Vienna, Austria.

Zamorano, F., Wouwer, A. V., & Bastin, G. (2010). A detailed metabolic flux analysis of an underdetermined network of CHO cells. *Journal of Biotechnology, 150*(4), 497-508.

Zeng, A. P. (1996). Quantitative assessment of cell density effect on the metabolism and antibody production rate of hybridoma cells at high cell density. *Journal of Biotechnology, 45*(3), 243-251.

Zhu, J. (2012). Mammalian cell protein expression for biopharmaceutical production. *Biotechnology Advances, 30*(5), 1158-1170.

Zupke, C., & Stephanopoulos, G. (1994). Modeling of isotope distributions and intracellular fluxes in metabolic networks using atom mapping matrices. *Biotechnology and Bioengineering, 10*(5), 489-498.

Zupke, C., & Stephanopoulos, G. (1995). Intracellular flux analysis in hybridomas using mass balances and in vitro (13)C NMR. *Biotechnology and Bioengineering, 45*(4), 292-303.